Microenvironment Mediated Resistance to HER2 Targeted Therapeutics in HER2+ Breast Cancer

By

Spencer S Watson

A Dissertation

Presented to the Department of
Cell, Developmental, & Cancer Biology
Oregon Health and Science University
School of Medicine
In partial fulfilment of the
requirements for the degree of

Doctor of Philosophy
In Cancer Biology

May 2017

School of Medicine

Oregon Health & Science University

Certificate of Approval

This is to certify that the PhD Dissertation of

Spencer Watson

"Microenvironment Mediated Resistance to HER2 Targeted Therapeutics in HER2+ Breast Cancer"

Has been approved

_____

Mentor/Advisor: Joe W. Gray, Ph.D.

_____

Member/Chair: Rosalie Sears, Ph.D.

_____

Member: Lisa M. Coussens, Ph.D.

_____

Member: Owen J.T. McCarty, Ph.D.

_____

Member: James Korkola, Ph.D.

_____

Member: Amanda Lund, Ph.D

Table of Contents

Tables and Figures

Abbreviations

2DG	-	2-Deoxy-D-glucose
ADC	-	Antibody-drug conjugates
ADP	-	Adenosine diphosphate
AEV-H	-	Avian erythroblastosis virus H
AJCC	-	American Joint Committee on Cancer
AR	-	Androgen receptor
AREG	-	Amphiregulin
ATP	-	Adenosine triphosphate
BFB	-	Breakage fusion bridge
BR	-	Biological replicates
CAF	-	Cancer associated fibroblast
CEP17	-	Chromosome enumeration probe 17
CGH	-	Comparative Genome
CML	-	Chronic myeloid leukemia
ConA	-	Concanavalin A
CTLA	-	Cytotoxic T-lymphocyte-associated protein
DCIS	-	Ductal carcinoma in situ
DM	-	Double minute
DSB	-	Double stranded breaks
DSG2	-	Desmoglein II
ECD	-	Extracellular domain
ECM	-	Extracellular matrix
EdU	-	5-ethynyl-2'-deoxyuridine
EGF	-	Epidermal growth factor
EGFR	-	Epidermal growth factor receptor
EMT	-	Epithelial to mesenchymal transition
ER	-	Estrogen receptor
FAK	-	Focal adhesion kinase
FBS	-	Fetal bovine serum
FDA	-	Food and Drug Association
FGF	-	Fibroblast growth factor
FGFR	-	Fibroblast growth factor receptor
FFPE	-	Formalin-fixed paraffin embedded

FISH	-	Fluorescent in situ hybridization
GEF	-	Guanine exchange factor
GSEA	-	Gene set enrichment analysis
HER2(3,4)	-	Human epidermal growth factor receptor 2, 3, and 4
HER2E	-	HER2 Enriched
HGF	-	Hepatocyte growth factor
HGFA	-	Hepatocyte growth factor activator
HIF-1	-	Hypoxia induced factor 1
HR	-	Hormone receptor
HRG1β	-	Heregulin 1 beta
HSP90	-	Heat shock protein 90
HSR	-	Homologous staining region
IGF	-	Insulin-like growth factor
IGF-1R	-	Insulin-like growth factor 1 receptor
IGFBP-2	-	IGF binding protein 2
IHC	-	Immunohistochemistry
KRT	-	Cytokeratin
L-HER2+	-	Luminal HER2+
LCA	-	Lens cullinaris agglutinin
LINCS	-	Library of Network-Based Cellular Signatures
LOESS	-	Local polynomial regression
MAPK	-	Mitogen activated protein kinase
MaSCs	-	Mammary stem cells
MDSC	-	Myeloid derived suppressive cell
MEMA	-	MicroEnvironment MicroArray
MEP	-	Microenvironment perturbagen
MIB	-	Multiplexed kinase inhibitor bead
MMP	-	Matrix metalloprotease
MPS	-	Massively Parallel Sequencing
MTD	-	Maximum tolerated dose
mTORC	-	Mammalian target of rapamycin complex
NACA	-	Non-adherent cell array
NAF	-	Normal activated fibroblast
NBL	-	Normal-breast like

NO	-	Nitric oxygen
NRG1β	-	Human epidermal growth factor receptor 2
NSCLC	-	Non-small cell lung carcinoma
NMR	-	Nuclear magnetic resonance
PD-L1	-	Programmed cell death ligand 1
PDK1	-	Phosphoinositide-Dependent Kinase 1
PFA	-	Paraformaldehyde
PHA-E	-	Phaseolus vulgaris erythroagglutinin
PI3K	-	Phosphatidylinositide 3-kinase
PIP3	-	Phosphatidylinositol (3,4,5)-trisphosphate
PLC	-	Pregnancy lactation cycle
PLCγ	-	Phospholipase C-γ
PMCA2	-	Plasma membrane calcium ATPase2
PR	-	Progesterone receptor
ROS	-	Reactive oxygen species
RPPA	-	Reverse phase protein array
RSV	-	Rous sarcoma virus
RT	-	Room temperature
RTK	-	Receptor tyrosine kinase
RUV3	-	Removal of unwanted variance 3
SF	-	Scatter factor
SMA	-	Smooth muscle actin
T-DM1	-	Trastuzmab emtansine
T-reg	-	T-regulatory cell
TAM	-	Tumor associated macrophage
TCGA	-	The Cancer Genome Atlas
TEB	-	Terminal end bud
TKI	-	Tyrosine kinase inhibitor
TN	-	Triple negative
TNM	-	Tumor, node, metastasis
TR	-	Technical replicates
TSA	-	Trichostatin A
VDR	-	Vitamin D receptor
WGA	-	Wheat germ agglutinin

Acknowledgements

I would first like to thank my mentor Dr. Joe Gray for all his support, guidance, and inspiration. He has greatly expanded my vision of what is possible in science, and any future success I have in research I owe in no small part to him. I would also like to thank Dr. Jim Korkola who has been an amazing co-mentor to me, and a constant source of great advice. The freedom and support they have given me these last six years have been invaluable.

In addition, I am extremely grateful to my thesis advisory committee, Drs. Lisa Coussens, Rosie Sears, and Owen McCarty. I believe their insight and uncompromising standards have made me a better researcher. Drs. Coussens and Sears in particular have been incredibly generous with providing both intellectual and material aid to my work.

I also need to acknowledge my fellow OHSU PMCB classmates, they have been a constant source of support and encouragement, and I wish all of them the very best in their future endeavors.

Finally, I would like to thank the OSLER OCTRI TL-1 training grant, and the NIH NCI Ruth L. Kirschstein predoctoral F31 fellowship for their generous financial support.

Dedication

I would like to dedicate this work to my wife Jessica, and my sons Noah and Calvin. Thank you for your endless patience throughout this process, I truly could not have done it without you

Academic Curriculum Vitae

Spencer S. Watson
watsons@ohsu.edu
watsonspencer@hotmail.com

Education

2011 – 2017 Oregon Health and Science University, Portland Oregon
Ph.D. in Cancer Biology

2000 – 2003 Oregon State University, Corvallis Oregon
Bachelor of Science, Biology Major Chemistry Minor

Summer 1999 School for Field Studies, Queensland Australia

Professional Experience

2011-2017
OHSU Biomedical Engineering, Portland Or
Graduate Program for Molecular and Cell Biology
Knight Cancer Biology Graduate Program
Ph.D. Candidate, Joe Gray Lab

- Functional genomics of breast cancer.
- Advanced high throughput cellular imaging, quantification, and analysis.
- Interrogation of tumor microenvironments utilizing array based technology.
- Functional analysis of breast cancer drug resistance.
- Focus on therapeutic resistance and microenvironment influences on cellular plasticity in breast cancer.

2006-2011
OHSU/Shriners Hospital for Children, Portland Or
Research Assistant, Ronen Schweitzer Lab

- Genetic studies of embryogenesis and tendon formation.
- 3D renderings of early limb development using multiphoton imaging.
- Image cytometry of electron microscopy imaged collagen fibril phenotypes.
- Immunohistochemistry analysis of developmental anatomy.
- Study of tendon stem cell recruitment and differentiation.
- Management of mouse colony.
- Focus on link between early cellular differentiation of tendomuscular progenitors and evolutionary biology.

2003-2005
OHSU Behavioral Neuroscience Portland Or
Research Assistant, Chris Cunningham Lab

- Conditioned Place Preference experiments with mice.
- Intragastric self-administration of alcohol experiment with rats and mice.
- Animal Surgery; mice and rats.
- Focus on generating a rodent model of alcoholism for treatment trials.

Summer 2002
OHSU Pediatrics Department Portland, Or
Student Research Assistant, De-Ann Pillers Lab

- Studying role of ureaplasma infection in neonates leading to chronic lung disease.
- Tested patient samples using PCR, and gel electrophoresis.
- Maintained cell cultures for ELISA testing.
- Aided other researchers with cell cultures, plasmid preps, genotyping of mice, and data entry.
- Focus on long term cohort study design.

Summer 2001
OHSU Pediatrics Department Portland, Or
Student Research Assistant, De-Ann Pillers Lab

- Studying role of ureaplasma infection in neonates leading to chronic lung disease.
- Tested patient samples using PCR, and gel electrophoresis.
- Compiled patient records into worksheets, performed statistical analysis.
- Aided other researchers with genotyping of mice, and data entry.

Summer 2000
OHSU Pediatrics Department Portland, Or
Volunteer, De-Ann Pillers Lab

- General Laboratory Assistance.
- Tested patient samples using PCR, and gel electrophoresis.
- Worked on grant proposals.
- Data entry, and general assistance to other researchers, including assisting with echocardiograms in mice.

Fellowships/Awards

2013 – 2014 Oregon Clinical and Translational Research Institute OSLER TL1 fellowship
2016 – 2017 National Cancer Institute Ruth L. Kirschstein National Research Service Award (NRSA) for Individual Predoctoral Fellows (F31)

Skills

Extensive advanced fluorescent microscopy techniques. High content Image cytometry with Olympus Scan^R, GE InCell, ImageJ, and CellProfiler. Programming and computational biology, with focus on bioinformatics using Python Bioconductor and R*. Computational analysis of RNAseq and RPPA data. Cell spot microarray development and design. Western blot and CoIP protein analysis. Mouse colony management and animal surgery.

Selected Research Publications

G.K. Mack, **S.S. Watson**, G.A. Pantely, J. Pang, R. Hohimer, D.J. Sahn, D.M. Pillers.
Deterioration of cardiac function associated with cardiac hypertrophy in a heterozygous murine model of congenital muscular dystrophy.
Oral presentation at the Western Society for Pediatric Research Annual Meeting, Carmel, CA 2001.
Journal of Investigative Medicine 49(2):151A, 2001.

T.T. Colaizy*, G. Sexton, E. Walker, **S.S. Watson**, D.M. Pillers.
Association of PCR detection of ureaplasma urealyticum in endotracheal aspirates of very low birth weight infants with incidence of chronic lung disease of prematurity.

Platform Presentation. AAP 2002 National Conference and Exhibition, 2002. Journal of Perinatology 22(7):603-604 (2002).

T.L. Fidler, **S.S. Watson**, B.G. Obrerlin, & C.L. Cunningham.
Consecutive days of passive ethanol infusion result in higher levels of ethanol self-infusion than do alternate days of passive ethanol infusion in rats.
Published in Alcoholism; Clinical and Experimental Research 28(5);143A, 2004.

T.L. Fidler, **S.S. Watson**, A.M. Struthers, & C.L. Cunningham.
Intragastric Ethanol Self-Administration in Selectively Bred HAD-1 and LAD-1 Rat Lines.
Published in Alcoholism; Clinical and Experimental Research 29(5);98A, 2005

J.A. Staverosky, B.A. Pryce, **S.S. Watson**, R. Schweitzer.
Tubulin polymerization-promoting protein family member 3, Tppp3, is a specific marker of the differentiating tendon sheath and synovial joints.
Published in Developmental Dynamics 238(3):685-92, 2009

S.S. Watson, T.J. Riordan, B.A. Pryce, R. Schweitzer.
Tendons and muscles of the mouse forelimb during embryonic development.
Published in Developmental Dynamics 238(3):693-700 2009

B.A. Pryce[1], **S.S. Watson[1]**, N.D. Murchinson, J.A. Staverosky, N Dunker, R. Schweitzer.
Recruitment and maintenance of tendon progenitors by TGFbeta signaling are essential for tendon formation.
Published in Development 136(6):1351-61 2009

Y. Li, Q. Qiu, **S.S. Watson**, R. Schweitzer, R.L. Johnson.
Uncoupling skeletal and connective tissue patterning: conditional deletion in cartilage progenitors reveals cell autonomous requirements for Lmx1b in dorsal-ventral limb patterning.
Published in Development 137(7):118-8 2010

W. Liu, **S.S. Watson**, Y. Lan, D.R. Keene, C.E. Ovitt, H. Liu, R. Schweitzer, R. Jiang.
The atypical homeodomain factor Mohawk controls tendon morphogenesis.
Published in Molecular Cell Biology 30(20):4797-807 2010

A.H. Huang[1], T.J. Riordan[1], B. Pryce[1], J.L. Weibel[1], **S.S. Watson[1]**, F. Long[2], V Lefebvre[3], B.D. Harfe[4], H.S. Stadler[1], H. Akiyama[5], S.F. Tufa1, D.R. Keene[1], R. Schweitzer[6]
Musculoskeletal integration at the wrist underlies modular development of limb tendons.
Published in Development 2015 Jul 15;142(14):2431-41.

S.S. Watson, M. Dane, K. Chin, M. Nederlof, M. Liu, T. Liby, W. Thompson, R. Smith, D. Kilburn, M. Whitman, D. Sudar, G.B. Mills, L. Heiser, O. Jonas, J.W. Gray, J. Korkola.
Microenvironment Mediated Mechanisms of Resistance to HER2 Inhibitors Differ Between HER2+ Breast Cancer Subtypes
(Manuscript Under Consideration at Cell Systems, May 2017)

Presentations

Keck / Department of Defense Retreat April 27 2013, Portland Oregon
Oral Presentation “Interrogating Tumor Microenvironment Interactions with Array Based Technology”

Nature CNIO Conference October 27 2013, Madrid Spain
Presented Poster "Interrogating Plasticity and Drug Resistance with MicroEnvironment MicroArrays"

OHSU CDB Student Seminar Series May 10 2014, Portland Oregon
Oral Presentation "Interrogating the Impact of the Tumor Microenvironment on HER2+ Breast Cancer Drug Resistance"

AACR Annual Meeting April 5 2014, San Diego California
Presented Poster "Interrogating HER2 plasticity and lapatinib resistance with MicroEnvironment MicroArrays"

OHSU Research Week May 6 2014, Portland Oregon
Presented Poster "Interrogating HER2 plasticity and lapatinib resistance with MicroEnvironment MicroArrays"

ISAC CYTO Conference May 17 2014, Ft Lauderdale Florida
Presented Poster "Interrogating HER2 plasticity and lapatinib resistance with MicroEnvironment MicroArrays"

NIH Integrative Cancer Biology Program PI Meeting May 2014, Rockville Maryland
Presented Poster "Interrogating Plasticity and Drug Resistance with Microenvironment Microarrays"

High Content Analysis & Phenotypic Screening Conference January 26 2015, San Diego California
Presented Poster "Interrogating Plasticity and Drug Resistance with MicroEnvironment MicroArrays"

OHSU CDB Student Seminar Series March 23 2015, Portland Oregon
Oral Presentation "Microenvironment Mediated Mechanisms of Resistance to Anti-HER2 Agents in HER2+ Breast Cancer"

OHSU Research Week May 8 2015, Portland Oregon
Presented Poster "Interrogating HER2+ breast cancer plasticity and resistance to lapatinib with MicroEnvironment MicroArrays" Awarded Best Poster

OHSU CDCB/OCSSB Retreat August 12 2015, Portland Oregon
Presented Poster "Interrogating HER2+ breast cancer plasticity and resistance to lapatinib with MicroEnvironment MicroArrays"

Cold Spring Harbor Laboratory Biology of Cancer Meeting May 12 2015, Cold Spring Harbor New York
Presented Poster "Interrogating Mechanisms of HER2+ Breast Cancer Lapatinib Resistance with Microenvironment Microarrays"

NIH Library of Integrated Network-Based Cellular Signatures (LINCS) Outreach Retreat April 2016, Portland Oregon
Oral Presentation "Microenvironment mediated mechanisms of resistance to anti-HER2 agents in HER2+ breast cancer"

Gordon Research Seminar Mammary Gland Biology Conference May 28 2016, Lucca Italy
Oral Presentation "Phenotypic Subtypes of HER2+ Breast Cancer Rescued from Lapatinib by Discrete Microenvironment Factors"

Gordon Research Conference Mammary Gland Biology Conference May 29 2016, Lucca Italy

Oral and Poster Presentation “Phenotypic Subtypes of HER2+ Breast Cancer Rescued from Lapatinib by Discrete Microenvironment Factors”

OHSU CDCB Student Seminar Series November 2016, Portland Oregon
Oral Presentation “Microenvironment Mediated Mechanisms of Resistance to Anti-HER2 Agents in HER2+ Breast Cancer”

OHSU CDCB Student Seminar Series March 6 2017, Portland Oregon
Oral Presentation “Microenvironment Mediated Mechanisms of Resistance to HER2 Inhibitors Differ Between HER2+ Breast Cancer Subtypes”

AACR Annual Meeting April 1 2017, Washington D.C.
Presented Poster “Microenvironment Mediated Mechanisms of Resistance to HER2 Inhibitors Differ Between HER2+ Breast Cancer Subtypes”

References

Joe Gray Ph.D.
Gordon Endowed Chair
Chair, Department of Biomedical Engineering
Director, OHSU Center for Spatial Systems Biomedicine
Associate Director for Translational Research
Oregon Health and Science University Knight Cancer Institute
Center for Health and Healing,
3303 SW Bond Ave, Room #13000
Portland, OR 97239, Mail Code: CH13B
Grayjo@ohsu.edu
Phone: 503-418-9302

Lisa Coussens Ph.D.
Professor and Chair
Cell, Developmental & Cancer Biology Department
Associate Director of Basic Research, Knight Cancer Institute
Oregon Health & Science University
3181 SW Sam Jackson Park Rd
Mailcode L215
Portland, OR 97239
coussenl@ohsu.edu
Phone: 503-494-7811

James Korkola Ph.D.
Assistant Professor
OHSU Center for Spatial Systems Biomedicine
Oregon Health & Science University
Collaborative Life Sciences Building (CLSB)
2730 SW Moody Avenue, Portland, OR 97201
Mail Code: CL3G
korkola@ohsu.edu
Phone: 503-494-4943

Abstract

Microenvironment Mediated Resistance to HER2 Targeted Therapeutics in HER2+ Breast Cancer

Spencer S. Watson

Department of Cell, Developmental, & Cancer Biology

School of Medicine

Oregon Health & Science University

May 2017

Thesis Advisor: Joe W. Gray, Ph.D.

The HER2+ subtype of breast cancer typically results from amplification of the proto-oncogene *ERBB2*, that causes overexpression of the mitogenic cell surface receptor kinase HER2. Absent targeted therapies, this subtype is one of the most aggressive and invasive of all the breast cancer subtypes. However, because overexpressed HER2 is often the key oncogenic driver in this subtype, it has been a successful target for clinical agents that inhibit it specifically. Trastuzumab, pertuzumab, T-DM1, and lapatinib, are all FDA approved drugs that have significantly improved progression-free survival in HER2+ patients. Despite this, long term survival benefits have been hampered by *de novo* or emergent resistance to these targeted agents. While cell-intrinsic secondary mutations that result in drug tolerance have been well studied, the less well understood and remarkably complex cell-extrinsic tumor microenvironment has shown a substantial capacity to cause drug resistance in otherwise drug sensitive tumor cells.

We developed a high throughput, reductionist approach to interrogate this complexity, and determine potential microenvironment-mediated signaling events that could impart drug resistance to HER2+ cancer cell line models. We printed a library of biologically active human extracellular matrix and cell adhesion proteins as 300 μm diameter spots to which cancer cells were specifically adhered. These cell-spot arrays were further exposed to a library of human paracrine signaling proteins creating more than 2500 protein combinations. Arrays were immunofluorescently assayed for cell count, proliferation, and markers of mammary cell state following treatment with either the HER2 targeting drug lapatinib, or DMSO control. High-content imaging, singe-cell image cytometry, and RUV3 and LOESS data normalization were employed to analyze the effect each protein combination had on resistance to lapatinib. We determined that the growth factors NRG1β and HGF had the strongest impact on drug resistance in the selected cell lines, with ECM and cell adhesion proteins modulating their effect. The data demonstrated that the growth factor NRG1β resulted in drug resistance in the HER2 amplified breast cancer cell line AU565, but not the HER2 amplified line HCC-1954, that was instead rescued from drug effect by the growth factor HGF. Remarkably, NRG1β was observed to convert lapatinib treatment from an inhibitor of proliferation to a potent stimulant. However, response to NRG1β and HGF was found to be mutually exclusive between multiple HER2+ cell lines. This mutually exclusive response was further shown in a panel of 8 HER2+ cell lines, where it was determined that cell lines rescued from lapatinib by NRG1β belonged to a unique subgroup of the HER2+ subtype termed L-HER2+, and lines rescued by HGF belonged to a subgroup termed HER2E. Both subtypes were defined by expression profile analysis and patient data derived from The Cancer Genome Atlas. Further experiments validated these responses in 3D and murine cancer models.

Comparisons between these subtypes revealed that L-HER2+ lines demonstrated increased reliance on PI3K signaling, resulting in a feedback response to HER2 inhibition that increased cell surface levels of the NRG1β receptor HER3. Exogenous NRG1β combined with increased surface levels of HER3 enhanced the formation of HER2-HER3 dimers. Dimerization with HER3 also caused a conformational

shift in the ATP binding pocket of HER2, blocking the binding site of lapatinib and neratinib, resulting in drug resistance. We determined that drug sensitivity could be restored in L-HER2+ lines exposed to NRG1β by inhibiting dimerization of HER2-HER3 with the HER2 targeting antibody drug pertuzumab. HER2E lines were found to more dependent on the MAPK pathway, and did not demonstrate the HER3 feedback response observed in L-HER2+ lines, but did have innately higher levels of the HGF receptor MET. We determined that drug sensitivity could be restored in HER2E lines exposed to HGF by targeting MET with the TKI crizotinib.

The data and supporting evidence in this thesis suggest that the L-HER2+ and HER2E subtypes of HER2+ breast cancer are fundamentally different diseases, demonstrating unique expression profiles, phenotypes, pathway utilization, drug sensitivities, and response to their surrounding environment. This evidence leads us to conclude that tailoring therapeutic strategies to these unique breast cancer subtypes based on both their individual characteristics, and on the composition of their primary or metastatic microenvironment, could improve the efficacy of existing therapeutic agents.

In addition, this thesis highlights the importance of understanding the environmental context of cancer cells in combatting resistance to targeted therapies. This work demonstrates that the tumor microenvironment can not only provide compensatory signals to abrogate the inhibition of a single kinase, but can actually alter the target of a drug to completely blockade inhibition. Here we detail mechanisms by which subtype-specific interplays of cell-extrinsic and cell-intrinsic factors can dramatically influence drug resistance in HER2+ breast cancer.

Chapter 1. Introduction to HER2+ Breast and the Tumor Microenvironment

1.1. Historical Synopsis of Breast Cancer Research

The major themes of this thesis involve the intersecting factors of breast cancer subtype heterogeneity, the tumor microenvironment, HER2 amplification-associated tumorigenesis, and resistance to HER2 targeted therapeutics. As such, it is important to provide the contextual background and relevant history of each topic, and how they intertwine with the foundational studies of cancer research. This chapter will introduce a brief history of how cancer research led to the identification of *ERBB2* as a proto-oncogene, and how that informed both clinical stratification of breast cancer diagnosis and targeted therapy. Next, an overview of the signaling environment of the normal mammary duct will introduce key endogenous factors that influence transformed mammary cells. A detailed description of the biology of the HER2 oncoprotein will demonstrate how *ERBB2* amplification can drive mammary tumorigenesis, and how specific inhibition of HER2 has led to clinically successful therapeutic strategies. Finally, this chapter will provide an overview for how cell intrinsic mechanisms and the cell extrinsic tumor microenvironment can cause drug resistance in otherwise drug responsive cancer cells.

***

Mammary gland carcinoma is one of the oldest known cancers in medicine [1, 2]. However, for most of recorded history the only treatment for breast cancer was crude surgical resection, which had extremely limited efficacy [3]. One of the first milestones in the treatment of breast cancer was the advent of the radical mastectomy, starting with Bernard Peyrilhe in 1773, and later put into common practice by William S. Halsted in 1882 [4, 5].

One of the first indications that tumors arose from genetic aberrations in single cells came from Theodor Boveri in 1902. Boveri, along with Walter Sutton, were both instrumental in the identification of chromosomes as mediators of inherited traits, and this work led Boveri to postulate that chromosomal damage from external factors such as radiation or chemical insults could result in uncontrolled cellular proliferation [6, 7]. Thomas Hunt Morgan et al. would later validate much of Boveri's postulates with their work on the Mendelian genetics of *drosophila melongaster* in 1915 [8].

The next breakthrough in the understanding of tumorigenesis came from the study of oncogenic retroviruses. Retroviruses replicate their genomes by integrating them into the DNA of their host via reverse transcriptase [9], and this mechanism results in the potential to both incorporate host genes into the viral genome, as well as introduce exotic genes into a host. Rous sarcoma virus (RSV) is an avian retrovirus discovered to cause sarcoma tumors in chickens by Peyton Rous in 1911 [10]. Studies with RSV led to the development of a focus assay for viral quantification in 1958 [11]. This assay utilized RSVs ability to transform cultured fibroblast cells to titrate precise quantities of viral particles [12]. Viral focus assays facilitated a wave of oncoviral research in the 1960s [13, 14], resulting in the discovery of *src* as the the gene responsible for RSVs oncogenic capacity in 1970 [15]. Further studies revealed that *src* was not an exotic gene unique to the viral genome, but was in fact cellular in origin [16]. Comparisons between the protein products of viral *src* (*v-src*) and cellular *src* (*c-src*) showed that *v-src* was oncogenic due to a C-terminal deletion and several point mutations in its SH3 domain that eliminated a negative regulatory mechanism, causing the protein to have constitutive activity [17, 18]. This changed the paradigm for what was defined as an oncogene, revealing that endogenous genes could be oncogenic given some sort of gain-of-function alteration.

The cellular origin of *src* gave rise to the concept of cellular proto-oncogenes, endogenous genes whose mutation or overexpression could cause cellular transformation. Over 30 such genes have been defined as having transformative capacity in avian and rodent retroviruses [19]. Of these, genes coding for proteins

HER2, PI3K, MYC, ABL, and RAS were all later identified as drivers of human cancers [20-24]. *Ras* in particular, identified soon after *src* in 1979, was an important milestone in the understanding of genetic drivers of cancer. Experiments introducing DNA from human tumor cells into mouse fibroblast cells identified a distinct region of DNA responsible for fibroblast transformation, and that region was homologous to viral *ras* [24]. This finding provided clear evidence that human homologs of known viral oncogenes were drivers of cancer.

The discovery of the transformative capacity of the viral oncogene *v-erbB* in avian erythroblastosis virus, and the identification of its human homolog erbB (the Epidermal Growth Factor Receptor gene *EGFR*) in 1984 was another breakthrough [25, 26]. The rodent derived oncogene called *neu* [12] was discovered about the same time. *Neu* was determined to be partially homologous to *EGFR*, but with key differences that marked it as a related but unique oncogene [27]. The human homolog of *neu* was found to be the *EGFR*-like gene *ERBB2*, that coded for a tyrosine kinase that was named HER2 in 1985 [28, 29]. HER2 is a cell surface Receptor Tyrosine Kinase (RTK) that normally stimulates mitogenic pathways by dimerizing with other erbB family receptors [30]. However, HER2 is unique in that it doesn't require activation by a ligand in order to signal, so activating mutations or overexpression of HER2 results in oncogenic transformation [31, 32]. Following its identification, HER2 was found to be frequently amplified and overexpressed in many cases of breast cancer [20]. Importantly, the overexpression of HER2 was linked to an aggressive form of breast cancer, and became a key prognostic indicator [20]. Due to the importance of HER2 identification to both breast cancer classification and treatment, it will be covered in greater detail later.

Advances in understanding of the basic causes of cancer biology let to increased clinical cancer research. Spurred on by promising results from the advent of chemotherapy in the 1950's and 60's, cancer began to be seen as a possibly treatable malady, rather a terminal diagnosis [33, 34]. Breast cancer in particular received a great deal of clinical attention, and histological analysis of patient tumors began to suggest that this was a not a homogenous disease. These pathologic studies of breast tumors informed the first clinical

subdivision of the disease, resulting in the Tumor, Node, Metastasis (TNM) grading system to divide tumors by stage of progression, which was formalized in the first American Joint Committee on Cancer (AJCC) cancer staging handbook in 1977. Additional risk factors were identified in the 1970s and 80s to further stratify mammary carcinomas, specifically these were expression levels of hormone receptors (HR) Estrogen Receptor (ER) and Progesterone Receptor (PR) in patient tumor biopsies [35-37]. The role of ER and estrogen signaling in breast cancer led researchers to attempt to target its function specifically with the selective estrogen receptor modulator tamoxifen, that became the first successful targeted therapy for breast cancer following its first clinical trial in 1971 [38]. However, not all patients responded to the drug, indicating a significant degree of heterogeneity between tumors with similar HR status and TNM grade.

The identification of HER2 as an oncoprotein, and its subsequent correlation to an aggressive variant of breast cancer in 1985 resulted in its adoption as another prognostic risk factor in the assessment of patient tumors [39]. Identification of ER, PR, and HER2 as prognostic risk factors, along with large retrospective studies of tumor samples correlated with patient outcomes, led to the 2011 St. Gallen International Expert Consensus recommendation to divide breast cancer into 5 subtypes [39]. The formal classification stratified breast tumors based on high or low expression of ER, PR, HER2, and the cellular proliferation marker Ki-67. These breast cancer subtypes are defined below. The informal name is given along with clinical classification. The terms Luminal A and Luminal B were derived from the naming scheme used for molecular subtyping. However, they stated that they lacked the molecular classification for delineating between Luminal A and B at that time, and that clinical nomenclature should still refer to these subtypes based on the HR status [39].

i. **Luminal A** ER+ / HER2- / PR high / Ki-67 low

ii. **Luminal B HER2-** ER+ / HER2- / PR high or low / Ki-67 high (> 14%)

iii. **Luminal B HER2+** ER+ / HER2 overexpressed or amplified / PR+ / any Ki-67

iv. **HER2+** HER2 overexpressed or amplified/ ER- / PR-

v. **Triple Negative** ER- / PR- / HER2-

For reasons that will be discussed later, Luminal B HER2+ is not a subset of the HER2+ subtype, but is instead a subset of luminal breast cancers that has HER2 positivity. The two 'Luminal B' subtypes were later collapsed into one subtype that could be either HER2 positive or negative [40]. Clinical HER2 positivity is based on a histological grading system, where HER2 biopsy staining is assessed by a trained pathologist; 0 to +1 staining is considered negative, +2 is considered borderline, and +3 is referred to as HER2+ [41]. Later, an additional imaging test for the *ERBB* gene was developed to identify amplification in patient biopsies, which will be discussed in more detail later. The HER2+ subtype has also been previously stratified clinically as either ER+ or ER- in trials combining tamoxifen with trastuzumab [42]. However, this yielded inconclusive benefit, and so this stratification has not yet been made a formal clinical distinction [42].

Modern research has continued to find new and more robust methods for classifying breast tumors. Charles Perou et al. used gene expression patterns to stratify breast cancer into 5 different 'intrinsic' molecular subtypes, providing a molecular definition of Luminal A, Luminal B, HER2E, Normal-like, and Claudin-low subtypes [43]. These molecular subtypes revealed a wide range of heterogeneity within the classical clinical subtypes [44]. Carlos Caldas et al. expanded on gene signature classification by integrating genomic and transcriptomic data to describe 10 unique 'IntClust' subtypes [45]. Subtypes can also be further stratified by unique driver and secondary mutations [46]. Indeed, the history of medical oncology in breast cancer has been to increasingly subdivide the disease into more and more specific and unique maladies, providing us with a more nuanced understanding of the disease.

The Cancer Genome Atlas (TCGA) continued this trend with studies that revealed significant genomic and transcriptomic and proteomic differences within the intrinsic molecular subtypes [46]. Interestingly,

they identified consistent differences between clinically assessed HER2+ tumors and molecularly defined HER2E tumors [46]. These subtypes did not directly correlate with the HER2+ or Luminal-B/HER2+ clinical subtypes, nor were they encompassed by the HER2E molecular subtype, suggesting that they represent two distinct new molecular subtypes of HER2+ breast cancer. The research presented in this work will focus on defining two subtypes of HER2+ breast cancer that differ in biological function, interaction with their microenvironments, and responsiveness to HER2 targeted therapies.

1.2. Overview of Normal Mammary Duct Biology

The mammary glands of humans consist of a complex of 10 to 20 simple apocrine glandular lobules. Each lobule is made up of millions of smaller lactiferous ductules (or acini) that produce and secrete milk that is then extricated through a network of ducts to reach the nipple. The basic unit of this structure in a mature gland is the terminal end bud (TEB), a secretory alveoli connected to a contractile duct. The generation, maintenance, and function of TEBs involves a complex set of interactions between the varying cell types of the stroma and the forming duct.

The basic structure of the mammary duct is comprised of three compartments; the luminal cavity, the epithelium, and the surrounding stroma (Figure 1.1). The stroma is largely made up of adipose cells, but is also the site of the vasculature, stromal fibroblasts, and immune cells such as macrophages, mast cells, and eosinophils. The epithelium of the TEB tip is unique from the rest of the ductal structure, with a layer of cap cells surrounding several stratified layers of body cells. The stromal and epithelial compartments are separated by the basement membrane, a layer of Extracellular Matrix (ECM) proteins that both support the duct structure, and serve as a barrier to prevent invasion into the stroma. Important constituents of the basement membrane are collagen IV, laminin, and nidogen, which also serves as mediators of juxtacrine signaling for epithelial and stromal cells. The basal myoepithelial cells in the epithelial compartment are directly adjacent to the basement membrane. The myoepithelial cells have

diverse functions in the ductal structure; they produce the basement membrane, they remodel the surrounding ECM to facilitate ductal branching, they have contractile force to mechanically drive milk excretion, and they reinforce the cell fate of adjacent luminal epithelial cells [47, 48]. Basal cells form a mesh network around the duct, and typically have elongated mesneschymal cell shapes. The luminal epithelial cells are between the myoepithelial cells and the luminal cavity. The epithelial cells are cuboidal in appearance and form a simple-cuboidal barrier around the luminal cavity. Additionally, they are a vital component in hormone induced communication with the stroma, and have a high capacity to undergo epithelial to mesenchymal transition (EMT) during ductal branching and formation [49, 50]. During lactation, cells in the TEB epithelial compartment differentiate into lactiferous alveoli cells that produce and secrete milk into the luminal cavity. An imporant aspect of the pregancy-lactation cycle (PLC) is the massive wave of proliferation and differentation in TEBs throughout the mammary ducatal tree tiggered by increased production of signaling hormones estrogen, progesterone, prolactin, and others during pregnancy. This is followed by the process of involution, in which the expansion of the mammary gland is reveresed by systematic apoptosis.

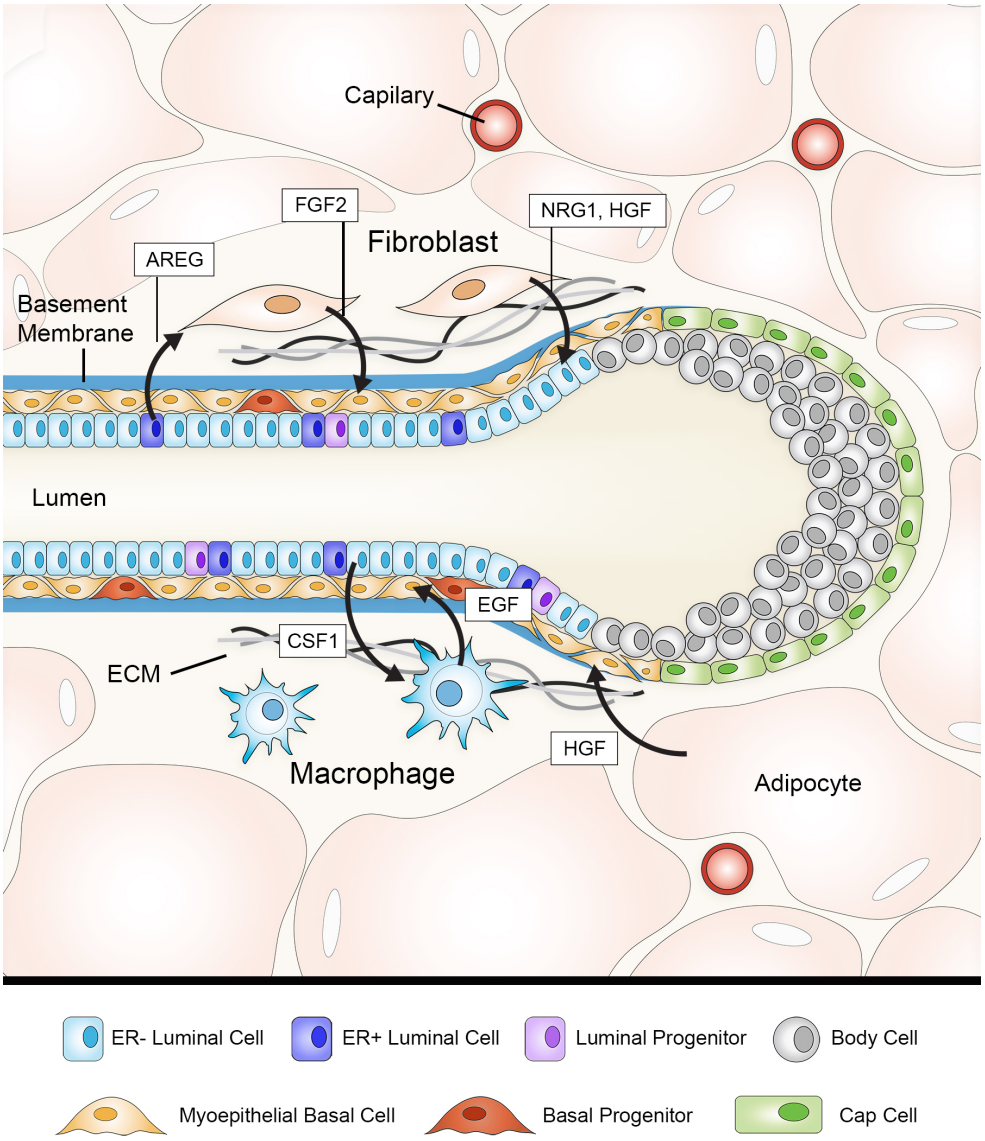

Figure 1.1. Signaling Networks of the Mammary Duct. Diagram of mammary duct TEB depicting varying cell states within the epithelial lineage and paracrine signaling interactions with the surrounding stromal cells. Figure is not representative of relative cellular size, or precise cellular localization in the forming TEB. Figure was inspired by ©Gjorevski, Nelson et al., 2011, originally published in Nature Reviews 12:581-593, and ©Joshi et al., 2012, originally published in Trends in Endocrinology & Metabolism 23(6):299-399.

Identification of cell states within the duct is largely based on cell shape and morphology, as well as by over 15 cell-type specific markers [51]. Key examples that differentiate between basal and luminal mammary duct cells (Figure 1.2) are cytokeratins 5 and 14 (KRT5, KRT14), smooth muscle actin (SMA), and p63 that are markers of basal cell types. Luminal cells have high expression of KRT8/18, KRT19, Androgen Receptor (AR), GATA3, E-Cadherin, and Vitamin D Receptor (VDR). The presence or absence of these and other markers within certain cell types indicates their place in the lineage hierarchy of the duct, but co-expression of basal and luminal markers also reveals a large amount of heterogeneity within the ductal cell types, which will be discussed in more detail later. Multiplexed histology studies showed that there are at least 11 differentiation states within the luminal branch of the mammary lineage hierarchy, and at least 2 basal states [51].

Luminal and basal epithelial cell types are the key mediators of growth and morphogenesis in human mammogenesis, responding differentially to hormone and growth signals following puberty to dramatically increase the size and complexity of the ductal tree. A major distinction between these cell types in development is their expression of hormone receptors ER and PR. Basal cells lack these receptors, but a third of luminal epithelial cells express both, and are often termed hormone 'sensor cells' because of their ability to propagate the hormone signal to other cells in the forming duct [52]. Luminal cells undergo a wave of proliferation in response to estrogen signaling, followed by secretion of amphiregulin (AREG) that activates EGFR signaling in stromal fibroblasts, increasing their mobility and proliferation [53]. In turn, fibroblasts produce Fibroblast Growth Factors (FGF) FGF2 and FGF7 that signals proliferation and morphodynamics in basal cells through FGF Receptor (FGFR) FGFR2 [54] (Figure 1.1). This simplified overview highlights how paracrine signals coordinate the actions of all three cell types to maintain orderly expansion of the ductal tree as it invades the fat pad during puberty

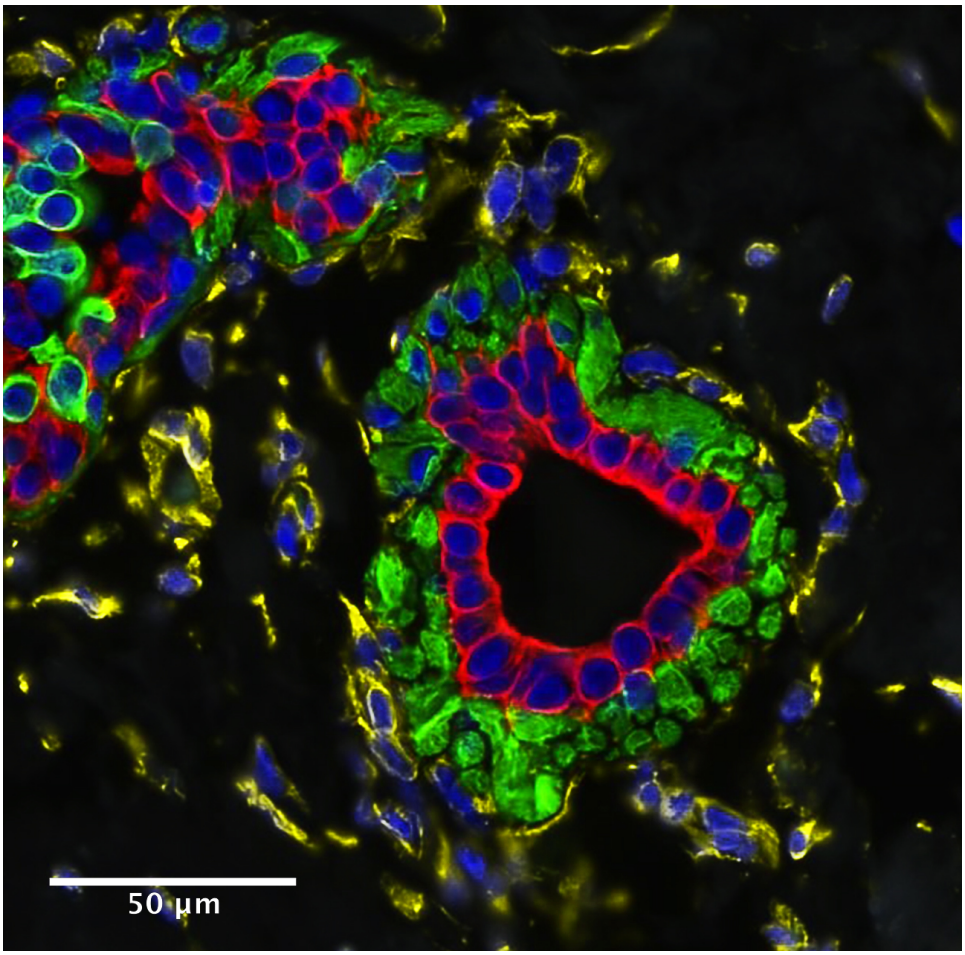

Figure 1.2. Identification of Mammary Cell States by Cytokeratin Markers. Microscopic image of human mammary duct cross section immunofluorescently labeled for the luminal marker KRT19 (red), the basal marker KRT14 (green), the mesenchymal fibroblast marker vimentin (yellow), and DAPI (blue). Image provided by ©Koei Chin 2017, used with permission.

Cellular communication between luminal and basal cells and their surrounding stroma is essential to the maintenance and function of the mammary duct in the mature duct. Part of this maintenance involves the concept of mammary stem cells (MaSCs). Studies that support the presence of MaSCs in the human duct report that they have low replication rates, are capable of self-renewal, and are bipotent progenitors of both luminal or basal cell fates [55]. In humans, MaSCs are thought to be located in the myoepithelial compartment near the terminal of TEBs, and are ER and PR negative [56]. Hormone stimulation has been demonstrated to activate MaSCs to proliferate and differentiate [57]. As the MaSCs are hormone receptor negative, it is currently unclear what specific signal activates them, but it is likely communicated from hormone receptor positive ductal 'sensor cells'. MaSCs are thought to differentiate into HR- basal progenitor cells following activation, as well as HR- and HR+ luminal progenitor cells that can then further differentiate into mature luminal and basal ductal cells. This concept has led to several models of mammary epithelial lineage hierarchies. In some models, bipotent stem cells give rise to bipotent luminal progenitors, and unipotent basal progenitor cells, where the luminal progenitors can then give rise to mature luminal cells, luminal hormone-sensor cells, and alveolar cells [58]. In other models MaSCs are multipotent, and give rise to luminal, basal, and alveolar unipotent progenitors [59]. Identification of position within the linage of these models rely on combinations of cell state marker expression mentioned previously, where the presence or absence of particular markers indicates the cells progression towards its terminal cell fate. However, progression through these lineages may not be strictly linear, especially with transformed cancer cells, and context driven factors can cause progenitors to switch lineage paths, or even move backwards in the lineage, de-differentiating to a more progenitor-like state [60, 61].

The progression of progenitor cells to their terminal cell fate is not cell intrinsic in the mammary duct, but instead is driven by environmental signals from surrounding cells in the duct. Indeed, determination of cell fate in the mammary duct is believed to be highly local-context dependent. For example, promotion of luminal progenitors to a mature luminal fate is driven by adjacent basal cells signaling to luminal progenitors via NRG1 to activate the STAT pathway, which is essential for proper duct formation and

milk production [48]. Mature luminal cells have also been shown to secrete CSF-1, recruiting stromal macrophages to the ductal basement membrane [62], that can in turn maintain basal cells via EGF signaling [63] (Figure 1.1).

This section highlights how paracrine signaling networks between the different cell types in the mammary duct promotes and maintains growth, cell fate, and glandular function. It also demonstrates how varied the phenotypic cell states can be within the epithelial lineage hierarchy of the duct, which may have profound impacts in cancer depending on the cell of origin that first undergoes transformation.

1.2.1. *NRG1 biology and expression*

As noted above, paracrine signaling ligands can trigger proliferation, motility, and differentiation in cells of the mammary duct. We observed in the studies presented in this thesis that transformed mammary cancer cells that share phenotypic similarity with normal mammary cell types retain similar responses to environmental cues that are intrinsic to those cell types. Chapters 3 and 4 will detail studies that identify two mammary stromal derived growth factors, NRG1β and HGF, that have the capacity to elicit HER2 targeted drug resistance in HER2+ breast cancer cell lines. Here I will discuss the biology of these two growth factors.

***

Neuregulin 1 β1 (NRG1β), previously known as heuregulin 1 (HRG1β), is a cell surface transmembrane glycoprotein produced from the neuregulin 1 gene. The neuregulin 1 gene is part of a family of 4 *NRG* genes, but is unique in that it produces at least 6 different protein variants via alternative splicing (types I through VI). The general structure of most NRG1 proteins consists of a cytoplasmic domain (with variants a, b, or c), a transmembrane domain, a protease cleavage site, an EGF-like domain (α, β, or γ), a

glycosylation site, an IgG-like domain, and an N-terminal domain (types I-VI). The EGF-like domains of NRG1β and NRG1α are specific ligands for the HER3 and HER4 ErbB receptors [64]. NRG EGF-like domains bind to domains I and III of ErbB receptors [64]. However, as these are not secreted factors. The EGF-like domain (along with the rest of the ECDs) must be released from the membrane bound protein by protease cleavage in order to activate receptors. This function is commonly performed by proteases ADAM10, ADAM17 and BACE1, typically produced by stromal fibroblasts [65]. Once released into the extracellular environment, ECD domains of the NRG1β ligand initially bind to integrins αVβ3 and α6β4 on the target cell surface. Further processing liberates the EGF-like domain from the other ECD domains, or facilitates direct interaction between the EGF-like domain and HER3 [66]. The exact mechanism of this interaction is still unclear.

Functional NRG1β signaling requires four intersecting factors; expression of NRG1, stromal derived proteases, and HER3 expression and cell surface localization on the target cell (along with possible roles of key integrins). NRG1 is highly expressed in a diverse range of tissues, including the thyroid, mammary ducts, lymph nodes, the lung, and the brain [67, 68]. ADAM10 and ADAM17 are highly expressed in many tissues, but most highly expressed in the lung, thyroid, brain, liver, and bone marrow [68]. HER3 is highly expressed in most tissues in the body, including those where NRG1 and protease expression overlap. Stromal fibroblasts produce NRG1β and proteases, and can greatly increase production of both when transitioning into Cancer Associated Fibroblasts (CAFs) in multiple cancer types and metastatic locations [69]. However, basal myoepithelial cells can also produce NRG1β, and even luminal epithelial cancer cells have been shown to produce NRG1β when treated with HER2 targeted drugs [48, 70].

The normal role of NRG1 in mammary duct development and homeostasis is to promote luminal progenitor cells into mature luminal states. Myoepithelial cells produce NRG1 in response to internal p63, and this activates the HER4 and STAT pathway to promote the mature luminal expression pattern. Additionally, stromal fibroblasts produce NRG1 during mammogenesis to elicit proliferation in luminal

epithelial cells near TEBs [71]. However, luminal cells are not the only target of NRG1, in 3D matrigel experiments of disassociated mammary epithelium it was found that treatment of basal myoepithelial cells with NRG1 resulted in a morphogenic formation of alveolar structures [72]. Interestingly, treatment with HGF in this same experiment elicited a completely different morphogenic response, forming branched tubules instead of alveoli, which will be discussed more below. NRG1β and HER3 also appear to be important in glucose sensing, uptake, and metabolism in breast tissue and breast cancer [73].

NRG1 signaling is a vital component of both neural and mammary gland development, and in some cases cell survival [74]. As will be discussed in Chapter 3, luminal HER2+ breast cancer cell lines cannot survive without HER3. It also appears that NRG1 signaling drives different responses to the normal mammary duct cell types, resulting in luminal maturation and proliferation in luminal epithelia, and resulting in a specific morphogenic pattern in basal epithelia.

1.2.2. *HGF biology and expression*

Hepatocyte Growth Factor (HGF), also known as Scatter Factor (SF), is a paracrine signaling ligand that activates the oncogenic RTK MET [75]. HGF is initially translated as a proform protein (pro-HGF), consisting of two major components; an alpha chain, and a beta chain. HGF can also be alternatively spliced into isoforms NK1 and NK2, but these will not be discussed. The N-terminal alpha chain of pro-HGF contains a PAN/APPLE-like domain and 4 Kringle domains [76]. The beta chain contains an inactive serine proteinase domain, and is connected to the alpha chain by a short peptide linker. Following translation, pro-HGF is secreted into the extracellular space where it can either remain soluble in the interstitial fluid, or bind to ECM proteins. The extracellular serine protease Hepatocyte Growth Factor Activator (HGFA) cleaves the linker region on pro-HGF, and both the alpha and beta chains change conformations so that the beta chain can reattach to the alpha chain in a new orientation via a disulfide bond [77].

The receptor for HGF is the cell surface RTK MET, occasionally also called HGF Receptor (HGFR). Like HGF, MET is also produced as a proform and enzymatically cleaved and reordered to create a mature MET receptor that is trafficked to the plasma membrane. The mature receptor has 3 extracellular domains, the most N-terminal of which is the Sema domain that recognizes and binds HGF. The cytoplasmic domains consist of a phospho-serine containing juxtamembrane domain, a tyrosine kinase domain, and a c-terminal tail with two main auto-phosphorylation sites. MET is activated when ligand binding causes dimerization of two receptors, and this brings the kinase domains into close proximity with the tyrosine residues of the opposing c-terminal regulatory domains. The tyrosines Y1349 and Y1356 are multipurpose docking sites on the MET c-terminal domains that can bind the adapter proteins GRB2 and GAB1 [78]. Through these adapter proteins MET phosphorylation is linked to the Mitogen-Activated Protein Kinase (MAPK) pathway, the PI3K pathway, the STAT pathway, and potentially others depending on the cell type, to stimulate cell survival, proliferation, motility, and morphogenesis [78].

HGF is produced by fibroblasts and adipocytes in mammary tissue in response to a range of stimuli, including estrogen, and inflammatory cytokines [79, 80]. HGF/MET signaling has been found to play several roles during the course of mammary duct development. Interestingly, HGF signaling elicits different responses in different mammary cell types. In experiments with disassociated mammary epithelium cultured in collagen gels, treatment with HGF caused a wave of proliferation in luminal cells, but triggered morphpogenic branching and ductal tubule formation in basal cells [81]. This suggests that response to HGF, like NRG1, is cell-type specific during mammary development.

HGF is highly expressed in mammary glands, liver, lung, thyroid, and adrenal glands [68]. HGFA, the protease required for HGF activation, is produced by liver parenchymal cells and circulated throughout the body in serum [82]. HGFA typically circulates as an inactive precursor and is activated in response to tissue injury [83]. The normal mechanisms of this signaling pathway in response to injury or wound healing

suggests they could be hyper-activated in the tumor microenvironment. Evidence for this comes from studies of elevated levels of HGF, HGFA, and MET in human breast tumors, which were linked to poor prognosis [84, 85].

1.3. Expression and Biology of the Oncoprotein HER2

HER2 (or HER2/*neu*) is a cell surface transmembrane RTK encoded by the *ERBB2* gene. It is part of the ErbB family of RTKs that include EGFR (HER1), HER3, and HER4. This family of signaling proteins is regulated via numerous mechanisms (transcriptional, translational, localization, and ubiquitination), but is regulated most directly by paracrine signaling ligands. There are at least 12 ligands that are recognized by the different ErbB receptors (ex. EGF, AREG, TGFα, BTC, NRG), and binding of ligand to its appropriate receptor triggers a conformational shift in the receptor protein structure (from 'closed' to 'open'), which results in ErbB receptor pairs dimerizing, and propagating the signal to the cell interior via their cytoplasmic kinase domains [64]. However, HER2 is unique in this family as it is the only receptor that does not bind a ligand. HER2 is permanently locked in an active or 'open' conformation [86]. Normally, HER2 heterodimerizes with one of the other ErbB family receptors after they are activated by ligand binding, as HER2 homodimerization is a lower affinity interaction [87]. But when HER2 is highly overexpressed (as it is in HER2+ cancer) the low affinity of this interaction is overcome by the massive increase in receptor concentration. Mutations or post translational modifications to HER2, such as the Δ16 splice variant, can provide further mechanisms to overcome low affinity and enhance the homodimerization of HER2 [88]. HER2 homodimers can signal independent of any ligand signal, and so are unbound from external regulation.

HER2 is a normal constituent of many epithelial layer cells during the course of human development [89], but in normal adult tissue homeostasis it is most highly expressed in breast mammary ducts, the uterus, appendix, bladder, nasopharynx, bronchus, and skeletal and cardiac muscle [68]. In addition, HER2 has

been found to be essential for both mammary [90] and cardiac development and function [91]. Because of this, anti-cancer drugs that target HER2 (such as trastuzumab) often have the side effect of cardiotoxicity [92], that can be exacerbated in cases of co-morbidity like diabetes or hyperglycemia, hypertension, or dyslipidemia [93]. In addition, HER2 signaling is a vital regulator of pulmonary tissue response to acute injury [94]. Thus, it is important that targeted agents against HER2 in HER2+ breast cancer have efficacy at physiological concentrations that have little effect on cells with normal expression levels of HER2, but are instead inhibitory of cancer cells that overexpress HER2.

The HER2 protein has 4 Extracellular Domains (ECDs), a juxtamembrane domain, a transmembrane domain, a cytoplasmic tyrosine kinase domain, and a cytoplasmic regulatory carboxyl-terminal (c-terminal) tail (Figure 1.3). The ECDs I and III are the classical ligand recognition domains in ErbB family receptors. Binding of a ligand to these domains in other ErbB-family RTKs causes a conformational shift exposing domain II, and shifts the protein into the 'open' or active conformation [95]. However, HER2 is constitutively in this conformation in the absence of ligand [86]. The 'open' conformation allows interactions with domain II on adjoining ErbB receptors that facilitates dimerization. For the purpose of illustration, I will use the example of how HER2 interacts with EGFR, and later contrast this with how this differs to interaction with HER3. HER4 typically has low expression in breast cancer tumors, and high expression is linked to good prognosis, and so HER4 will not be discussed in this overview [96].

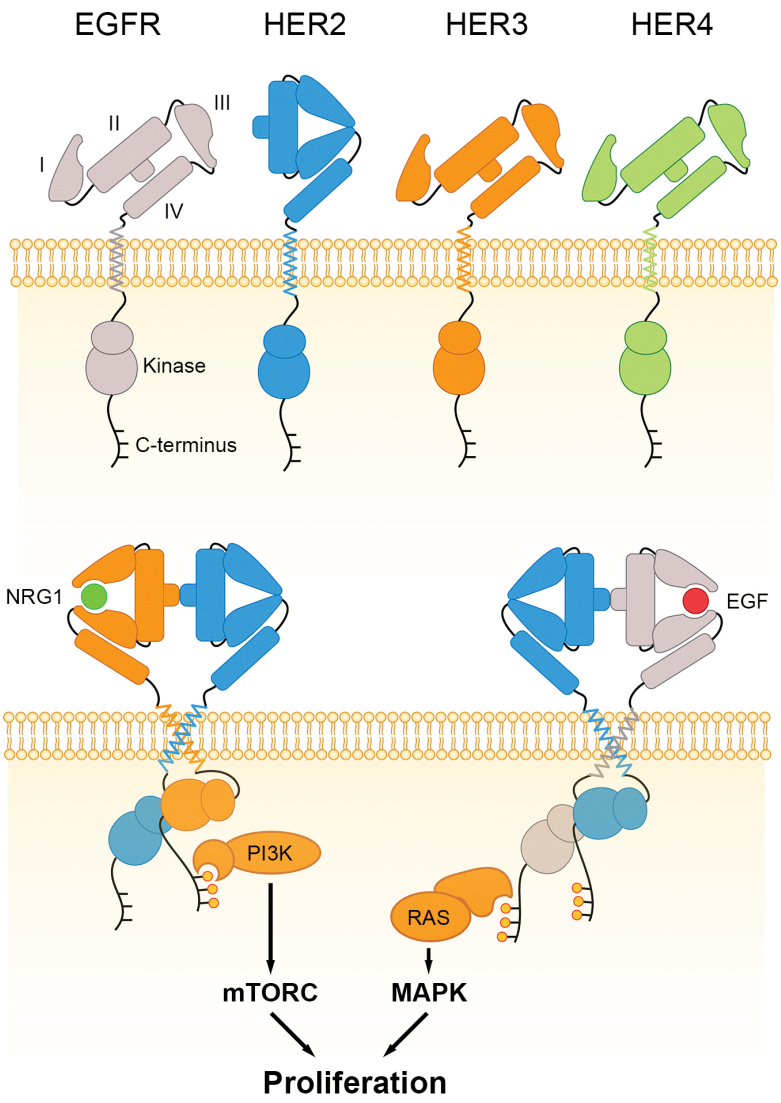

Figure 1.3. The Structure and Function of ErbB RTKs in Mammary Epithelial Cells. ErbB family RTKs are activated by ligand binding to take on an open conformation, facilitating binding with other ErbB family members. Dimerization brings the cytoplasmic kinase domains near the c-terminal regulatory domain of its dimer partner. Phosphorylation of tyrosines on the c-terminal domains couples the activated receptor to PI3K, MAPK, STAT, and other mitogenic signaling cascades. HER2 and HER3 are notable exceptions, as HER2 does not require a ligand to dimerize, and HER3 lacks any kinase activity. Figure adapted from ©Baselga & Swain, 2016, originally published in Nature Reviews Cancer July 2009, 9:463-475.

Contact between domain II sections of HER2 and EGFR facilitates dimerization through interaction between adjacent dimerization arms. This stabilizes the extracellular regions, and results in interaction between partner cytoplasmic kinase domains [97]. Dimerization of these two receptors leads to very specific conformations between the kinase domains, where the kinase domain of one takes what is classically called the 'activator' (or 'donor') position, and the kinase domain of the other takes the 'receiver' (or 'acceptor') conformation [98]. The 'activator' and 'receiver' nomenclature stems from studies of EGFR homodimers, and so is not necessarily descriptive of the role each ErbB kinase plays in every receptor combination. Instead, 'activator' and 'receiver' define an N-C linear order. For the purposes of this overview these will instead be termed the 'First' and 'Second' kinase positions, where the C-terminal region of the First position kinase binds to the N-terminal region of the Second position kinase (Figure 1.4). The asymmetric kinase structure both further stabilizes the dimer, and brings the C-terminal regulatory domains of each protein to the sites of phosphorylation on the adjoining receptor, resulting in auto-phosphorylation of the tyrosine residues. This kinase dimer structure also plays a regulatory role in the conformation of the ATP-binding pocket of each kinase [99]. The ATP-binding pocket of the First position kinase has been found to be in the inactive (or DFG in/α-C out) conformation, and the Second position kinase pocket in the active conformation [100, 101]. An important consequence of this is that HER2 targeting small molecule Tyrosine Kinase Inhibitors (TKIs) such as lapatinib and TAK-285 preferentially bind the inactive conformation of the ATP pocket, and so their efficacy is greatly reduced when the pocket is in the active conformation. It has been suggested that kinase domains can switch places, and this would allow inhibitor binding to HER2 and EGFR kinase domains as they enter First kinase position [102]. Ward et al. demonstrated that HER2 preferentially takes the First position in pairings with EGFR, and the Second position in pairings with HER4 [98]. Interactions with HER3 were not shown, but there is a great deal of structural homology between HER3 and HER4, suggesting similar relationships with HER2. For reasons that will be discussed later, it is most likely that HER2 occupies the Second position in HER2-HER3 heterodimers.

The major phosphorylation sites on HER2's regulatory C-terminal domain are the tyrosine residues 1112, 1139, 1196, 1221/1222, and 1248. Tyrosine 877 is a Src binding domain [103]. Phosphorylation of tyrosine 1112 is a binding site for the E3 ubiquitin ligase CBL that results in the polyubiquitination of HER2 and its proteasomal degradation [104]. Tyrosine 1139 is a GRB2 and GRB7 binding domain [105]. GRB7 is on the *ERBB2* amplicon, and so is frequently overexpressed in HER2+ disease. Tyrosines 1196, 1221/1222, and 1248 are canonical Shc binding domains. Autophosphorylation of tyrosines 1248 and 1221/1222 couples HER2 to the MAPK pathway, which is the predominant pathway employed by HER2-HER2 homodimers [106, 107]. HER2 lacks any p85 binding sites which can directly link it to the PI3K pathway, but HER2 homodimers can activate PI3K signaling through adapter proteins such as Shc or GAB [108-110]. Which pathway is activated by HER2 signaling in each cell type is dictated by expression levels of the other ErbB dimer partners, as well as adapter proteins.

The multiple adapter binding sites of HER2 containing complexes give them a great deal of flexibility in downstream signaling cascades. The primary HER2 pathways involved in cell survival and proliferation are the JAK/STAT, phospholipase C-γ (PLCγ), Mammalian Target of Rapamycin Complex (mTORC), and MAPK pathways. Below we will focus on the mTORC and MAPK pathways, as they were found to be the dominant oncogenic signaling pathways in the studies presented in Chapters 3 and 4. HER2 homodimers and HER2-EGFR heterodimers predominantly signal through the MAPK pathway, so to briefly summarize this cascade; phosphorylation of tyrosine 1248 or 1221/1222 on HER2's C-terminal domain by EGFR serves as a binding site for the adaptor protein SHC, that is coupled to GRB2, that is coupled to SOS, a Guanine Exchange Factor (GEF) for RAS. Association between this complex and HER2 brings SOS to the plasma membrane where it can activate membrane bound RAS, RAS then in turn recruits RAF, and this in turn activates the MAPK cascade of MEK and ERK. The end result is the phosphorylation and activation of transcription factors that increase transcription of genes involved in proliferation. How HER2 complexes signal through PI3K in mammary cells will be discussed in the next section.

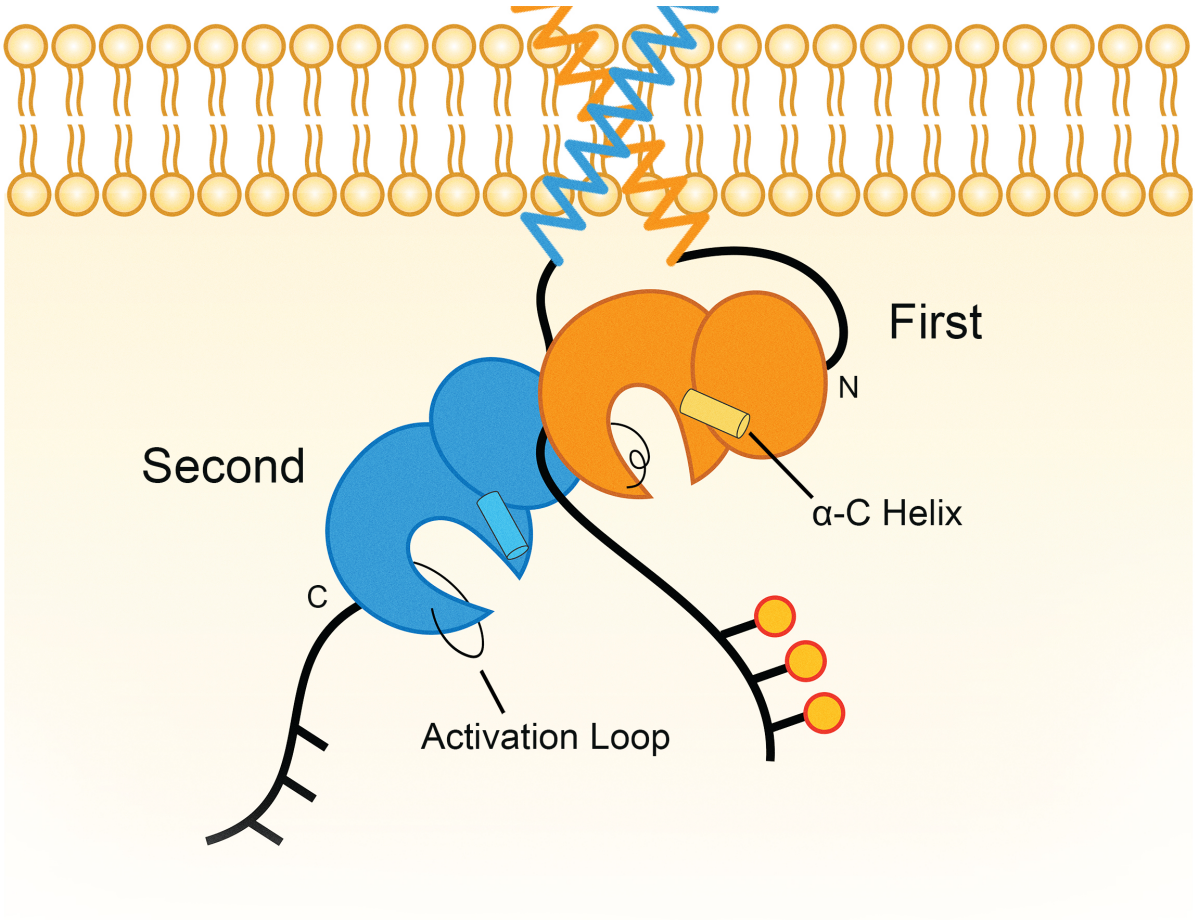

Figure 1.4. Asymmetric ErbB kinase domain dimerization. Kinase domains of ErbB dimers form linear pairings where the C-terminal end of the First position kinase binds to the N-terminal domain of the Second position kinase. Asymmetric dimerization causes a conformational shift in the activation loop of the ATP binding pocket; the First position kinase takes an inactive conformation where its α-C helix is facing out, while the Second position kinase takes an active conformation where its α-C helix is facing in. Figure based on data from ©Novotny, Shokat et al., 2016, originally published in Nature Chemical Biology 12:923-930.

A major regulator of ErbB signaling to the MAPK pathway, or any membrane-bound receptor driven pathway, is its trafficking to and from the plasma membrane. Using the previous example of the MAPK pathway; the primary consequence of HER2 activation is the stabilization of complexes like GRB2/SOS near the membrane so they can interact with membrane bound constituents of the signaling pathway. Internalization of the ErbB receptor via endocytosis shuts down activity of the pathway. However, another unique feature of HER2 that contributes to its potency in receptor kinase complexes in human cells is its specific localization on the plasma membrane. HER2 is found to be predominantly localized to cellular membrane protrusions in mammary epithelial cancer cells, and largely absent on the bulk membrane [111]. It is currently unclear if the localization of HER2 to cellular protrusions impedes their signaling capability [111]. These cellular extravasations, that can be similar to filopodia or invadopodia, are distinct domains from the bulk membrane, with differential expression plasma membrane proteins. One of these differences that has a direct bearing on HER2 activity is the absence of clathrin coated pits on cellular protrusions [111]. The mechanism for internalization and subsequent degradation of ErbB receptors, which is an important negative regulator of ErbB activity, normally involves clathrin-mediated endocytosis [112]. The lack of clathrin coated pits at the site of HER2 localization makes HER2, and HER2 containing complexes, exceedingly stable and long-lived on the cell surface. Interestingly, these cellular protrusions may not only be the preferred site of HER2 localization, but may also be a direct result of HER2 overexpression [113].

Other proteins also contribute to making HER2 a prolific and largely unrestrained mitogenic kinase. In particular, the chaperone protein Heat Shock Protein 90 (HSP90) is an important regulator of HER2 localization, both in terms of inhibiting internalization, and also contributing to rapid endosomal recycling back to the cell surface. HSP90 binds to the cytoplasmic domain of HER2 via its interaction with CDC37, and multiple theories exist for how this inhibits internalization [114]. Two possibilities are that the CDC37-HSP90 complex conceals internalization signals on HER2, or that the complex interferes with HER2 entering sites of forming endocytic vesicles via interactions with raft proteins like flotillins [115]. HSP90 is

also thought to bind to f-actin within the cellular protrusions, sequestering HER2 to areas of the membrane without clathrin coated pits [116]. Another possibility that may have biological relevancy for the mechanisms of drug resistance discussed later is that HSP90 constrains HER2 to the cell surface by inhibiting internalization, and by ensuring its rapid recycling back to the cell surface, rather than to lysosomal degradation [117].

It has been reported that the interaction between HER2 and HSP90 is regulated by cytoplasmic calcium levels, and the calcium ion pump Plasma Membrane Calcium ATPase2 (PMCA2) is important in maintaining an appropriate low calcium level for their interaction [116]. Knockdowns of PMCA2 in that study were shown to greatly increase the extent of HER2 internalization, and greatly decreased cell proliferation. Other inhibitors of HSP90 are also capable of increasing HER2 internalization and decreasing its mitogenic activity, such as geldanamycin, and 17AAG [117, 118].

As the mechanisms detailed above are specific to HER2, resistance to regulation by internalization is most likely conferred to HER2 binding partners such as EGFR and HER3. This can lead to enduring hyper-activation of multiple signaling pathways when HER2 is overexpressed. In addition, some of the ErbB pairings have further unique characteristics that can have profound effects on drug resistance, such as the case with HER3.

1.3.1. *HER3 biology and dimerization with HER2*

The ErbB family receptor kinase HER3 is an important co-factor in HER2 signaling. HER3 is overexpressed in 50-70% of breast cancers, and is often co-overexpressed in ER+ HER2+ breast cancers [119, 120]. HER3 has multiple features that make it unique among RTKs. The primary difference between HER3 and other ErbB family kinases is that it lacks a functional kinase domain, and so cannot function as a homodimer, and must instead heterodimerize in order to signal [121].

The extracellular domain of HER3 shares a great deal of structural homology with EGFR and HER4, and remains in an inactive or 'closed' conformation in the absence of ligand binding. ECDs I and III serve as ligand binding domains that are specific for the EGF-like domains of paracrine signaling proteins NRG1 and NRG2, binding of these ligands triggers a conformational shift to an active conformation that enables heterodimerization with EGFR, HER2, or HER4 [64]. However, HER3 is unable to phosphorylate tyrosine residues on the c-terminal domain of dimer partners following dimerization because it lacks any known kinase activity, but as it does contain a kinase domain so it is classified as a pseudokinase [121].

There are 11 phosphorylation sites on the c-terminal tail of HER3 known to serve a range of regulatory functions, but the phosphorylation site most relevant to breast cancer is tyrosine 1289. Phosphorylation of tyrosine 1289 on HER3 serves as a binding site for the p85 subunit of PI3K. This in turn sequesters PI3K at the plasma membrane where it can phosphorylate the membrane lipid phosphatidylinositol (4,5)-bisphosphate (PIP2), converting it to PIP3. PIP3 serves as a binding site for both Phosphoinositide-Dependent Kinase-1 (PDK1) and AKT, bringing them together so that PDK1 can phosphorylate and activate AKT. Activation of AKT results in a signaling cascade that activates mTORC, that in turn activates ribosomal protein S6, leading to transcriptional enhancement of genes involved in cellular proliferation.

AKT/mTORC is a common and potent mitogenic pathway in breast cancers, and particularly important in HER2+ breast cancer. One of the major reasons for this is because it is the primary pathway activated by HER2-HER3 heterodimers, which are the most potent kinase pairings of all the ErbB combinations [122, 123]. Because HER3 lacks kinase activity, it is unable to phosphorylate HER2. Instead, signaling is almost exclusively via HER2 phosphorylating the p85 binding site on HER3. This is clinically important since HER3 frequently is overexpressed when HER2 is amplified in breast cancers [96, 120]. HER2 and HER3 are each other's preferred binding partner [122], having the highest affinity of interaction, and having the highest

rate of kinase activity [123]. As discussed above, binding of HER3 to HER2 likely confers all the stability characteristics of the latter to the former, including sequestration to membrane protrusions, low rate of internalization, and rapid recycling back to the plasma membrane.

Despite the high affinity of HER2-HER3 interactions, HER2-HER3 dimers typically are not the predominant pairing at steady state when HER2 is overexpressed, even when HER3 is co-overexpressed [124]. This is due to HER3 being sequestered in the endoplasmic compartment of the cytoplasm, rather than the cell surface [125]. Work by Mark Moasser et al. demonstrated that HER3 is under multiple levels of regulation, and is part of a feedback response to loss of AKT/mTORC signaling [125]. HER3 is typically maintained at an elevated but homeostatic level in the endosomal compartment of the cytoplasm of HER2+ breast cancer cells when overexpressed. When HER2, PDK1, or PI3K activity is inhibited, levels of pAKT drop and this results in several responses that increase surface levels of HER3 [125]. The first response is endosomal trafficking of HER3 from the cytoplasm to the cell surface, and data from the work discussed in Chapter 3 suggests that this response can occur in less than two hours [126]. Loss of pAKT levels also triggers increased expression and binding of transcription factors such as FOXO1 and FOXO3a to the promoter regions upstream of HER3 to enhance transcription of HER3 [127]. Another response to loss of HER2 signaling removes inhibitory checks on HER3 protein translation by decreasing expression of HER3-targeting miRNAs such as miR106b, and by increased induction of the mRNA cap binding protein 4EBP1 [126]. The combination of these events results in increased HER3 protein production. HER3 protein levels can increase 10-fold under prolonged HER2 targeted drug treatment, such as lapatinib or neratinib, eventually overcoming drug effect through the increased formation of TKI resistant HER2-HER3 heterodimers. This upregulation of HER3 typically takes at least 48 hours to reach peak feedback response [125].

The HER3 feedback response can also occur in response to MAPK inhibition [128]. Loss of pERK in BT474 HER2+ breast cancer cells treated with the MEK inhibitor AZD6244 was associated with an increase in

pAKT along with an increase in association between the p85 subunit of PI3K and HER3 [128]. This demonstrates the capacity the HER3 feedback has to overcome inhibition of multiple mitogenic pathways. However, the mechanism underlying this response to MEK inhibition is currently unknown.

HER2-HER3 heterodimers play a major role in HER2 targeted drug resistance, which will be discussed in greater detail in Chapters 3 and 4. An important aspect of this resistance is the structural conformation of the kinase domains of the dimer. Unlike the extracellular and juxtamembrane domains of the HER2-HER3 heterodimer, the cytoplasmic domains form an asymmetric dimer, similar to the HER2-EGFR dimer discussed previously (Figure 1.4). However, this pairing is unique because HER3 has no kinase activity and cannot phosphorylate HER2, so the HER3 kinase domain must assume the First position in the kinase domain pairing, relegating HER2 to the obligate Second position. As stated above, stabilization of HER2-HER3 dimers by NRG1 causes a conformational shift in the ATP binding pocket of HER2 that diminishes the binding affinity of HER2 targeting TKIs [99].

All of this makes HER2-HER3 heterodimers both incredibly potent and resilient stimulators of proliferation, which is why there has been a great deal of basic and clinical research into how to inhibit these structures. As discussed previously, HER3 has no known kinase activity, and so cannot be directly targeted by TKIs. Because of this current agents focus on inhibition with monoclonal antibody drugs targeting HER3 to block its ability to dimerize; such as patritumab, or targeting its most frequent activating ligand NRG1 [129, 130]. However, there are potential consequences with targeting HER3 directly in patients. HER3 is very highly expressed in most tissues in the body, including the brain, GI tract, and cardiac muscle, so directly targeting HER3 might result in serious side effects for patients [68].

Targeting only the mechanism of HER3 activation by HER2 is likely to be far more tissue specific than targeting all HER3 functions, and so the most effective strategy for blocking HER2-HER3 signaling in cancer cells remains targeting HER2. However, how a HER2+ cancer cell responds to inhibition of

HER2-EGFR or HER2-HER3 dimers cannot be assumed to be homogenous. HER2+ tumors have a high degree of heterogeneity in terms of additional mutations, HR expression, RTK expression, and cellular phenotype [46]. Later sections will discuss how these different cell types can vary dramatically in their response to treatment.

1.4. HER2+ Breast Cancer

The above overview on the biology of the HER2 protein largely deals with activity of the wild-type protein under normal expression levels. However, several important mechanisms are given for how HER2 overexpression or constitutive activity can be oncogenic. Indeed, HER2 overexpression represents both a significant and serious risk factor in breast cancer, and a prime opportunity to improve patient survival with targeted treatment. This section will discuss how HER2 was identified as an oncoprotein, how *ERBB2* amplification occurs, mechanisms by which HER2 drives tumorigenesis, and the biology and characteristics of the HER2+ subtype of breast cancer.

***

Viral oncogene research played a key role in the discovery of ERBB2 as an important oncogene. Early work with the avian erythroblastosis virus (AEV-H) resulted in the identification of viral *erbB* as the oncogene responsible for AEV-H mediated transformation [25]. The advancement in cDNA cloning technology in the 1980's led to the seemingly unrelated discovery of the EGF receptor gene, along with its amplification in human A431 cancer cells [26]. Following this, it was discovered by Downward et al. in 1984 that the gene for EGFR shared a great deal of homology with the viral oncogene *v-erbB*, terming it *c-erbB* (now known as *EGFR*) [131]. These findings provided strong evidence for the oncogenic potential of cellular *erbB*.

Concordantly, in 1981 a focus assay screen for oncogenes discovered consistent sequences from neuro- and glioblastomas in BDIX mice capable of transforming NIH353 fibroblast cells [12]. These sequences were later termed '*neu'*, and found to produce a tumor antigen called p185 [132]. *Neu* and p185 were found to have homology with *c-erbB* and EGFR, respectively [132]. However, after successfully cloning human cDNA sequences complimentary to *c-erbB*, Lisa Coussens et al. discovered in 1985 that the homology between *neu* and *erbB* was restricted to the tyrosine kinase domain [27]. Additionally, while human *erbB* mapped to and was overexpressed on chromosome 7 in human A431 cancer cells, probes against *neu* lacking the kinase domain were only detectable on chromosome 17 [27]. This clearly demonstrated that *neu* and *erbB* were similar but disparate oncogenes. Later that same year Coussens et al. would identify human *neu* as a cell surface tyrosine kinase, and rename it HER2 [28].

Further evidence clearly identified HER2 and *neu* as cellular oncogenes. Comparisons between *neu* from neuro- and glioblastomas and *neu* isolated from normal tissue (*c-neu*) revealed that *neu* was oncogenic due to a point mutation in the transmembrane domain (V664E), which rendered it highly resistant to internalization [31]. The activated oncogene, now dubbed *neu*T, was found to be transformative on its own in MMTV-*neu*T mouse models, while overexpression of *c-neu* typically required some additional mutations to cause tumors in MMTV-*neu* models [133, 134]. This provided strong evidence that *c-neu* was in fact a proto-oncogene. Conversely, human HER2 overexpression alone was determined to be sufficient for transformation in mouse NIH3T3 and NR6 fibroblast cells, as well as in MMTV-HER2 mouse models [135-137]. As discussed previously, human HER2 is naturally resistant to endocytic internalization, especially when overexpressed, so this may offer an explanation for the difference in transformative capacity.

Another important milestone in 1985 was the observation by King et al. that a gene similar to *v-erbB*, but distinguishable from *EGFR*, was frequently amplified in human breast cancers [29]. Dennis Slamon et al. then found in 1989 that amplification of the HER2/*neu* proto-oncogene occurred in 25-30% of breast cancer patients, and was correlated with a highly aggressive and invasive form of breast cancer [20]. These

findings directly led to the use of HER2 expression as a prognostic risk factor in clinical treatment, and the identification of the HER2+ subtype discussed previously.

The HER2+ subtype of breast cancer is an aggressive, invasive, and metastatic disease. Additionally, amplification of HER2 is observed in ~25% of all breast cancer instances [138]. In the absence of treatment, the HER2+ subtype is most often lethal, and so proper identification of HER2 overexpression has been an essential tool in clinical treatment. Initial assessment of HER2 expression and grading was done by immunohistochemistry (IHC) in patient biopsies as discussed previously [41]. Later, Joe Gray et al. developed Fluorescence In Situ Hybridization (FISH) assays to identify amplification of the *ERBB2* amplicon [139]. The FISH HER2 assay reports *ERBB2* amplification as a ratio of detected probes against *ERBB2* to those of Chromosome Enumeration Probe 17 (CEP17), with a ratio greater than 2.2 being considered HER2-amplified. Importantly, this assay can differentiate between two major types of *ERBB2* genomic amplification as discussed below.

Amplification of *ERBB2* is the most frequent cause of overexpression of HER2, which is driven by genomic amplification of the 17q12 amplicon. The advent of technologies such as Comparative Genome Hybridization (CGH), and Massively Parallel Sequencing (MPS) allowed identification and precise mapping of the *ERBB2* amplicon in breast cancer, as well its differential amplification between subclonal regions within tumors [140, 141]. In addition to HER2, the *ERBB2* amplicon includes several other genes that have been implicated in breast cancer progression, including *STARD3*, *GRB7*, *PSMD3* and *PERLD1* [142]. It should be noted that mutations in *ERBB2* itself [143], or overexpression of signaling ligands such as NRG1 [144], can also result in similar hyper-activation of the HER2 pathway in the absence of HER2 overexpression, however the rates of these aberrations tend to be very low compared to HER2 amplification [145]. Due to the innate biology of HER2 discussed in detail previously, amplification of the *ERBB2* amplicon is sufficient to hyper activate multiple oncogenic signaling pathways to transform cells.

However, advanced HER2+ breast cancers often carry additional mutations in tumor suppressor genes, such as *TP53* mutations which occur in about 50% of HER2+ breast cancers [146].

ERBB2 amplification can occur by multiple mechanisms, typically resulting in either homologous staining regions (HSRs) within a chromosome, or double minute (DM) extrachromosomal bodies, both identifiable by the FISH assay. HSRs are large copy number gains that are typically observed to be contiguous along one or more chromosome regions, while DMs are small circular plasmid-like extrachromosomal bodies. DMs are found in about 30% of HER2+ breast cancers, with the majority of cases either having HSRs, or a mix of the two [147]. Interestingly, comparative studies found no correlation between response to trastuzumab and the type of *ERBB2* amplification [147]. However, DMs have been associated with lower HER2 protein, and reduced correlation between amplification and IHC score [148]. One proposed mechanism of *ERBB2* amplification involves extrareplication and recombination, where 4 aberrant additional replication forks can occur within 2 normal replication forks, generating two additional copies of the genomic fragment undergoing replication [149]. Disruption of these aberrant forks leaves the two extra fragments with exposed ends, allowing them to either ligate with each other forming DMs, or recombining back into the chromosome forming HSRs [149]. Another well-established mechanism of ERBB2 amplification that can result in HSRs and DMs is the Breakage-Fusion-Bridge (BFB) cycle [150, 151]. Briefly, Double Stranded Breaks (DSBs) that removes a telomere from the end of a chromosome will leave exposed ends, if this chromosome then goes through replication that will allow the exposed ends of the two homologous chromosomes to ligate together, resulting in a single chromosome with two centromeres. When the two centromeres are pulled to opposite poles during anaphase a chromosome bridge forms that will eventually break in a random location, leaving one daughter cell with extra chromosomal material. Because this still results in a chromosome without a telomere, the entire process can repeat, creating HSRs on a single chromosome. Additionally, a double strand break on a fused chromosome in the BFB cycle can result in recombination between adjoining HSRs. DMs result when a

double strand break removes one of the centromeres, and the recombination eliminates the second, this results in DMs (Figure 1.5).

The amplification of the *ERBB2* amplicon, and the associated overexpression of HER2 in breast cancer, has profound impacts on patient outcome. The HER2+ subtype typically had such poor outcomes largely due to both the high incidence of metastasis, as well as the morbidity associated with the common sites of metastasis. HER2+ disease has been found to metastasize to liver, lung, brain, and bone, and often does so at a higher frequency than other breast cancer subtypes, based on a study of 3726 patients, 509 of whom were HER2+ [152]. Additionally, this was one of few studies that stratified HER2+ disease by expression profiling and HR status, demonstrating how each category had differential frequency of site-specific metastasis (Table 1.1). ER/PR negative HER2+ tumors had higher frequency of metastasis to the brain and lung, while ER/PR positive HER2+ tumors had higher frequency of metastasis to bone. This suggests that hormone positivity may be a marker for differential biology within the HER2+ subtype. ER+ and ER- HER2+ tumors differed in their tissue preference, however the liver, lung, brain, and bone were commons sites of metastasis for both.

HER2 overexpression in mammary duct cells results in hyper-stimulation of mitogenic pathways that remove checks on cell cycle progression, inhibit apoptosis, and upregulate genes involved in proliferation. A further consequence of HER2 overexpression is that cancer cells become dependent on HER2 signaling for continued growth, becoming what is termed ‘oncogene-addicted’, meaning that loss of HER2 signaling in HER2+ cells often results in cell death [153]. Oncogene-addiction can be exploited in HER2+ breast cancer for the purpose of targeted therapy.

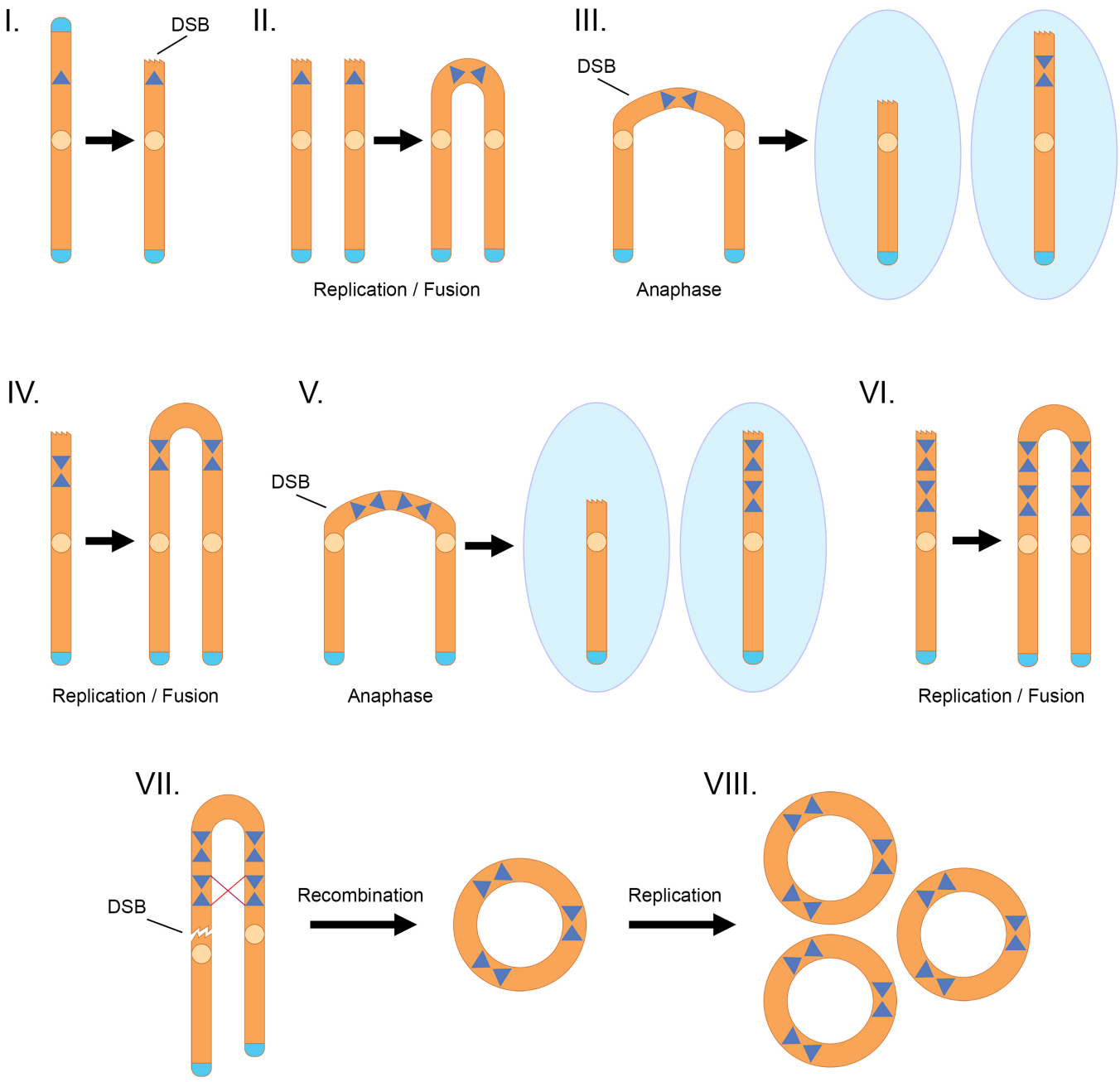

Figure 1.5. Breakage-Fusion-Bridge cycle of gene amplification. Copy number gains by BFB can occur through the following process: I. DSBs remove the telomere of a chromosome. II. If the chromosome goes through replication before repair the exposed ends of the two homologous can fuse. III. The two centrosomes are pulled to opposite sides of the dividing cell during anaphase, eventually causing a DSB in random location that can leave a daughter cell with an extra copy of a genomic region. IV-VI. The chromosome with copy number gain still lacks a telomere, and so can repeat the BFB cycle, causing HSRs. VII. When DSBs coincide with homologous recombination between HSRs, this removes both centrosomes and creates a plasmid-like ring structure (DMs). VIII. DMs can then independently undergo replication within the cell. Figure adapted from ©Matsui et al., originally published in BioMolecular Concepts 2013 4(6):567-589.

Before the advent of targeted treatment, the patients with HER2+ subtype tumors had significantly worse outcomes than patients with non-HER2 amplified disease [154-156]. However, the identification of a dominant cell surface kinase driving proliferation presented a unique opportunity to exploit cancer cell dependency on HER2, and employ a targeted drug strategy that could improve on chemotherapy alone.

1.5. Targeted Therapeutics Against HER2

In 1975 Niels K. Jerne, Georges J.F. Köhler, and César Milstein developed the ability to produce inhibitory monoclonal antibodies to combat disease. They were awarded the Nobel prize in 1984 for their pioneering work on the development of monoclonal antibodies [157]. Cloning of the gene for HER2/*neu* in the 1980s led to the identification of its gene product, the specific tumor antigen p185 [132]. A monoclonal antibody against HER2 was generated, the murine anti-p185 antibody mumAb4D5, that was found to be inhibitory to HER2 activity [158]. Because a mouse antibody would trigger an immune response if used in human patients, the antibody was humanized by Carter et al. in 1992, allowing for its use to specifically target HER2 in cancer patients [159]. Successful clinical trials beginning in 1992 eventually culminated in the FDA approval of trastuzumab (Herceptin) in 1998. Briefly, the mode of action of trastuzmab is to bind to an epitope on the extracellular domain IV of HER2, and so preferentially targets cells with extremely high surface level expression. Binding of trastuzumab to domain IV of HER2 both interferes with its activity, and engages the native immune system to target cancer cells (Figure 1.6). Trastuzumab increased overall survival rate in patients with HER2+ breast cancer by 37% over chemotherapy alone, and 10 year survival from 75% to 84%, and is now part of standard of care treatment for patients with HER2 overexpression [160].

Table 1.1. **Subtypes of HER2+ Breast Cancer Show Preferential Sites of Metastasis**

Subtype	# of Patients	Brain		Liver		Lung		Bone		Distant Nodal		Pleural		Other		Unknown	
		#	%	#	%	#	%	#	%	#	%	#	%	#	%	#	%
Luminal A	458	35	7.6	131	28.6	109	23.8	305	66.6	73	15.9	129	28.2	62	13.5	36	7.9
Luminal B	378	41	10.8	121	32.0	115	30.4	270	71.4	88	23.3	133	35.2	73	19.3	13	3.4
HER2+ ER/PR+	117	18	**15.4**	52	44.4	43	**36.8**	76	**65.0**	26	22.2	40	34.2	16	13.7	6	5.1
HER2+ ER/PR-	136	39	**28.7**	62	45.6	64	**47.1**	81	**59.6**	34	25.0	43	31.6	23	16.9	6	4.4
Basal-like	159	40	25.2	34	21.4	68	42.8	62	39.0	63	39.6	47	29.6	38	23.9	11	6.9
TN non-basal	109	24	22.0	35	32.1	39	35.8	47	43.1	39	35.8	31	28.4	28	25.7	6	5.5
P		< .001		< .001		< .001		< .001		< .001		.3214		.0056		.1338	

Legend: ER = Estrogen Receptor alpha, PR = Progesterone Receptor. *P* values were obtained using Pearson's χ^2 test.

Table 1.1. Subtypes of HER2+ Breast Cancer Show Preferential Sites of Metastasis. Clinical metastasis incidence data for 253 HER2+ breast cancer patients. Frequency of site-specific metastasis among HER2+/ER+ and HER2+ER- patients who developed distant disease. Data in bold indicates different metastatic frequencies between subtypes HER2+ disease. Data derived from Metastatic Behavior of Breast Cancer Subtypes, ©Hagen Kennecke et al. 2010. Originally published in Journal of Clinical Oncology 2010 July 28:3271-7.

There was increased interest in the research and pharmacology fields to develop new targeted therapeutic agents against HER2 following the success of trastuzumab. Targeting the kinase function of HER2 with small molecule TKIs proved another successful strategy, leading to the development of lapatinib (Tykerb), afatinib (Gilotrif), and neratinib (Figure 1.6). Lapatinib was FDA approved as part of a combination therapy with capecitabine as a second line therapy for patients who had progressed on trastuzumab. In this context lapatinib significantly improved disease progression over chemotherapy alone, but failed to improve overall survival [161].

Clinical use of trastuzumab turned the deadliest subtype of breast cancer into one of the most manageable, but it is by no means a cure. Firstly, less than 50% patients responded to treatment, showing *de novo* resistance. This demonstrates significant heterogeneity within the HER2+ subtype. Additionally, over 40% of patients that initially responded to HER2 targeted drugs developed acquired resistance and progressed under treatment, resulting in only slight improvement on overall survival [162, 163]. There has been a concerted effort in oncogenic pharmacology to develop new and ever more effective strategies to both inhibit HER2 and overcome mechanisms of resistance. Multiple agents employ a similar approach to trastuzumab, using monoclonal antibody binding to HER2-specific epitopes to either interfere with activity, introduce a conjugated drug, or engage the immune system. Trastuzumab both interferes with HER2 activity and activates the immune system to target HER2 overexpressing cells, but the more recent FDA-approved agent from Genentech trastuzmab emtansine (TDM-1, Kadcyla), adds to this by conjugating a cytotoxic agent. Interestingly, while trastuzumab does not appear to be internalized upon binding to HER2 [164], TDM-1 is internalized, allowing for the delivery of the conjugated emtansine to the cell, resulting in cell death. TDM-1 is one of a new class of targeted agents called antibody-drug conjugates (ADCs). MM-302 from Merrimack is another ADC that recently made it to phase II clinical trials before being halted due to lack of improvement over trastuzumab [165]. NewVax from GalenaBiopharma is a peptide vaccine that mimics HER2 to engage the immune system against HER2 overexpressing cells following standard of care treatment to prevent recurrence, and is entering phase III

trials. Margetuximab from Macrogenics is another HER2 targeting mAb, which improves on trastuzumab in terms of specificity, and is currently in phase III clinical trials. And finally, pertuzumab (Perjeta) is a FDA-approved antibody drug from Genentech that acts specifically to interfere with HER2 dimerization with HER3, EGFR, or other HER2 receptors by binding to domain II of HER2 (Figure 1.6). Pertuzumab has been found to improve survival in combination with trastuzumab in clinical trials [166]. Chapter 4 will discuss that the chief mode of pertuzumab in combination with HER2 TKIs may be in abrogating HER3 mediated resistance mechanisms.

In addition to antibody drugs, small molecule TKI agents that specifically inhibit HER2 kinase activity have shown great promise in both research and clinical settings including lapatinib, afatinib, and neratinib. The mode of action of each of these TKIs is competitive inhibition of the ATP-binding pocket on the tyrosine kinase domain, however they differ significantly in both specificity and binding affinity. Bindings of these TKIs to HER2 typically results in either apoptosis or inhibition of proliferation.

Afatinib is a dual kinase inhibitor, targeting both HER2 and EGFR, and is FDA-approved for use in non-small cell lung carcinoma (NSCLC), and is additionally in phase III trials for breast cancer. Afatinib binds covalently to its targets, classifying it as an 'irreversible' inhibitor [167]. Lapatinib is also a dual inhibitor of EGFR and HER2, however it is a 'reversible' inhibitor that does not form a covalent bond with its binding target. Lapatinib has been FDA approved for breast cancer patients already receiving capecetabine (Xeloda), but has also shown benefit for patients receiving trastuzumab [168]. This makes lapatinib a very promising agent for clinical treatment of HER2+ breast cancer. However, because drug resistance remains a persistent problem in this agent as well, much of this thesis will focus mechanisms of resistance to lapatinib.

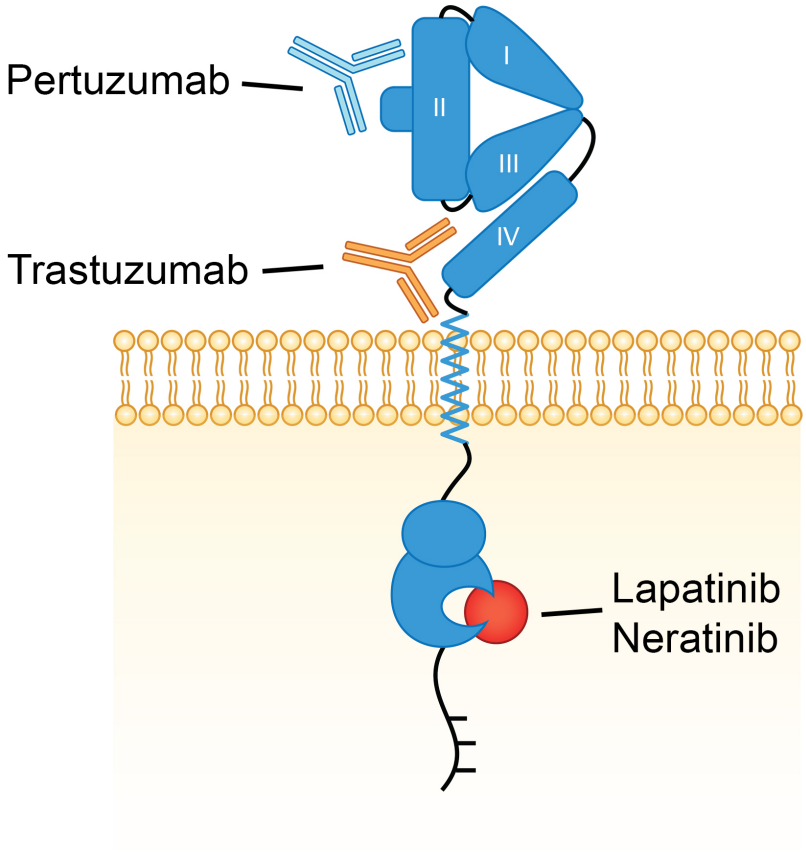

Figure 1.6. Binding sites of targeted inhibitory agents against HER2. Graphic depicts binding sites on the HER2 protein for inhibitory agents that target ECDs (pertuzumab and trastuzumab), and the cytoplasmic tyrosine kinase (lapatinib and neratinib). Figure adapted from ©Baselga & Swain, 2016, originally published in Nature Reviews Cancer July 2009, 9:463-475.

Other agents have attempted to improve on the efficacy of lapatinib. Neratinib is an irreversible HER2/EGFR TKI like afatanib, however unlike afatainib and lapatinib it is more specific to HER2, and is a much more potent inhibitor [169]. Puma Biotechnology entered neratinib in phase III trials for HER2+ breast cancer treatment [170], but it was found to show no additional benefit over trastuzumab, and was plagued by issues of severe diarrhea in patients. However, more recent promising results from the ExteNET phase III clinical trial has spurred the FDA's Oncologic Drug Advisory Committee to recommend FDA approval of neratinib (Nerlynx), with a final decision expected in 2017. Additionally, large high throughput screening studies from the lab of Kevan Shokat have identified additional new agents that can engage in state-agnostic kinase binding, which seeks to bypass the issue with lapatinib's ATP-pocket accessibility discussed previously [99]. However, agents such as these that may counter mechanisms of HER2 targeted drug resistance are not yet available in the clinic.

Despite promising results from several new and existing agents, clinical use of HER2 targeted therapeutics still faces the persistent problem of both *de novo* and acquired resistance. The difference in responses between patients suggests extensive heterogeneity between the tumors of HER2+ patients. A more nuanced understanding of intratumoral heterogeneity and phenotypic characterization may help us better identify which treatments are best suited for each patient.

1.6. Cell State Phenotype and Determination in Breast Cancer Cells

The 4 classical subtypes of breast cancer do not represent homogenous diseases. Instead, nearly all of the cell states within the normal mammary epithelial lineage are found in varying degrees within the tumors of each subtypes [44]. Luminal A and Luminal B tend to consist of largely luminal and luminal-progenitor phenotypes, while TN and HER2+ are mostly basal lineage phenotypes. In general, these tumor cells are simulacrums of normal mammary cell types, typically referred to as 'luminal-like', 'basal-like', 'mesenchymal-like' or 'progenitor-like'. Most of the phenotypes seen in the epithelial lineage are

recapitulated to some extent in breast cancer phenotypes, but identification of true breast cancer stem cells similar to MaSCs in tumors is still controversial.

Histological determination of cellular phenotype in breast tumors relies on the cell state markers discussed in a previous section. Cells in the luminal branch of the mammary lineage hierarchy are defined by their expression of cytokeratins KRT8, KRT18, KRT19, the hormone receptors ER and AR, and the vitamin receptor VDR [51]. Cells in the mammary lineage are defined by expression of KRT5, KRT14, SMA, CD10, and p63 [51]. Mesenchymal-like phenotypes are identified by their expression of vimentin [171]. In addition to these, markers of stemness can help define the cells similarity to progenitor or mature mammary cell states, such as CD24, CD44, and ALDH1 [172, 173]. However, markers and histology offer only a partial description of cancer cell phenotypes within tumors, and don't provide adequate information to infer relatedness to normal mammary cell types. Here, 'omic' approaches to describing cancer cell phenotype can provide a more robust portrait of tumors, and find commonalities between heterogeneous phenotypic cell states to better identify breast cancer subtypes.

The advent of cDNA microarrays allowed Charles Perou et al. to investigate differences in gene expression profiles both within and between different breast cancer instances [43]. They analyzed mRNA expression patterns of 42 resected breast tumors and performed hierarchal cluster analysis on the resulting data. Twenty-two of their samples had matched samples, meaning they were different samples taken from the same tumor. This allowed them look for genes expressed in all samples that had more variable expression between different tumors than they had between matched samples. Genes that met these criteria were then included in what was called the intrinsic gene subset. Cluster analysis of the 42 samples with the 'intrinsic' gene set grouped the tumor samples into 5 subtypes; Luminal-like (further broken down into Luminal A and Luminal B), Basal-like, Normal Breast-like (NBL), Claudin-low, and HER2-enriched (HER2E) [174]. This nomenclature denotes the similarity each subtype has to the expression profile of a normal mammary cell type. An important note was how closely the HER2E subtype clustered with

the basal-like subtype, expressing many basal-linked genes [43]. Interestingly, basal-like tumors expression profiles had a lot of similarity with luminal progenitor cells [175], and remarkably the expression profile HER2E cells did not match up with any normal mammary cell type [46].

This intrinsic molecular subtyping of breast cancer was found to be predictive of patient outcome, and response to treatment, providing a much more robust classification than classical immunohistochemistry and the use of just ER, PR, HER2, and Ki67 [154, 176]. Other gene sets were developed from the differential expression between the intrinsic subtypes, including proprietary signatures meant for clinical application, and the PAM50 assay. The PAM50 assay is a 50 gene qPCR assay that uses RNA extracted from FFPE, that was found to be predicative of relapse risk in breast cancer patients [177]. This later became the Prosigna Breast Cancer Predictive Gene Signature Assay provided by NanoString for clinical use.

Comparisons between intrinsic molecular subtypes and classical clinical subtypes revealed extensive heterogeneity within the 4 clinical subtypes [44]. How this impacts the classification of the HER2+ will be discussed in more detail later.

TCGA perfromed an even more comprehensive omic characterization of breast cancers [46]. They performed multi-parametric analytics on tumor samples from 825 patients; including RNAseq, Copy Number Analysis (CNA), DNA methylation analysis, whole-exome sequencing, microRNA sequencing, and Reverse Phase Protein Analysis (RPPA). These studies revealed additional heterogeneity within the molecular subtypes, suggesting the possibility that some subtypes were themselves comprised of multiple discrete subtypes. In particular, they performed important comparisons between molecular and classical determination of subtypes for patients with clinically assessed HER2+ tumors, identifying two unique subtypes. These HER2+ subtypes are the subject of Chapters 3 and 4.

1.6.1. *Sources of breast carcinoma phenotypic heterogeneity*

Phenotypic heterogeneity observed within and between tumors, along with the similarity of some molecular subtypes to normal mammary cells, raises the question if cancer cell phenotype is related to the initial cell type that underwent oncogenic transformation. It's possible that tumors with high intratumoral heterogeneity may have arisen from multipotent progenitor cells, or that luminal and basal cancers arose from those respective progenitors, and carry with them many of the same phenotypic traits, such as motility, proliferative rate, response to specific growth factors, and expression of ER/PR. There are currently competing theories to explain the phenotypic heterogeneity of cancer cells; the idea of 'cell of origin' or 'mutation of origin'.

To briefly summarize; the theory of 'mutation of origin' is that all breast cancers arise from a multipotent progenitor cell, and the transforming mutation or genomic aberration dictates the lineage path the cell follows. There is evidence supporting the idea that mutations can determine cellular phenotype in studies with PIK3CA mutations in breast cancer mouse models. In one study, introduction of the H1047R helical domain mutation in the gene for PI3K resulted in basal-like cancer cells expressing luminal markers, and introduction into luminal-like cells resulted in expression of basal markers [178, 179]. Conversely, the similarity of intrinsic molecular subtype expression profiles to those of normal mammary cells is strong evidence for the 'cell of origin' theory. Luminal-like cancer signatures were determined to be most similar to those of luminal epithelial cells [175], and Claudin-low signatures overlaped with post-EMT luminal cells [180].

Like many concepts in cancer, the driver of cancer cell phenotype is most likely not strictly 'cell of origin' or 'mutation of origin', but a hybrid of the two. Cell of origin, driver and secondary mutations, and the selective pressures of the tumor environment all influence cancer cell state. Additionally, cancer cell phenotypes are highly plastic, rather than defined immutable states, especially in the case of basal-

like cells. Multiple mechanisms have been identified that allow cancer cells to move in essentially any direction on the lineage tree to best suit their growth requirements [60, 181-185].

There are generally two ways for mammary cancer cells to switch between phenotypes; they can de-differentiate to a more stem-like state to regain multipotency, or they can trans-differentiate directly from one terminally differentiated state to another. Prime examples of de-differentiation to precursor states are cellular responses to drug treatment and EMT. Breast cancer cell lines have been found to take on bipotent stem-like states in response to cisplatin treatment, expressing progenitor markers and giving rise new ratios of cell states [181]. Drug treatment or signals from the tumor microenvironment can also trigger EMT in luminal-like cancer cells, and from this mesenchymal state the cells can give rise to luminal-like, basal-like, or Claudin-low cell states [60, 182, 183]. In contrast, juxtacrine signaling from protocadherins like FAT4 on neighboring cells or mechanotransduction from stiff ECM environments can activate the hippo pathway and induce the nuclear localization of TAZ/YAP, which works in concert with SWI/SNF chromatin remodeling complexes to cause the direct trans-differentiation from luminal-like to basal-like phenotypes [184, 185].

How subtypes of cancer obtain or maintain the mixture of cell phenotypes that allow them to progress has major implications on potential new treatments. Proper identification of cell state phenotype can also aid in the identification of tumor cell populations that are resistant or responsive to specific targeted agents. The next section will discuss how phenotypic heterogeneity within the HER2+ subtype may be the result of distinct subgroups within the clinical HER2+ classification, and Chapter 3 will discuss how these new subtypes have unique drug sensitivities.

1.7. HER2+ Phenotypic Subtypes by Cell State Markers and Transcriptomics

Some differences in cell state phenotypic contributions are so penetrant between tumors that they represent not heterogeneity, but unique and divergent subtypes, and this may be the case with the HER2+ subtype. As previously discussed, TCGA compared the clinical and molecular classification of HER2+ patient tumor samples. They determined that tumors clinically classified as HER2+ did not all correspond with their molecular HER2E PAM50 gene signature [61]. Instead, they found one subgroup of HER2+ expressed the HER2E gene signature, and these clustered closely with basal-like cancers [61]. The other HER2+ subgroup did not express the HER2E gene signature, and these were found to cluster more closely with luminal-like tumors [61]. In comparing the gene expression profiles and RPPA data between these two HER2+ subgroups they found 302 significantly differentially expressed genes, and 36 differentially expressed proteins. This led them term these subgroups HER2E (basal-like), and Luminal-HER2+ (luminal-like), which were all classified as just HER2+ by clinical classification.

In addition to protein and transcriptomic differences, TCGA determined that the two subtypes of HER2+ significantly differed in terms of common somatic mutations. Mutations in *TP53* were found to be enriched HER2E tumors, while *GATA3* mutations were enriched in L-HER2+. It should be noted that this was found in supervised clustering using either gene expression profile or ER status to define the classifications. The variance in mutations and gene expression within the subtypes leaves open the possibility that there are still more specific subtypes within HER2E and L-HER2+.

The closest clinical sub-classification of HER2+ breast cancers that correlates with HER2E and Luminal-HER2+ (L-HER2+) classifications is stratification by ER status. Few clinical studies have contrasted hormone receptor positivity with drug response and outcome in studies of HER2+ patients, but these studies did conclude that ER and PR status in patients was predictive of response to chemotherapy, lapatinib, pertuzumab, and trastuzumab [186-188].

These studies have not yielded new guidelines for patient treatments, and sub-classifying HER2+ by hormone receptor status is not universally accepted or utilized in treatment. The recommended standard of care treatment for HER2+ breast carcinomas remains the same for patients regardless of their ER status, with the occasional exception of including tamoxifen regimens for ER+ patients. However, this is starting to change [189].

Very recently, clinicians have begun to find that response to treatment in HER2+ patients correlates with subtypes of HER2+. Edith Perez et al. used the Prosigna algorithm (PAM50) to stratify clinically identified HER2+ patients from the NCCTG (Alliance) N9831 trial as either HER2E, basal-like, or luminal-like, and found that luminal-like and HER2E patients had significantly better responses to the combination of trastuzumab and chemotherapy than basal-like tumors [189]. Their findings are indicative of the recent shift towards treating HER2+ breast cancer as multiple different diseases, rather than a single heterogeneous disease.

While there may be some momentum towards stratifying HER2+ as a disease, or at least better characterizing cancers that can overexpress HER2, how HER2+ subtypes differ biologically remains largely unknown. How these subtypes differ in terms of intracellular signaling, response to HER2 targeted drug treatment, and interaction with the tumor microenvironment will be discussed in detail in Chapters 3 and 4. Below is an overview of the varying known mechanisms that can result in resistance to treatment in the HER2+ subtypes.

1.8. Intrinsic Mechanisms of Drug Resistance

All HER2 targeted therapies disrupt the first step in a pathway that leads to hyper-proliferation. However, dozens of steps follow in the signaling cascade stimulated by HER2, and so activating mutations or aberrations in these pathway components can trigger drug resistance. Factors that influence these cascades

can arise from within the cell, as well as from the surrounding environment; referred to as 'cell intrinsic' and 'cell extrinsic' respectively. I will highlight several important mechanisms that influence response to HER2 targeted therapies.

ERBB2 amplification is by far the most common method by which HER2 signaling becomes hyper-activated, but *ERBB2* activating mutations can also be transforming in the absence of amplification [143]. The lack of HER2 overexpression in these cases may render ineffective agents that only use HER2 overexpression as a target for drug delivery (such as ADCs), and do not specifically interfere with HER2 activity. These activating mutations are most frequently found in the kinase domain, and the mutations G309A, D769H, D769Y, V777L, P780ins, V842I and R896C have all been found to be oncogenic in the absence of *ERBB2* amplification [143]. However, these mutations are rare, occurring in about 2% of breast cancer patients, and only 1.4% of HER2+ patients [145]. The HER2 pathway can also become hyper-activated in the absence of HER2 overexpression or mutation by enhanced autocrine secretion of the HER3 ligand NRG1, which causes enhanced stabilization of endogenous HER2-HER3 heterodimers [144].

Despite instances of mutations in the absence of overexpression, the most pernicious mutations act in conjunction with overexpression. Mutations such as L755S in HER2 are not transformative themselves, but their presence in conjunction with overexpression has been linked to lapatinib resistance in patients and cell lines [143, 190]. L755s is a kinase domain mutation that lowers the binding affinity of reversible inhibitors such as lapatinib, but this can be overcome with irreversible HER2 TKIs such as neratinib [143, 190]. Similar activating HER2 mutations have also been identified in other cancers, such as lung adenocarcinomas [191]. Post translation HER2 modifications can also result in drug resistance [88-192]. The Δ16 splice variant of HER2 is a post translational aberration which omits exon 16 of HER2, resulting in a HER2 protein variant that can easily homodimerize, causing enhanced oncogenic capacity and resistance to trastuzumab [88]. p95-HER2 is another HER2 splice variant that is truncated so that it lacks the extracellular antibody epitope sites of all existing HER2 targeting antibody drugs [193]. p95-HER2 is a far

more common alteration than somatic HER2 mutations, observed in about 25% of HER2+ tumors. Because it lacks the epitope recognized by antibody based drugs, p95-HER2 tumors show better response to lapatinib compared to trastuzumab [192].

There are several steps in the downstream mitogenic cascade that can harbor an activating secondary mutation, rendering agents targeting HER2 largely ineffective. Common genes with activating mutations in breast cancer (as well as lung and colorectal cancers) that bypass HER2 inhibition include *BRAF*, *KRAS*, *PIK3CA*. Loss of PTEN also reduces the effectiveness of HER2 targeted drugs. As discussed previously, phosphorylation of c-terminal tyrosine residues on EGFR or the 1221/1222 tyrosine on HER2 (which would normally be inhibited by HER2 targeted TKIs) stimulates RAS on the plasma membrane to activate RAF, so oncogenic mutations in *KRAS* or *BRAF* can bypass this point of regulation and maintain MAPK signaling in the presence of drug treatment [194, 195]. Activating mutations in the PI3K coding gene *PIK3CA*, such as the common H1047R mutations, have been linked to resistance to both trastuzumab and lapatinib [196], as has loss of the PI3K antagonist phosphatase PTEN [197, 198]. These mutations can maintain activity of the AKT/mTORC pathway in the presence of HER2 inhibitory drugs.

The above are all largely examples of *de novo* resistance, rather than a response to drug treatment or acquired resistance. Perhaps the most common form of acquired resistance is 'adaptive' resistance, where regulatory networks are buffered to abrogate loss of any one part of signaling cascades. The levels of activated proteins in cell signaling cascades normally exist under a range of regulatory mechanisms that maintain homeostasis through positive and negative feedback loops, mechanisms that become adjusted to heightened levels of mitogenic proteins in oncogene-addicted cells. Two illustrative examples are AKT and HER3. When pAKT levels fall as the result of lapatinib treatment inhibiting PI3K, the pathway responds with reduced activation of IRS-1 which normally inhibits PI3K, increasing activity to restore levels of pAKT [199]. This causes a rebound in pAKT levels following initial inhibition under lapatinib treatment in breast cancer cells, but other mechanisms also may be at play [200]. The decrease of pAKT and

downstream mTORC activity has been shown to increase transcription factor binding (such as FOXO1 and FOXO3) resulting in the increased expression of a range of RTKs such as HER3, Insulin-Like Growth Factor 1 Receptor (IGF-1R), and MET, that have the potential to restore AKT/mTOR or MAPK pathway activity under lapatinib treatment [201].

Another prevalent form of cell intrinsic drug resistance involves the expression of mitogenic RTKs, that can differ between cancer cell types. Additionally, cancer cell types can differ in their propensity to signal through different signaling cascades, such as STAT, mTORC, or MAPK. Because of this, responses to drugs targeting specific RTKs or signaling cascades are heterogeneous. How this pertains to HER2+ breast cancer is discussed in detail in Chapters 3 and 4.

Epigenomic feedback responses are another form of adaptive resistance that upregulate a large range of RTKs. This effect is termed kinome adaptation, and is a prime example of 'acquired' resistance [202]. Kinome adaptation is similar to adaptive resistance in that it is a direct response to loss of part of a signaling cascade. However, it involves more enduring epigenomic alterations and chromatin remodeling [202]. This results in a slower response, but one that persists even after the inhibited signaling pathways have been restored. In a study by Gary Johnson et al., HER2+ cell lines were treated with lapatinib, and RNAseq was used to assess changes in kinase expression for the fraction of the kinome present [202]. Several compensatory kinases were found to be significantly upregulated in response to treatment, including MET, DDR1, FGFRs, and IGF-1R [202]. An important note is that adaptive and acquired resistance are not mutually exclusive mechanisms. Instead they can be viewed as a two-step response to treatment where adaptive responses are the first line of defense, and acquired resistance is the fall back if loss of signaling endures.

These compensatory receptor kinases rely on paracrine signaling ligands from the tumor stroma, and so represent an interplay between intrinsic drug response, and the cell extrinsic microenvironment. Stromal

derived compensatory signals that aid in bypassing points of pathway inhibition are one of the many ways the cell extrinsic tumor microenvironment can provide drug resistance to cells that would otherwise be responsive to treatment.

1.9. The Tumor Microenvironment and Drug Resistance

Tumor characteristics may differ widely between patients, and between metastatic sites within a patient. Even within a single tumor there are extensive intratumoral differences in vascularization, immune infiltrate, genomically distinct sub clonal populations, and cancer cell phenotypes. In addition, the tumors reside in a highly variable and evolving microenvironment. This environmental context that determines which cancer cell mutations and phenotypes confer the greatest fitness advantage, providing selective pressure for the most resilient cancer phenotypes. In addition to being influenced by their environments, tumors can also disrupt and remodel it to aid in progression. Understanding this two-way communication between the tumor and its microenvironment is crucial to improving treatments, largely because these interactions have the potential to protect tumors from therapy, and cause treatments to accelerate progression.

***

The study of the tumor microenvironement began with early observations of tumor metastasis by Ernst Fuchs in 1882 and Stephen Paget, who is thought of as the conceptual father of the field due to his well-known “seed and soil” theory presented in 1889 [203]. They proposed that metastatic disease is not solely driven by the cancers cells, the ‘seed’, but that there must be aspects of the local non-tumor environment, the ‘soil’, that pre-disposes a tissue to supporting metastatic colonization. Early research in the field largely focused on immunology and tumor angiogenesis. This research clearly demonstrated that modification of the tumor microenvironment was an essential step in cancer progression [204-207]. Since the

1980s this field has greatly expanded to encompass a range of biologic disciplines, with ever increasing interconnectedness. Here I will present a brief overview of the major microenvironment factors that have been implicated in therapeutic resistance in breast cancer, and how these may differ between primary and metastatic anatomical locations. These factors can be generalized as:

I. The extracellular matrix
II. Stromal fibroblasts
III. Immune cell infiltrate
IV. Vascularization and hypoxia

The ECM surrounding mammary ducts is normally composed of two layers; the basement membrane, and the interstitial ECM. The basement membrane surrounds the mammary duct, is in direct contact with myoepithelial cells, and is comprised largely of collagen IV, laminins, nidogen, and perlecan which are produced and secreted by both the myoepithelial cells and the stromal fibroblasts [208]. The interstitial ECM resides between the basement and the surrounding stroma; it is comprised of collagens I, III, and V, as well as fibronectin, decorin, and biglycan, that are all produced and secreted by stromal fibroblasts. These ECM structures support the tissue organization of the duct, and serve as a barrier to the invasion of ductal carcinoma in situ (DCIS) into the surrounding tissue. Disruption of the surrounding ECM is an important step in cancer progression, and this remodeling can have further consequences on drug sensitivity.

One of the first events in ECM remodeling that can cause resistance to targeted treatments involves the release of growth factors bound to the ECM [209]. Secreted factors can bind to and be sequestered by the ECM, either in active or pro-forms. Enhanced production of proteases in and around tumors, such as Matrix Metalloproteases (MMP) 7 and 9, not only degrades ECM structures, but also releases bound

growth factors that can activate RTKs on cancer cells that overcome the effects of targeted therapeutics [209]. ECM stiffness has also been shown to influence drug sensitivity [210-212]. Enhanced secretion of fibronectin, hyaluronan, and laminins in the tumor microenvironment increases the stiffness of ECM networks, which hyper-activates the integrins that bind to laminins and collagen I leading to activation of Focal Adhesion Kinase (FAK) complexes which can in turn activate the PI3K and MAPK pathways to overcome drug treatment [210, 211]. This stiffness is also called the elasticity modulus of a tissue, and has been found to vary widely between the mammary duct and common sites of breast cancer metastasis; the lung being one of the least stiff, and bone being the most [211, 212]. Mina Bissel et al. found that HER2+ cell lines grown in matrigel, which is a 3D heterogeneous mixture of basement membrane proteins, were far more resistant to lapatinib than cells grown in normal tissue culture conditions, and that this could be ablated by knockdown of the collagen binding integrin-β1.

Stromal fibroblasts produce paracrine signals that can cause inflammation, motility, and even cancer progression and drug resistance. These factors are produced when breast tumors recruit and reprogram fibroblasts into CAFs. Over 80% of fibroblasts in breast cancer are reported to have a CAF phenotype [213]. The process of CAF reprogramming is usually thought of as a two-step process, where normally quiescent fibroblasts are activated by inflammatory cytokines, hypoxia, or growth factors like TGF-βs to become wound healing or 'normal-activated fibroblasts' (NAFs). As these signals never abate, cancer can be considered 'the wound that never heals'. This persistent activation eventually drives NAFs to undergo permanent epigenetic remodeling that drive them into a CAF phenotype, which in turn drives the high expression of ECM proteins such as collagens, tenascin C, ICAM1. Additionally, the NAF cells can express a range of MMPs that can release bound growth factors from the ECM [214]. Finally, fibroblast activation in breast, lung, skin, and liver cancers (to name a few) has been reported to result in the direct overexpression and secretion of a range of growth factors that can cause tumor progression and drug resistance such as IGFs, FGFs, IL-6, HGF, and NRG1 [69, 215, 216].

Infiltrating immune cells comprise another important cellular component of the tumor microenvironment. The normal role of immune cells in tumors, CD8+ cytotoxic T-cells in particular, is to recognize neo-antigens on cancer cells and trigger their elimination. However, factors secreted by cancer cells and CAFs, such as the chemokine CCL2, can protect tumors from immune-surveillance via the recruitment of immunosuppressive Myloid Derived Suppressive Cells (MDSCs) [217, 218]. The term MDSC is a catch-all phrase for cells of a myeloid lineage that share a commonality in suppressing immune surveillance, rather than a defined cell type. Tumor derived factors such as GM-CSF, SCF, and VEGF, along with CAF derived factors like IL-6, IL-10, and IL-1β, can stimulate the activation and proliferation of granulocytic precursors into granulocytic and monocytic MDSCs [219]. MDSCs can regulate levels of reactive oxygen species (ROS), nitric oxide (NO), L-arginine, and L-cysteine in the tumor microenvironment which negatively influence T-cell proliferation following antigen stimulation, suppressing the immune response [220]. They have also been reported to suppress T-cell function via activation of CD4+ T-regulatory cells (T-regs) [221]. As previously stated, part of the mode of action for trastuzumab is to engage the immune system against HER2 overexpressing cells, however T-cell suppression by MDSCs can limit the effectiveness of this mechanism.

Tumors can also recruit and corrupt normally suppressive cells to aid in cancer progression, such is the case with tumor associated macrophages (TAMs). Macrophages recruited to the tumor environment are educated by the local cytokine landscape to take on a number of roles. TAMs that take on a pro-inflammatory, or M1, phenotype can increase immune surveillance and aid in therapeutic response [222]. However, TAMs that take on an anti-inflammatory, or M2, phenotype can instead promote tumor growth by secreting growth factors and suppressing immune surveillance [223]. TAMs can block CD-8+ T-cell proliferation and activity indirectly by activating T-regs via TGF-β1 signaling [224], that can then inactivate CD-8+ T-cells via juxtacrine signaling through cytotoxic T-lymphocyte-associated protein 4 (CTLA-4) [225]. M2 TAMs can also inactivate T-cells directly by expressing the cell surface protein, Programmed Cell

Death Ligand-1 (PD-L1), that signals through the receptor PD-1 on T-cells to block their proliferation and activation [226].

Studies by Lisa Coussens et al. demonstrated that secretion of IL-10, which is elevated in TAMs, results in decreased IL-12 expression in breast tumor dendritic cells, and that this in turn inhibits CD8+ T-cell dependent responses to the chemotherapeutic drug paclitaxel [227, 228]. Additionally, recruitment and proliferation of TAMs was shown to be blocked by targeted inhibition of CSF-1R, the receptor for the tumor-derived factor CSF-1 [229].

Targeted treatment against these immune checkpoint blockades to improve response to chemotherapy has shown promising results, but faces many additional challenges. Cell death induced by cytotoxic treatment triggers the release of large amounts of adenosine (ATP and ADP) into the tumor microenvironment, which increases cancer cell proliferation and migration by signaling through puragenic receptors ($P2X_7Rs$) [230], and by signaling through the adenosine receptor A2AR in myloid cells to promote the M2 TAM phenotype [231], and inhibit CD-8+ T-cell activity [232].

The presence, contribution, and distribution of MDSCs, TAMs, T-regs, and other myloid lineages in the tumor microenvironment vary greatly between different metastatic sites, and so may determine localized responses to targeted therapy [233]. Additionally, because of the vital role of the immune system in both cancer progression and response to treatment, targeted therapies against immune checkpoint blockade such as ipilumumab (anti-CTLA4), and atezolizumab (anti-PD-L1), and new agents against A2AR are showing impressive efficacy in combination with chemotherapy. This raises the possibility that checkpoint inhibitors may increase the efficacy of HER2+ targeting drugs that engage the immune system, such as trastuzumab.

The final feature of the tumor microenvironment addressed here is an amalgamation of several different features that affect the availability and localization of oxygen and nutrients. Neoangiogenesis and tumor vascularization are vital interactions with the microenvironment that a tumor must facilitate in order to progress. However, unlike tissue vascularization following would healing, angiogenesis in cancer is abnormal and poorly regulated, resulting in 'leaky' vascular networks [234]. Mechanisms that result in abnormal vascularization include heightened concentration of VEGF, and dysregulation of MMP14, TGF-β1, or ALK5 [235, 236]. Additionally, because there are often poor lymphatic structures to drain the tumor, more fluid enters the tumor than leaves it, resulting in high interstitial pressure. High interstitial pressure and abnormal tumor vascularization can cause drug resistance by impeding drug delivery to large parts of the tumor [237]. This can also impede nutrient availability, driving cells into a non-proliferative quiescent state that, protects them during treatment so they can later reenter a proliferative state when vascularization progresses [238].

Incomplete vascularization of the tumor, along with high interstitial pressure, can also result in poor oxygen availability throughout the tumor; referred to as hypoxia. Hypoxia results in a range of responses in the tumor microenvironment, such as the secretion of VEGF from tumor cells, and increased adenosine levels released from necrotic cells. The best-studied effect hypoxia has on drug resistance is its stimulation and activation of the transcription factor hypoxia-induced factor 1 (HIF-1) in cancer cells. HIF-1 is a heterodimeric protein made of two constituents; HIF-1α and HIF1β. Stimulation of HIF-1 by hypoxia to translocate from the cytoplasm to the nucleus increases the transcription of genes involved in angiogenesis, glycolysis, and expression of growth factors such as IGF-2, TGF-α, TGF-β3, and IGF-BP2 to bypass the effects of targeted therapeutics [239]. This also activates MAPK signaling (via ERK), resulting in drug resistance to lapatinib in HER2+ cells [240, 241].

The key points of this overview of tumor microenvironment mediated drug resistance are as follows. First, it involves a broad range of competing, additive, and synergistic influences on both tumor cells and

the surround stroma. Second, with the exception of mechanical effects like ECM stiffness and interstitial fluid pressure, almost all of the mechanisms that influence drug resistance are mediated by cancer cell extrinisic signaling proteins. Juxtracrine signals are mediated through signals conveyed by ECM and cell adhesion proteins like collagen IV, nidogen, E-cadherin, and Notch. Paracrine signals are conveyed by growth factors, chemokines, and cytokines, such as EGF, NRG1, SDF-1, IL-6, and IL-10. While much of the intercellular communication in the tumor microenvironment is difficult to model, it is possible to learn a great deal about how these interactions influence drug resistance by focusing specifically on how the extrinsic paracrine and juxtacrine signals from the microenvironment can influence cancer cell response to targeted therapy.

1.10. Thesis Overview

Breast cancer is a devastating and unfortunately common disease. In 2017 it is estimated that there will be 252,710 new instances of invasive breast cancer in the U.S. alone [242]. Despite recent advances in treatment, the American Cancer Institute still projects over 40,000 deaths as the result of breast cancer for 2017. Much of the difficulty in treating breast cancer comes from the huge range of diversity in terms of mutations, phenotypes, and the intratumoral heterogeneity of both. Classifying tumors by their defining characteristics has greatly aided clinicians in identifying which subtypes respond best to available therapies, and over the past 4 decades has helped to improve patient outcomes. Clinical classification based on ER/PR/HER2 markers, along with the more recent advances in intrinsic molecular subtyping, has facilitated the use of targeted therapies specific to their biology, exemplified by the use trastuzumab and lapatinib against HER2+ breast cancer.

However, targeted therapies in HER2+ cancers typically represent only a modest improvement in overall outcome, and so are by no means a cure. The lack of efficacy in terms of long term survival has been attributed to both acquired and *de novo* resistance to targeted drugs. Outlined above are some of the most

well researched mechanisms employed by HER2+ cancer cells to bypass these agents on their own, as well as cell extrinsic influences the tumor microenvironment can provide to protect drug sensitive tumors from treatment. An important commonality in cell extrinsic protective mechanisms against HER2 targeted therapeutics reviewed above is that they rely on cellular communication, and the use of paracrine and juxtacrine signaling proteins to elicit drug resistance in cancer cells. The biggest obstacles to targeting these signals to restore sensitivity is that the exact signal combinations driving resistance *in vivo* are largely unknown, and how different cancer cell types respond to these signals remains under-researched.

A single tumor can be comprised of a range of cancer cell phenotypes, and each of these phenotypes can mirror how different cell types in the mammary lineage respond to extrinsic signals. Acquisition and maintenance of these phenotypes can depend on a complicated combination of factors, including their driving mutations, and their cell type of origin. The HER2+ subtype in particular has been found to be heterogeneous in terms of basal and luminal expression patterns, leading some researchers and clinicians to suggest that these represent biologically distinct subtypes of HER2+ breast cancer.

We interrogated how these HER2+ subtypes respond to the large range of potential signals in the tumor microenvironment, and how they might be differentially protected from HER2 targeted treatments by modeling this complexity in a high-throughput cell-array assay utilizing a panel of HER2+ breast cancer cell lines and a library of human ECM and paracrine signaling proteins. Each of the cell lines in the panel have been extensively characterized by multiple omic techniques, and reliably recapitulate a range of the phenotypic heterogeneity found in patients. The human protein library we designed also recapitulates much of protein landscape of different primary and metastatic tumor environments. Chapters 2 and 3 will detail the project to screen representative HER2+ cell lines across more 2500 combinations of protein signals under lapatinib treatment, and how differential response to NRG1β and HGF is intrinsic to the luminal and basal subtypes of HER2+ breast cancer.

These studies, along with supporting evidence presented in Chapter 4, detail how an interplay of heterogeneity within the HER2+ breast cancer subtype, and influences of the tumor microenvironment combine to create the potential for anatomic-site specific resistance to HER2 targeted therapies. Specifically, data from TCGA revealed that there exist at least two sub-categories of HER2+ tumors; basal-like, and luminal-like. This thesis will demonstrate how these two subtypes are biologically distinct in terms of drug response, phenotype, pathway utilization, and response to specific factors in the microenvironment that can cause resistance to HER2 targeted agents lapatinib and neratinib.

Chapter 2. The MicroEnvironment MicroArray

This work includes studies planned for submission to Nature Methods in 2017

2.1. Experimental Summary and Workflow

Our primary goal in studying microenvironment mediated mechanisms of drug resistance was to find specific and actionable molecular mechanisms that could be targeted to improve drug sensitivity in cancer cells. These mechanisms are often difficult to precisely identify within the signaling milieu to which cancer cells are exposed in *in vivo* cancer models, and traditional cell culture assays do not have enough throughput to interrogate all the potential signaling combinations. We developed a cell-spot imaging assay approach to address these obstacles that was both high-throughput to accommodate the large range of signals involved, but also reductionist so that specific signals or simple combinations of signals that cause drug resistance could be identified. This platform was termed the MicroEnvironment MicroArray (MEMA) (Figure 2.1). This section serves as both a detailed description of the method, as well as an explanation and justification for the platform design.

The MEMA technique was based on the work of Mark LaBarge et al. [243], and Juha Rantala et al. [244]. They each developed cell-spot assays that involved printing material onto a solid surface that could serve as micrometer scaled growth pads. Proteins combinations (such as matrigel) were printed with robotic contact-printers (of the type typically employed for printing DNA/RNA microarrays) onto surfaces treated so as to be either hydrophobic, or resistant to cell adhesion [243, 244]. Robotic printing created defined arrays of 200-400 μm spots to which cells adhered, so that after a brief culture period cells would attach

only to the printed spots, and remain there throughout the experiment, fixation, and over 20 stringent washes. Cell-spot arrays allowed additional treatments to be introduced to each spot before printing, creating an array of thousands of potentially unique perturbations within a single experiment. LaBarge et al. used this technique to assess the effects that ECM stiffness and elasticity modulus had on cancer cells [245], while Rantala et al. introduced a library of siRNAs packaged in liposomal transection reagent [244]. Additionally, Rantala et al. employed high content imaging and image cytometry using the Olympus Scan^R platform to perform quantification of single-cell responses to treatments [244].

Jim Korkola at OHSU and I utilized the strengths of each cell-spot array approach to engineer a novel platform to assess the impact signaling proteins from the microenvironment had on resistance to targeted therapeutics in breast cancer cell lines. The results of this project are presented in detail in Chapter 3, but here I will give a description of how this technique was developed, along with potential further applications.

The MEMA technique developed for the project involves solubilizing a library of 48 unique biologically active human ECM and cell-adhesion proteins in 384-well plates with an appropriate printing buffer. These 384-well 'source plates' are loaded into an Aushon 2470 contact printer, which is a highly automated robotic printer that dips a set of 48 pins into the source plate wells, and then deposits the proteins as 300 μm spots onto 8 replicate wells of 8-well cell culture dishes, typically in batches of 8-16 plates at one time. Printing was initially performed on a table-top Genetix Q-Array Mini during the developmental stage. However, this platform did not allow the level of automation and climate control that the Aushon 2470 provided. The printing program creates randomized duplicate matrices of 20x35 spots, or 'arrays', each of which has between 13-15 replicates spots of each protein in the ECM/cell adhesion library. For a single arm of an experiment 8 duplicate plates are created, each one with 8 arrays, for a total of 44,800 spots per set of arrays.

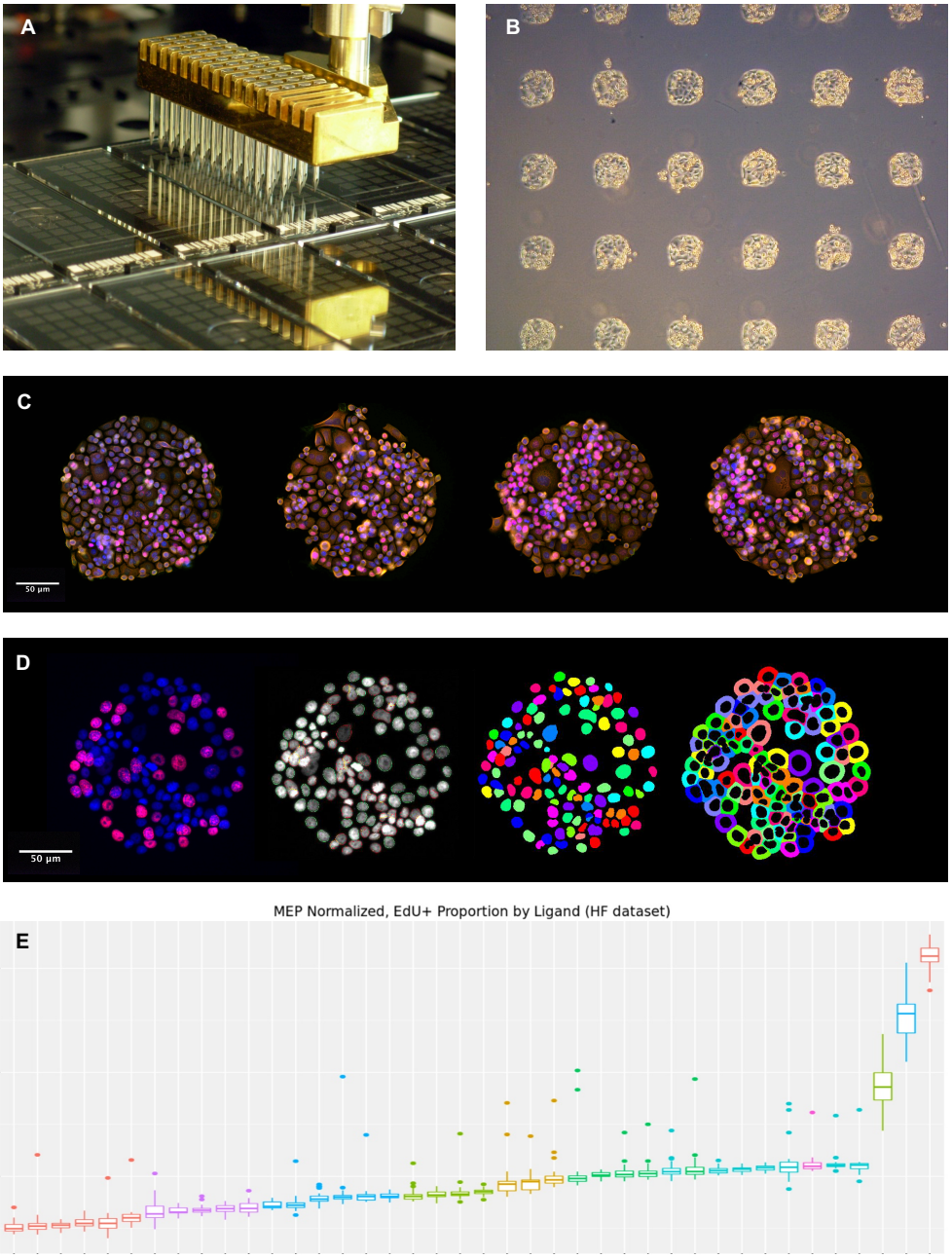

Figure 2.1. The MicroEnvironment MicroArray Platform. (2.1A&B) Libraries of human ECM and cell adhesion proteins are robotically spotted to form 300 µm culture pads to which cells are specifically adhered. A library of human soluble signaling ligands are added to culture medium, and arrays are treated with drug for 72 hours. (2.1C) Following treatment cells are fluorescently assayed for cell count by DAPI, proliferation by EdU, and differentiation by KRT19 and KRT14. (2.1D) Each spot is imaged for all fluorescent channels, and image cytometry is employed to detect each nuclei, and quantify the intensity of the fluorescent marker. (2.1E) Resulting data is normalized by RUV3 and LOESS regressions to find significant effects on drug resistance. Data analysis in 2.1E is provided by Mark Dane, used with permission.

Arrays are desiccated for 48 hours after printing, and blocked with a hydrophobic coat of F108 copolymer so that cells can only attach to the printed protein. Breast cancer cell lines are briefly trypsinized, and $2.5x10^5$ cells are added to each well in the 8-well plates for 30 minutes. This step allows the cells to evenly disperse across the array surface, and the light trypsinization ensures the cells can quickly and strongly bind to the printed proteins. However, as there is currently no way to ensure an exact number of cells adhering to each spot, two independent data normalization methods are used to correct for this and other sources of variation. These will be discussed later. Cells on the arrays are kept at normal culture conditions (37^0C, and 30% CO_2), and complete medium, which is their medium type recommended by ATCC supplemented with 10% Fetal Bovine Serum (FBS).

A second library of 56 different biologically active human signaling ligands (growth factors, chemokines, cytokines) is added to the medium on the arrays after cell adhesion to the arrays has been completed, so that each array receives a unique ligand, or a PBS control. This creates over 2500 different combinations of proteins in a single array set. The complete list of proteins is available on the Synapse website (https://www.synapse.org/#!Synapse:syn2874083.3). The experimental treatment is started at the same time as ligand treatment, and duplicate array sets receive either 150 nM lapatinib, or a DMSO control for 72 hours.

5-ethynyl-2'-deoxyuridine (EdU) is added to the medium of each array for 1 hour after 71 of drug treatment. EdU is a nucleoside analog of thymidine taken up by all viable cells, but only integrated into DNA in place of thymidine in cells that are actively in S-phase during this 1-hour period. EdU contains a functional group available for copper-catalyzed Click-chemistry, and so is a detectable marker of S-phase cells. The arrays are fixed with 2% PFA at the completion of the experimental treatment, and stained with the fluorescent nucleic acid stain DAPI, and a fluorescent detector of EdU. In addition, the arrays are also stained by fluorescent immunohistochemistry for mammary gland cell type markers cytokeratin 14 (KRT14), and cytokeratin 19 (KRT19), which will be discussed more later. These 4 markers provide

assessment of the impacts each protein combination had on drug resistance in terms of cell number per spot, ratio of cells actively proliferating, and potential effects on cell type differentiation and plasticity.

The next step involves assessing the fluorescent markers staining intensity with high-content imaging. A custom automated high-content fluorescent CMOS microscope was developed for the MEMA platform by Nikon and Damir Sudar. This scope allows for the rapid acquisition of 4 fluorescent channels at 20X magnification for each of the 89,600 spots in an experiment. 20X magnification is sufficient to resolve individual cells, and subcellular features. This image quality allows us to use CellProfiler image cytometry software to detect both cell nuclei and cytoplasm as mathematical objects, and to measure the integrated pixel intensity (the SUM of pixel intensities within an object divided by the area of the object) for each fluorescent channel in each cell. This approach is used to measure the number of cells on each spot, EdU positivity of each cell, size, shape, and position of nuclei and cytoplasm, and amount of KRT14 and KRT19 detected in each cell. I developed the CellProfiler pipeline used for MEMA analysis initially. Michel Nederlof then improved the pipeline with proprietary custom QI software, so that over 25 other features could be extracted and quantified from the image data. Data normalization, discussed below, is applied to the single-cell quantified measurements of each marker and cell feature, while the raw image data was stored on The Open Microscopy Environment (OMERO) servers.

Two stages of data normalization were developed to reduce data noise related to the intrinsic heterogeneity of cell-based assays, as wells as variable per-spot cell numbers between replicates. Data normalization techniques utilized the high number of replicates in each array, along with intrinsic positive and negative controls for drug treatments. The initial stages of these normalizations were developed by Juha Rantala and I, and employed multi-parametric gating schemes similar to flow-cytometry analysis, which removed erroneous data points that could result from improper object detection, apoptotic cell bodies, staining artifacts, or outlier biological responses. Staining intensities of fluorescent markers were

then normalized to the nuclear intensity of DAPI stains to account for variation in microscopic imaging. Multi-parametric analysis was performed in the Scan^R software package, and later moved to the FlowJo platform.

Data normalization was later improved by bioinformatics experts Laura Heiser and Mark Dane. Their group developed an R* based software pipeline that took single-cell measurements of cell count, marker intensity, and cellular features, and performed Removal of Unwanted Variance (RUV3) and LOESS (LOcal regrESSion) analyses, in addition to the previous normalizations, to correct for for spatial variances on the arrays [246]. RUV3 and LOESS regressions are analytical tools developed initially for analysis of cDNA microarrays, and were used to correct for signal gradients or area effects observed across array experiments, which can confound detection of legitimate biological responses. These variances fall into two categories; unique spatial aberrations (non-uniform signal gradients, or localized staining artifacts in a single array within an experiment), or uniform localized artifacts (consistent areas of lesser or greater signal across arrays, often stemming from printing errors). LOESS non-parametric regression was employed for spatial artifacts that were not uniform across all arrays, utilizing nearest-neighbor regression to smooth out signal topography in areas of artificial loss or gain of signal. However, consistent spatial artifacts across multiple arrays were not corrected by this method.

Mark Dane and Johann Gagnon-Batrsch developed the RUV3 approach, modified from the RUV method originally developed by Johann Gagnon-Bartsch [246], to correct for varying number of cells on spots across the array and between replicates, and to reduce data noise introduced by printing or cell seeding artifacts that are consistent across multiple arrays. This method allows for better comparisons both within and between MEMA experiments. The statistical model for RUV3 is:

$$y_{ij} = x_i\beta_j + \omega_i\alpha_j + \varepsilon$$

Where i is the array, j is the printed spot in the array, y is the measured value for one signal, $x\beta$ is the signal of interest, $\omega\alpha$ is the unwanted variation, and ε is random error. This method of normalization requires both replicates and negative controls to smooth out unwanted variations. The replicate MEMA spots in the PBS treated wells on each plate serve as the replicate values. However, because a discovery study such as this lacks absolute negative controls, these values need to be derived from the range in values between replicates for each protein combination. The mean is determined for each set of replicate spot cell counts in an entire set of arrays, and the respective mean is then subtracted from each value to produce a new data matrix of 'residual' values. These residual values are assumed to contain only noise rather than true biological responses, meaning that $\beta = 0$ in the above equation. RUV3 then solves for the $\omega\alpha$ term in the statistical model and applies this to calculate the $x\beta$ values which are the normalized signals of interest.

The combination of these normalizations methodologies performed well in repeated MEMA experiments. Normalized MEMA data identified responses to protein combinations in multiple cell lines under drug treatment that were later validated in more traditional cell culture assays. This data will be discussed in more detail in Chapters 3 and 4.

2.2. Development and Optimizations

Two years of development and optimizations were needed to produce a robust and reproducible technique. The initial stages of this primarily involved the identification and selection of proteins to populate the library. The criteria for the selected proteins were that they were:

I. Identified in the literature to be involved in the progression of breast cancer
II. Found to be present or overexpressed at sites of primary or metastatic breast tumors
III. Commercially available as biologically active human proteins

IV. Shown to have biological activity across a range of concentrations in cell based *in vitro* assays

Proteins that met both criteria I and II were preferred, but meeting either was sufficient for inclusion in the library. However, criteria III and IV were deemed essential for inclusion. Proteins in the library were classified as either ECM (secreted matrix proteins such as collagens, laminins, fibronectin), Cell Adhesion (cell surface proteins involved in adhesion and juxtacrine signaling such as desmoglein 2, E-cadherin, and integrins), or Ligands (secreted paracrine signaling molecules including growth factors, chemokines, and cytokines). Each protein was included in the library at the concentration that had been independently validated as the maximum range of ED_{50}'s for eliciting a biological effect in cell line models.

Proteins classified as ECM and Cell Adhesion were initially combined in pairwise combinations with Ligands before printing. Later, however, ECM and Cell Adhesion proteins were printed separately and soluble ligands were added to the medium. Duplicate arrays were printed so that each ligand in the library was added to an individual well to create pairwise combinations with each of the printed proteins. This increased response to soluble ligands in validation experiments. Additionally, it reduced potentially confounding experimental variables, such as growth factors being sequestered by ECM components, and the possibility that cells could respond to ligands escaping from adjacent spots.

Generating the arrays from the protein library met with several technical challenges. The foremost challenge was in the printing process, which proved highly variable depending on the temperature and humidity inside the array printing chamber. Much of this was due to variable viscosity between the protein samples, and the limitations of our initial array printer, which lacked large scale automation and reliable environmental control. We optimized our print buffer formulation to overcome the issues with differential viscosity. 100 mM Tris (pH 5.2), 5 mM EDTA, and 10% glycerol was experimentally

determined to be the ideal buffer. This resulted in even deposition of proteins between prints, but could also cause streaking of spots, so a 48-hour array desiccation step was added to allow the printed arrays to dry before the hydrophobic block step to ensure the spots did not streak. Other issues with reproducibility were addressed by acquisition of an Aushon 2470 microarray printing platform. This system had more advanced robotics, and better environmental sealing than our previous table-top Q-Array Mini printer, resulting in greatly decreased variability between prints.

The next technical hurdle involved optimizing cell culture conditions and seeding density on the arrays. While a large amount of replicates and RUV3 and LOESS data normalization can correct for a degree of heterogeneity between replicates, the cell seeding step is still essential to reproducibility between arrays. Consistent cell seeding required optimization of three equally essential steps; trypsinization, seeding density, and adhesion time. Adherent breast cancer cell lines require treatment with trypsin to release them from cell culture plastic dishes, which enzymatically cleaves cell surface adhesion proteins and releases the cells into suspension. However, these same surface proteins are required for adhesion to array spots, and since production of new adhesion proteins can be variable due to stochastic protein production between cells, it was beneficial to retain as much existing adhesion proteins as possible. Because of this, a set time of trypsin (or HyClone HyQtase) treatment was established for each cell line (typically 2-5 minutes) that would leave the cells only lightly attached to the culture surface so that they could be removed by forceful pipetting. Cells were then triturated, and added to the arrays. The number of cells needed for 72-hour experiments involving both drug and control treatments was experimentally established. Initial cell seeding quantity needed to be low enough so that control spots would not reach confluency until near the end of the experiment, but high enough so that some cells remained following drug treatment. How long the cells initially sat on the arrays during the adhesion step also influenced the number of starting cells per spot, so a consistent 30-minute adhesion time was used before non-adhered cells were removed by washing.

The amount of FBS added to the culture medium was another variable that influenced cell growth on the arrays. Breast cancer cell lines used in MEMA experiments typically require 10% FBS (full serum) for normal growth, and this also was deemed essential for proper binding to the arrays. However, it is possible that full serum can already contain saturating amounts of growth factors used in the MEMA, and serum starvation may be required to see a biological effect in some experimental designs. Full serum medium was used in drug trial MEMA experiments because we wanted to identify factors that would induce drug resistance. That could not be accurately determined unless the baseline conditions represented normal growth and drug response. Validation experiments with traditional cell culture assays supported this approach, reproducing MEMA findings, and showing that cells did not have a strong response to the protein factors in the absence of drug induced cell stress. This data is presented in Chapter 3.

2.3. Further Applications of the MEMA Platform

The primary application of the MEMA platform for the project in this thesis was to measure how the microenvironment affected cell count and EdU incorporation in lapatinib treated cells, which is detailed in Chapter 3. However, the MEMA is a flexible platform that can be used to interrogate the impact of microenvironment proteins on any endpoint that can be stained and quantified. The above studies demonstrate how modifications to MEMA print components, treatment conditions, and endpoint assays can be used to assess differentiation and proliferation in both adherent and non-adherent cell types.

An important aspect of cancer cell biology that can influence drug response is cell plasticity and differentiation, examples of which were given in Chapter 1. We tested the hypothesis in MEMA drug studies that certain protein signal combinations could cause drug resistance by driving the differentiation of cancer cells into drug tolerant cell states. We investigated correlations between cells state and drug resistance by plating AU565 and HCC-1954 HER2+ breast cancer cell lines on MEMAs, and treated for

72 hours with 750 nM lapatinib (adhering to the previously discussed workflow). Following this, cells were fluorescently stained with antibodies for cell state markers KRT14 (clone LL002, purchased from Abcam, 1:300 dilution) and KRT19 (clone RCK108, Purchased from Dako, 1:300 dilution) (Figure 2.2).

Analysis of this data did not reveal any significant correlation between the KRT14/KRT19 ratio following treatment and drug resistance that was specific to protein combinations. Interestingly, analysis instead revealed a differential effect on marker expression between the cell lines. Figure 2.3 shows averaged data points for each protein combination plotted by their average KRT14 expression versus their average KRT19 expression, both with and without lapatinib treatment. This data indicates that, with a few exceptions, marker expression was not heavily influenced by protein combinations in the absence of drug treatment in AU565 cells. However, the combination of drug treatment and protein exposure created a highly variable impact on marker expression that appeared to remain in a linear relationship (Figure 2.3A). In contrast, neither protein combinations nor drug treatment caused an appreciable effect on keratin expression in HCC-1954 cells (Figure 2.3B). There was a slight increase in KRT19 expression among data points under lapatinib treatment, but not to the extent observed in AU565. This study suggests that HCC-1954 is a less plastic cell line under drug treatment in comparison to AU565.

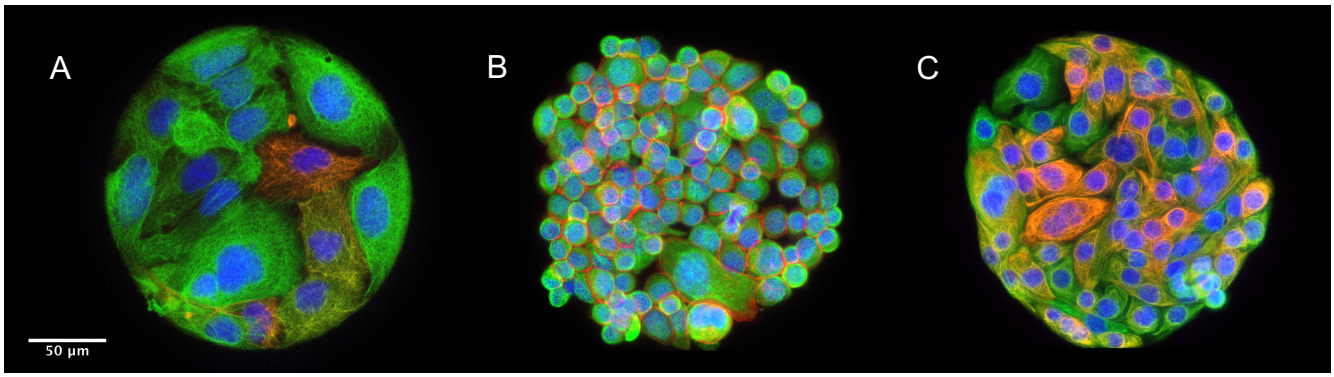

Figure 2.2. Fluorescent Markers of Mammary Lineage Differentiation. Following treatment, cells on MEMAs were fixed with PFA, permeabalized with triton X100, and fluorescent immunohistochemistry is used to detect KRT14 (red), KRT19 (green), and DAPI (blue). HCC1954 (2.2A), AU565 (2.2B), and JIMT1 (2.2C).

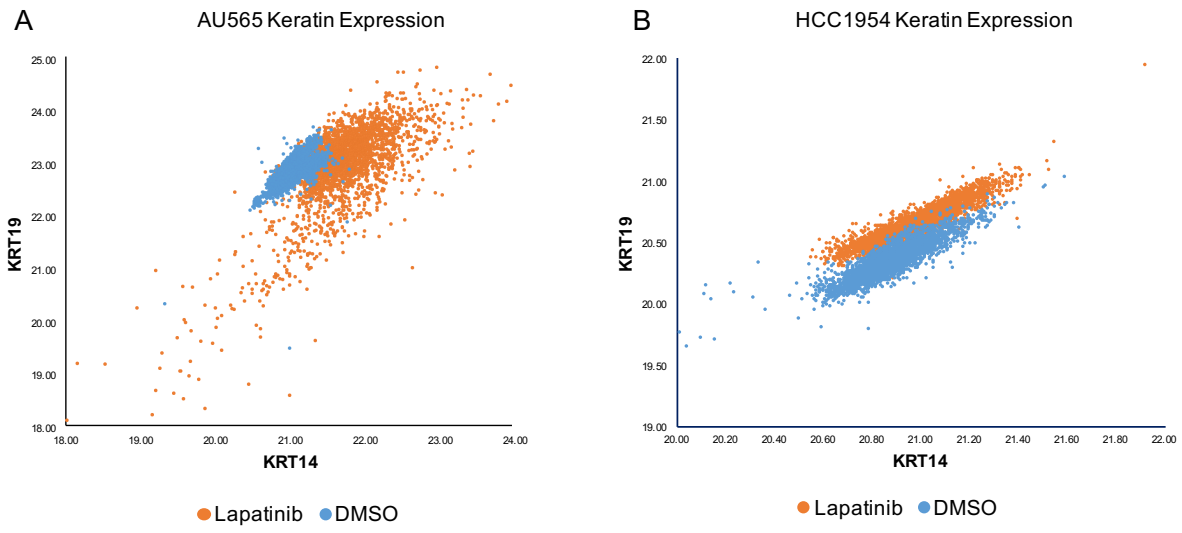

Figure 2.3. Cell Type Marker Expression Influenced by Lapatinib and MEMA Conditions. Average (n = 15) integrated intensity of KRT14 (x-axis) and KRT19 (y-axis) expression in AU565 and HCC-1954 treated with 750 nM lapatinib or DMSO control for 72 hours on MEMAs. Lapatinib treatment results in increased modulation of KRT14 expression in AU565 (2.3A) compared to HCC-1954 (2.3B).

A separate project was launched to better assess the influence protein combinations have on cell state markers, cell number, and proliferation in the absence of drug treatment. This project employed the MEMA platform to assess these endpoints across a large panel of breast cancer cell line, in collaboration with the NIH Library of Network-Based Cellular Signatures (LINCS). The project was designated the Microenvironment Pertubagen (MEP) arm of the LINCS consortium, and is headed by Joe Gray and Gordon Mills to investigate the effect specific protein combinations have on a range of cell biology across a large cell line panel. The LINCS consortium aims to integrate MEMA data with multiple omic characterizations of the same cell lines, engaging multiple lab groups from all over the U.S.

We reengineered the print formulation to facilitate the binding of non-adherent cell types. One of the main drawbacks of any cell-spot array technique is that it is only compatible with cells that adhere to cell culture surfaces. However, hematpoetic cancer cell lines (such as lines derived from leukemia cells) remain in suspension during cell culture, and never form strong adhesions to culture surfaces. Dmitri Rosanov, Chelsea Jenkins, Jeff Tyner, and I developed a variant of the MEMA to accommodate suspension cell lines, termed Non-Adherent Cell Arrays (NACAs). The goal of the NACA project was both to expand the range of cell lines compatible with the MEMA, and also to allow for a high-throughput screening technique for suspension cell lines that incorporated all the benefits of fluorescent microscopy. Fluorescent imaging of suspension lines is very difficult to do in a high content manner; the most widely used available technology is currently fluorescent-imaging flow cytometers, which are typically slow and costly. It was believed by colleagues in leukemia focused groups that an approach like the NACA could accelerate their projects, require fewer cells from patient samples, and allow them to interrogate new biological questions.

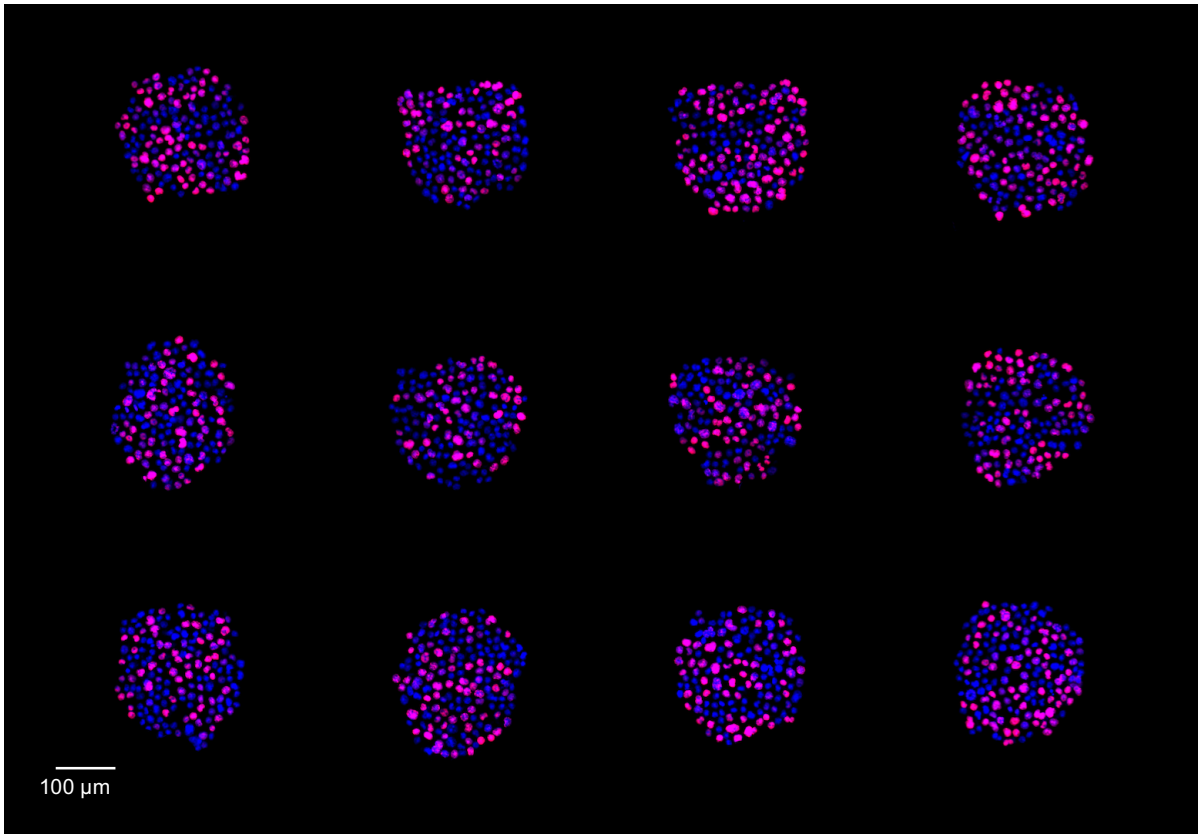

Figure 2.4. BaF3 cells adhere to and proliferate on NACA spots. NACA spots of collagen I supplemented with 1.5 mg/mL ConA. BaF3 cells added to arrays with full serum and 10 ng/mL IL-3. Following 24 hours, cells were fixed in PFA, permeabalized with triton x-100, and DAPI (blue) and EdU (pink) were fluorescently labeled. TR = 4, BR = 8. Cell lines provided by Chelsea Jenkins and Jeff Tyner, data used with permission.

The key component of NACAs was the development of a print formulation that could bind cell surface proteins in cell lines that lacked adhesion proteins. This was achieved by adding lectins to the print buffer, which bind to specific sugar moieties on glycosylated cell surface proteins. There are a large range of commercially available lectins with varying specificity for N-linked sugars on glycoproteins, such as glucose, galactose, mannose, and fucose. Initially, print buffers were supplemented with the lectin Concanavalin A (ConA), which binds mannose and glucose sugars. This approach was tested successfully in adhering the murine suspension cell line BaF3 to NACAs (Figure 2.4), which remained throughout the experiment, fixation, and EdU detection protocol.

A potential source of error in cell spot arrays is cells responding to signals from adjacent spots. An IL-3 containing assay was generated to address this in the NACA platform. BaF3 cells require the cytokine IL-3 in order to proliferate, so a repeating matrix of 5x5 spots within the NACA was generated so that the central spot of each matrix contained IL-3, and all surrounding spots were IL-3 negative. Cells were washed three times in IL-3 negative medium to remove presence of the cytokine, and then seeded on the arrays in IL-3 negative medium. The arrays were fixed in PFA after 48 hours, and EdU detection was performed to identify proliferating cells. Figure 2.5 shows a representative matrix from the experiment, where the center IL-3 positive spot has a very large percentage of cells proliferating, while all surrounding spots have very little EdU positive cells.

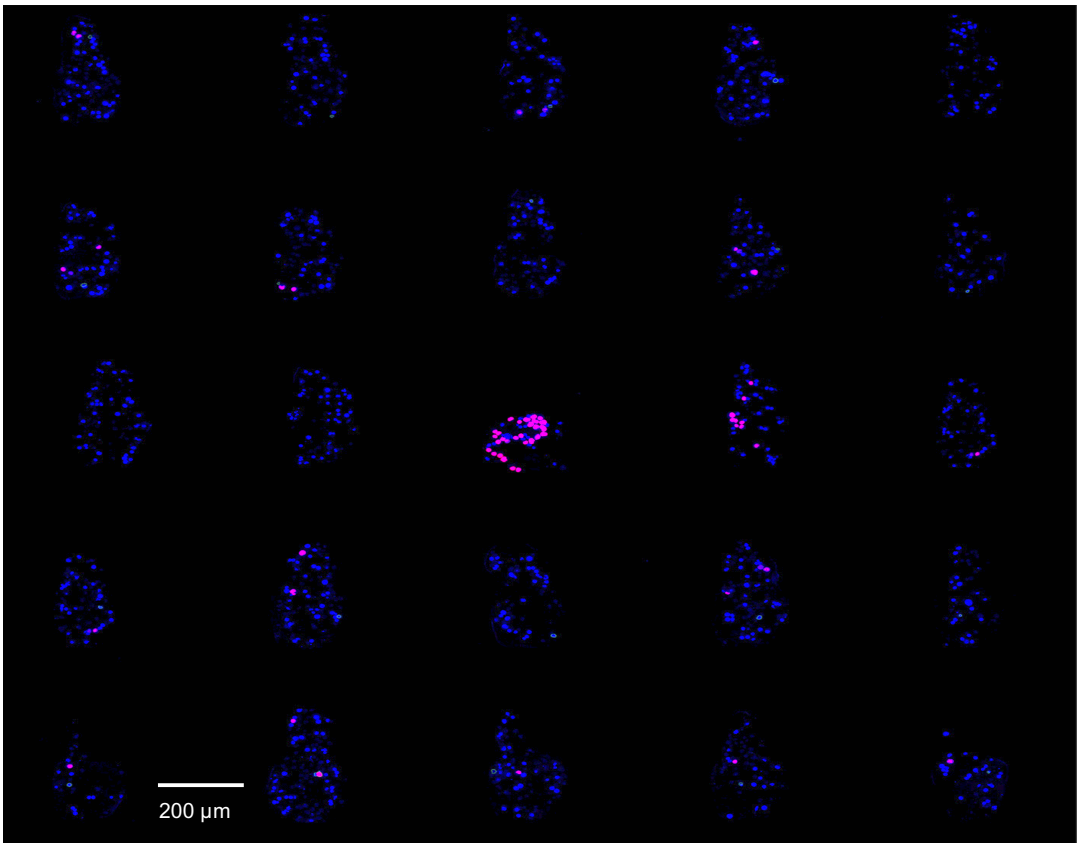

Figure 2.5. BaF3 cells respond to specifically printed IL3. NACA spots of collagen I, ConA, and either 10 ng/mL IL-3, or PBS control. The center spot contains IL-3, all surrounding spots do not. BaF3 cells were washed repeatedly in PBS and seeded on NACAs for 48 hours in medium with no additional IL-3. Nuclei were detected by DAPI (blue), and proliferation by EdU uptake (pink) following treatment. TR = 4, BR = 3. Cell lines provided by Chelsea Jenkins and Jeff Tyner, data used with permission.

The use of lectins to adhere cells to arrays was largely thought to be biologically inert, but some cell types, such as T lymphocytes, are activated by ConA in a process called agglutination [247]. A combination of lectins, rather than ConA alone, were used in suspension cell types where ConA could have biological activity. Three lectins were used at equal concentrations; Lens Cullinaris Agglutinin (LCA), Phaseolus Vulgaris Erythroagglutinin (PHA-E), and Wheat Germ Agglutinin (WGA) (purchased from Vector Laboratories). Each lectin binds different sugar moieties on glycoproteins, so three were used to ensure stronger cell binding, and each is reported to have little or no mitogenic activity.

The NACA was used in a selective gene knockdown project in collaboration with Jeff Tyner's lab. The project employed a library of siRNAs to knock down 95 unique genes frequently involved in drug resistance in leukemia patients [248]. siRNAs were pre-incubated in SilentFect liposomal transfection reagent before being added to replicate wells in source plates containing print buffer, and the lectin combination mentioned previously (LCA, WGA, and PHA-E). The human Chronic Mylogenous Leukemia (CML) cell line K-562 was plated on siRNA NACAs for 48 hours, and their remaining cell count and proliferation ratio were assessed. Figure 2.6 shows the results of this study, depicting EdU positive proportion of cells following treatment. Importantly, spots containing the AllStar CellDeath positive control siRNA had a significant negative impact on proliferation, indicating that siRNAs were successfully transfected. Other siRNAs that strongly reduced proliferation, such as those against ABL2 and EPHA6, had been previously independently validated in traditional liposomal transfection experiments to inhibit growth in K-562 cells.

***

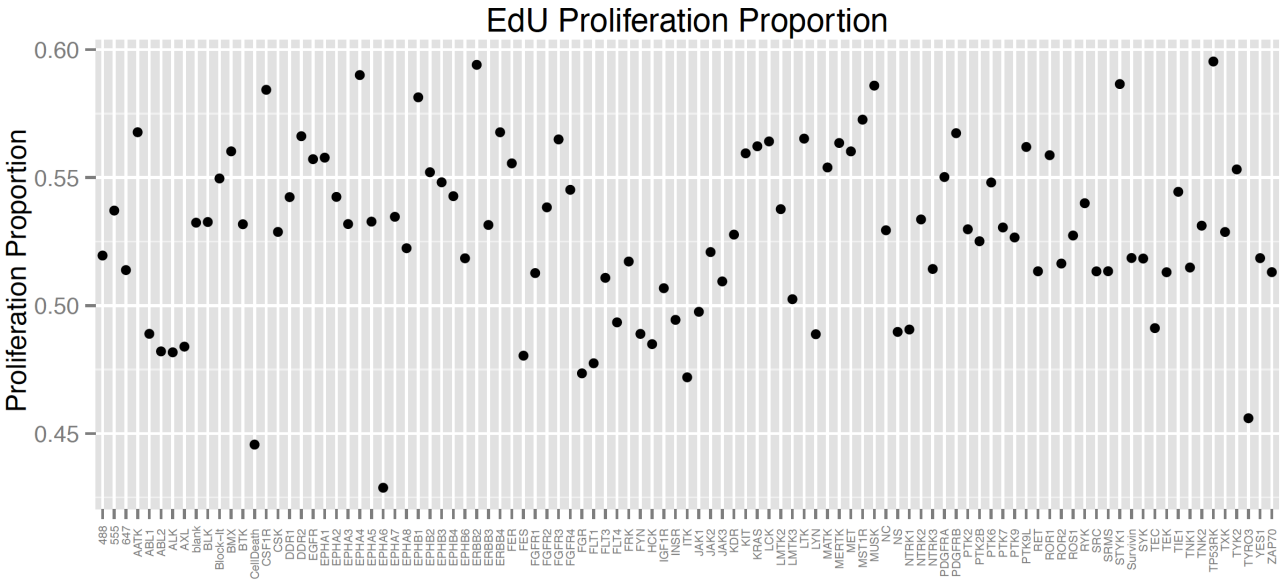

Figure 2.6. NACA siRNA array recapitulates known responses in K-562 cells. $1x10^6$ K-562 cells were seeded on siRNA NACAs containing collagen I, lectin combination, and a library of human siRNAs in liposomal transfection reagent. Immunofluorescent detection was used for nuclei and EdU detection. Graph shows proportion of proliferating cells for each siRNA and Cell Death control normalized to average cell count of each, n =15. Cell lines and siRNA panel provided by Chelsea Jenkins and Jeff Tyner. Data analysis provided by Mark Dane, used with permission.

Permutations of the MEMA platform, such as the NACA, the MEP LINCS project, and experiments focusing on exploring differentiation and plasticity, demonstrate the flexibility and versatility this technique has to interrogate many types of biology in a high-throughput manner. Chapter 3 will discuss in detail the data generated by the MEMA platform for HER2+ cell lines treated with the HER2 targeted TKI lapatinib. The data in Chapter 3 focuses on cell count and proliferation ratio following drug treatment, but the experimental permutations presented in this chapter suggests that many more data endpoints can be derived from MEMA-generated results.

Chapter 3. Microenvironment Mediated Mechanisms of Resistance to HER2 Inhibitors Differ Between HER2+ Breast Cancer Subtypes

Spencer S. Watson, Mark Dane, Koei Chin, Michel Nederlof, Moqing Liu, Tiera Liby, Wallace Thompson, Rebecca Smith, David Kilburn, Matthew Whitman, Damir Sudar, Gordon B. Mills, Laura Heiser, Oliver Jonas, Joe W. Gray, James Korkola

3.1. Abstract

Clinical responses of HER2+ breast cancers to tyrosine kinase inhibitors (TKIs) are limited by multiple resistance mechanisms including escape to protective microenvironmental niches. We describe use of MicroEnvironment MicroArrays to identify specific microenvironment signals that reduce sensitivity to HER2 targeted TKIs, lapatinib and neratinib. Interestingly, these differ between HER2E and Luminal-HER2+ subtypes. For example, hepatocyte growth factor (HGF) induces resistance in HER2E cells and neuregulin1-β1 (NRG1β) induces resistance in L-HER2+ cells. We attribute these divergent responses to differential use of PI3K and MAPK pathways and expression of HER3 and MET, respectively. NRG1β-mediated resistance in L-HER2+ lines is reversed by inhibiting HER2-HER3 dimer formation with pertuzumab, while HGF-mediated resistance in HER2E lines is reversed with the MET inhibitor, crizotinib.

The main text in this chapter is presented exactly as submitted to Cell Systems, only figure legends have been changed. A resubmission of this work is planned for June of 2017

3.2. Introduction

Amplification of HER2 occurs in ~25% of all invasive breast cancers, forming the HER2+ tumor subtype [138]. HER2+ tumors have worse outcomes than non-HER2+ luminal tumors in the absence of HER2

targeted therapy [154-156]. However, outcomes have been substantially improved with the use of therapeutic agents that target HER2. These include the monoclonal antibodies trastuzumab and pertuzumab, the antibody-drug conjugate trastuzumab emtasine (T-DM1), and tyrosine kinase inhibitors (TKIs) lapatinib, afatinib, and neratinib. Clinical studies with HER2-targeted agents have shown improved outcomes over chemotherapy alone for patients with HER2+ breast cancer in both the metastatic [161, 249] and adjuvant settings [250], but therapeutic resistance often arises. Indeed, treatments with trastuzumab, lapatinib, or neratinib in the metastatic setting fail to adequately inhibit the growth of HER2+ tumors in more than half of all cases [162, 163, 251]. Cell intrinsic compensatory mutations have been shown to provide drug resistance to subclonal HER2+ populations [252-254], however, several recent studies have demonstrated that extrinsic factors from the tumor microenvironment allow otherwise drug sensitive cells to escape therapeutic control. These factors include paracrine growth factors [255, 256], ECM proteins and physical structure [211, 257, 258] and hypoxia [259].

We focus in this paper on analysis of the impacts of signals provided by soluble and insoluble proteins from diverse microenvironment on responses to the tyrosine kinase inhibitors lapatinib and neratinib. We began by assessing the effects of >2500 combinations of 56 soluble and 46 insoluble extracellular matrix proteins from the microenvironment on the responses to lapatinib in HER2+ breast cancer cell lines using a powerful Microenvironment Microarray (MEMA) technology. We present the results of the entire screen but focus on two of the most potent signaling factors and their differential impacts on responses of cell lines representing the luminal-like (designated L-HER2) and basal-like (designated HER2E) subtypes of HER2+ tumors defined by The Cancer Genome Atlas (TCGA) project [260]. Specifically, we describe neuregulin1-β1 (NRG1β) as a potent resistance associated protein in L-HER2+ cells and hepatocyte growth factor (HGF) as a resistance associated protein in HER2E cells. We elucidate the involved mechanisms and show that NRG1β mediated resistance can be countered by co-treatment with pertuzumab and that HGF mediated resistance can be countered by co-treatment with crizotinib.

3.3. Results

3.3.1. *Microenvironment MicroArray identifies factors imparting lapatinib resistance*

We used MicroEnvironment MicroArrays (MEMAs) [243] to identify specific soluble and insoluble microenvironmental proteins that attenuate responses to lapatinib in HER2+ cell lines. MEMAs were comprised of >2500 different combinations of 56 soluble and 46 insoluble microenvironment protein. These proteins were chosen because of their involvement at sites of local and metastatic disease and represent components of lymphocytic infiltrates, stroma, blood and lymphatic system, local extracellular matrix, macrophages and endothelium. Each insoluble protein was mixed with collagen I to improve printing and cell attachment. Insoluble proteins were printed in multi-well plates as ~300 μm diameter spots that served as isolated growth pads for cells. Each insoluble protein composition was printed in ~15 replicate random locations. We added either AU565 cells (representing the L-HER2+ subtype) or HCC-1954 cells (representing the HER2E subtype) to each MEMA set, allowed the cells to attach to the spots overnight, and then treated each array with a single soluble ligand, and either 750 nM lapatinib or DMSO (Figure 3.1A). A list of the ECM components, soluble ligands, and their concentrations is available in the plate preparation document at the SAGE-Synapse website (https://www.synapse.org/#!Synapse:syn2874083.3). The cells were treated for one hour with EdU after 71 hours of lapatinib treatment, then fixed in 2% paraformaldahyde and immunfluorescently stained for DNA content (DAPI), EdU incorporation and differentiation markers (KRT14 and KRT19). The stained arrays were analyzed using a Nikon high content, high throughput imaging platform (Figure 3.1B) and the resulting multicolor images were quantified using image segmentation software. Data from 256 arrays were normalized by RUV3 and LOESS regression [246] to reduce variation in cell counts and staining intensity.

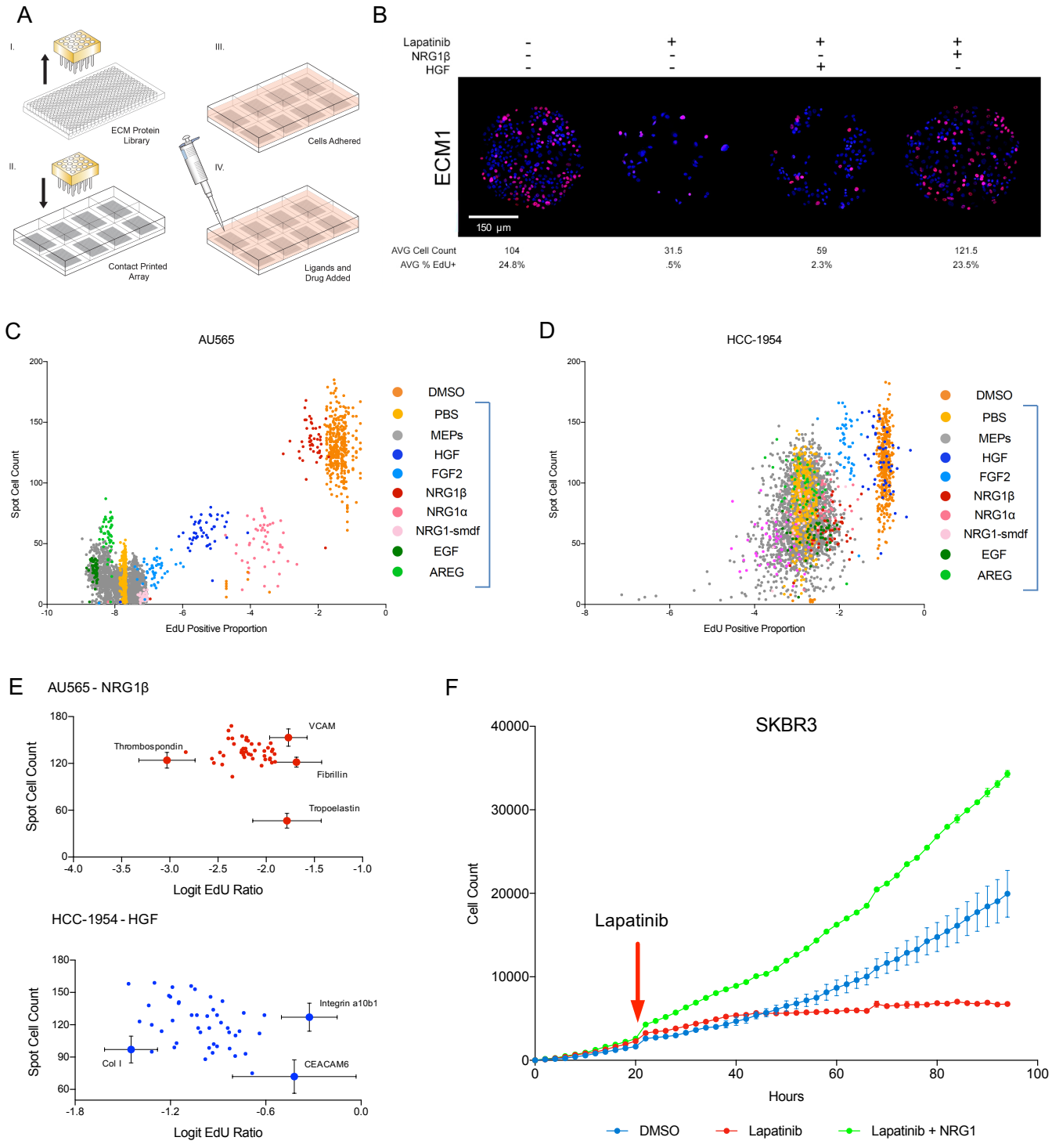
A
I.
ECM Protein Library
II.
Contact Printed Array
III.
Cells Adhered
IV.
Ligands and Drug Added
B
Lapatinib
NRG1β
HGF
ECM1
150 μm
AVG Cell Count 104 31.5 59 121.5
AVG % EdU+ 24.8% .5% 2.3% 23.5%
C
AU565
Spot Cell Count
EdU Positive Proportion
DMSO
PBS
MEPs
HGF
FGF2
NRG1β
NRG1α
NRG1-smdf
EGF
AREG
D
HCC-1954
Spot Cell Count
EdU Positive Proportion
DMSO
PBS
MEPs
HGF
FGF2
NRG1β
NRG1α
NRG1-smdf
EGF
AREG
E
AU565 - NRG1β
Thrombospondin
VCAM
Fibrillin
Tropoelastin
Spot Cell Count
Logit EdU Ratio
HCC-1954 - HGF
Integrin a10b1
Col I
CEACAM6
Spot Cell Count
Logit EdU Ratio
F
SKBR3
Lapatinib
Cell Count
Hours
DMSO
Lapatinib
Lapatinib + NRG1

Figure 3.1. MEMA studies reveal multiple protein combinations that confer lapatinib resistance to otherwise sensitive HER2+ breast cancer cell lines. (3.1A) Libraries of biologically reactive human ECM and cell adhesion proteins immobilized onto a solid surface by randomized robotic contact printing. Cells adhered to printed protein spots, and exposed to a library of soluble functionalized human ligand proteins and 750 nM lapatinib or DMSO control. (3.1B) Composite image of AU565 cells on MEMA spots containing immobilized ECM1 protein, treated with combinations of lapatinib, NRG1β, and HGF. Nuclei labeled with DAPI (blue), proliferation measured by nuclear EdU uptake (pink). (3.1C&D) Plots of mean cell count and EdU ratio logit (n=13-15) for AU565 and HCC-1954 cells on MEMA following 72 hours of 750 nM lapatinib treatment or DMSO treated control spots receiving no additional ligand exposure (orange). Protein combinations are highlighted in color by inclusion of selected ligands, all other microenvironment perturbants (MEPs) are colored gray. All conditions highlighted in blue bracket received lapatinib. (3.1E) Isolated plots from 3.1C of AU565 and HCC-1954 cells exposed to NRG1β and HGF respectively following lapatinib treatment. ECM/adhesion proteins influencing ligand mediated drug resistance are labeled. Error bars display SEM, n = 13-15. (3.1F) Mean cell count and SEM (n = 2, BR = 3) derived from live-cell imaging of nuclear GFP expressing SKBR3 cells treated with DMSO control, 500 nM lapatinib, or 500 nM lapatinib plus 25 ng/ml NRG1β over a 96-hour time course. NRG1β was added at time 0, and lapatinib was spiked in at the 24-hour time point. Image quantification and data analysis from 3.1C-E provided by ©Michel Nederlof and ©Mark Dane, used with permission.

We assessed the impacts of the diverse microenvironments on changes in the numbers of cells remaining after treatment and/or in the fraction of cells incorporating EdU after lapatinib treatment compared to DMSO control. We also assessed changes in basal and luminal mammary cell type markers KRT14 and KRT19, but they were not as associated with microenvironment mediated changes in lapatinib response and so they are not discussed further here. Figures 3.1C-E, and Supplemental Figure S3.1A show that several soluble and insoluble factors quantitatively influenced cell growth and fraction of cells incorporating EdU during treatment with lapatinib, including several soluble proteins previously reported [255]. Some insoluble proteins also influenced responses but the largest effects overall were produced by soluble proteins. Specifically, NRG1 isoforms attenuated response to lapatinib in AU565 while FGF2 and HGF attenuated response to lapatinib in HCC-1954. Interestingly, the degree of attenuation of response in AU565 differed between NRG1 isoforms and other EGF family members. For example, the number of AU565 cells remaining and the fraction of cells incorporating EdU after treatment with lapatinib, in the presence of NRG1β were similar to those values for AU565 cells treated with DMSO alone (no lapatinib). In contrast, treatment with lapatinib in the presence of NRG1-α1 resulted in a lower fraction of cells incorporating EdU compared to NRG1β and DMSO controls, but a higher number of average cells remaining than most of the lapatinib treated conditions, while NRG1-SMDF had little effect on response to lapatinib. Other ligands enhanced sensitivity to lapatinib, such as EGF in AU565 cells, and BMP4 in HCC-1954 cells.

Insoluble ECM proteins also affected response to lapatinib but the effects were less dramatic than for the soluble proteins. Figure 3.1E, for example, shows that NRG1β attenuation of response to lapatinib in AU565 cells is diminished by growth of cells on thrombospondin, and tropoelastin, and enhanced by growth on VCAM and fibrillin, while HGF attenuation of response to lapatinib in HCC-1954 cells was decreased by growth on collagen I, and enhanced by growth on integrin α10β1 or CEACAM6. Interestingly, none of the HER2+ cells grew well on nidogen (outlier not shown), one of the proteins secreted by myoepithelial cells to form the basement membrane separating normal epithelial cells by

expression and deposition of fibronectin, collagen IV, nidogen, and the bioactive laminins [47]. This suggests that nidogen may act as a growth "barrier" that contains normal and malignant epithelial cells.

Overall, NRG1β was the strongest microenvironmental inhibitor of lapatinib response in AU565 and HGF was the strongest inhibitor of response in HCC-1954. Importantly, NRG1β had little effect on response of HCC-1954 to lapatinib, and HGF had little effect on response of AU565 to lapatinib.

We assessed the effects of a range of NRG1β and HGF concentrations on responses to a range of lapatinib doses in a 2D live-cell assay in SKBR3 and HCC-1954 cells expressing nuclear GFP. HGF was able to abrogate lapatinib response in HCC-1954 cells in a dose dependent manner (Supplemental Figure S3.2). NRG1β attenuated response to lapatinib in SKBR3 cells, and interestingly this effect had already occurred at the earliest time point measured (2 hours post drug exposure) and was maintained for a full 96-hour time course (Figure 3.1F and Supplemental Figure S3.2).

Remarkably, several concentrations of NRG1β even caused SKBR3 cells to grow more rapidly in the presence of lapatinib than in untreated controls (Supplemental Figure S3.2) and that the stimulatory effect occurred as soon as lapatinib was added (Figure 3.1F). We suggest a mechanism for this in the following sections.

3.3.2. *HER2+ subtypes show differential response to NRG1β and HGF*

We explored the possibility that the observed differences in microenvironment-mediated attenuation of response to lapatinib between AU565 and HCC-1954 cells were due to differences in the intrinsic biology of L-HER2+ and HER2E subtypes by measuring responses to NRG1β and HGF in a panel of 8 cell lines. Four cell lines (JIMT1, HCC-3153, HCC-1954, and 21MT1) modeled the HER2E subtype and four (EFM192A, BT474, SKBR3, and AU565) modeled the L-HER2+ subtype (Figure 3.2A and 3.2B).

We used the irreversible TKI neratinib instead of lapatinib, since several of the cell lines exhibited *de novo* resistance to lapatinib, but all cell lines were sensitive to neratinib. We also explored the effects of varying concentrations of neratinib, NRG1β, and HGF. Figure 3.3A shows that NRG1β attenuated response to neratinib in the L-HER2+ lines but generally not in the HER2E cell lines, while HGF attenuated response to neratinib in the L-HER2E lines but had very little effect in the L-HER2+ cell lines. In many cases, L-HER2+ cells treated for 72 hours with neratinib in the presence of NRG1β showed a higher average cell count and a higher percentage of proliferating cells than untreated controls (Figure 3.3A and 3.3B), consistent with the stimulation of proliferation observed with the combination of NRG1β and lapatinib. We conclude from these studies that the differences in response to microenvironmental signals between L-HER2+ and HER2E cell lines are due primarily to subtype intrinsic differences.

3.3.3. *HER2+ subtypes show divergent expression of HER3 and MET*

We measured transcriptional profiles for HER2E and L-HER2+ cells using RNAseq [261] and assessed their differential biology in order to identify molecular processes that might account for the observed differences in response to microenvironmental signals. We found that HER2E lines before treatment generally expressed higher mRNA and protein levels of MET, and lower levels of HER3 compared to L-HER2+ lines (Figure 3.3C and 3.3D). The same relative expression trend is present in gene expression profiles for HER2+ human tumors analyzed by TCGA (Figure 3.3E). Protein analysis of 4 L-HER2+ lines and 4 HER2E lines treated for 48 hours with NRG1β, HGF, lapatinib, and combinations thereof demonstrated that treatment of both subtypes with lapatinib reduced levels of pHER3 and pAKT, and that pAKT expression in both subtypes could be restored by addition of NRG1β (Figure 3.3F). However, NRG1β restored pS6 levels, an indicator of active mitogenic signaling [262], only in the L-HER2+ lines while HGF restored pS6 levels only in HER2E lines.

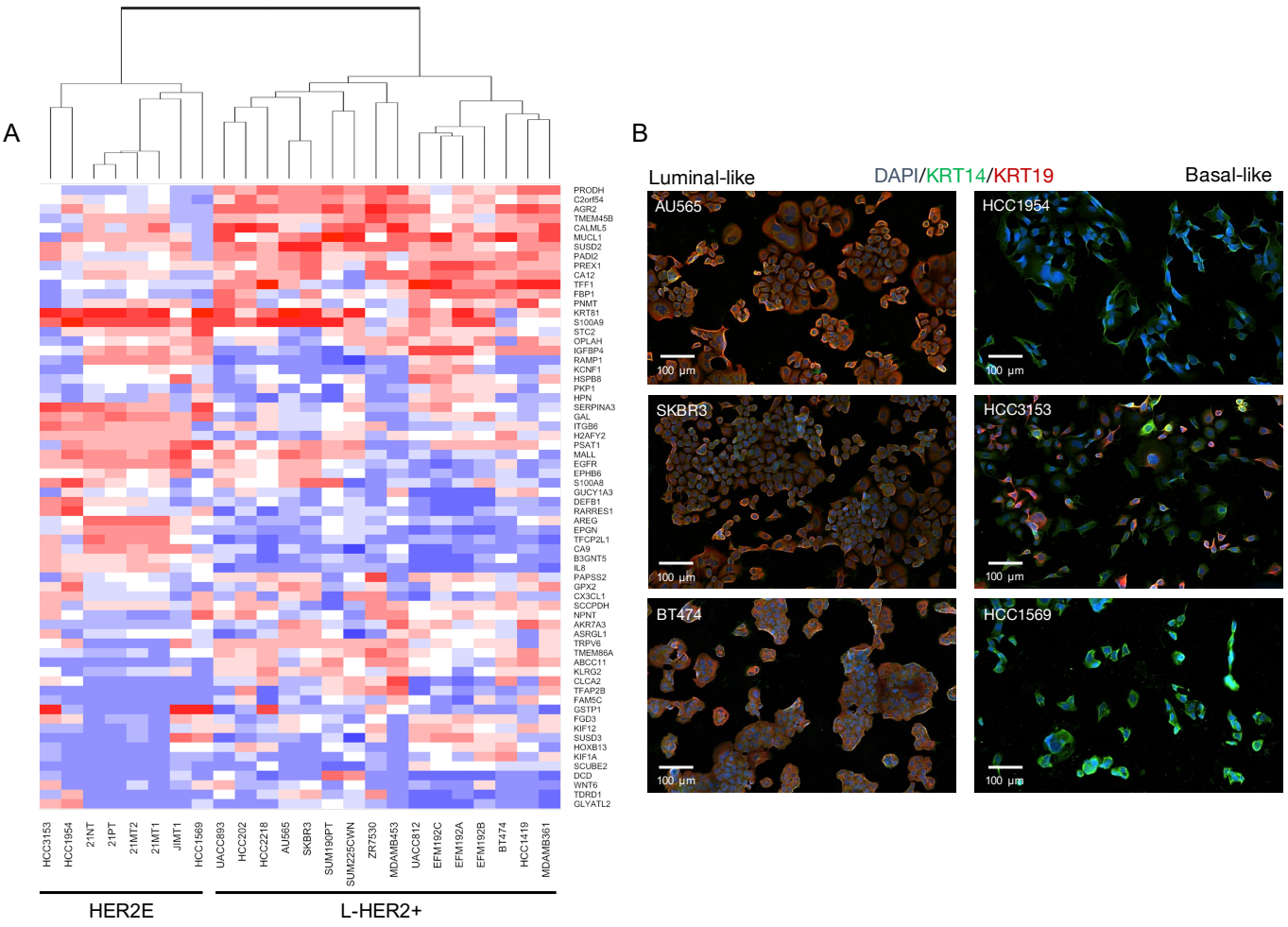

Figure 3.2. HER2+ cell lines are sub-classified into basal-like HER2E and luminal-like L-HER2+ phenotypes. (3.2A) Heatmap of mRNA expression of genes identified by TCGA as significantly different between HER2E and Luminal HER2+ patient tumors in a panel of HER2+ breast cancer cell lines. Gene expression was sorted for variance across cell lines, and the top 10% (66 genes) are used to cluster the panel. (3.2B) L-HER2+ and HER2E lines immunofluorescently labeled with DAPI (blue), KRT14 (green), and KRT19 (red).

3.3.4. *NRG1β and HGF effects also are observed in 3D cultures and xenografts*

We measured the responses of L-HER2+ cell lines (SKBR3, AU565) and HER2E cell lines (HCC-1954, 21MT1) grown in 3D matrigel to combinations of NRG1β, HGF, and neratinib to determine whether spatial organization and ECM structure altered the results observed for cells grown in 2D cultures (Figure 3.4A). We found that the cells were less responsive to neratinib at baseline in 3D, as has been previously reported with lapatinib [211]. However, we found that NRG1β reversed the inhibitory effects of neratinib in L-HER2+ cells and HGF reversed the inhibitor effects of neratinib in HER2E cells in 3D cultures, although the magnitudes of these effects were somewhat diminished compared to 2D. We also assessed the responses of L-HER2+ cells to lapatinib with and without NRG1β and HGF in BT474 cells grown as xenografts on murine flanks using the nanodosing technology described by Jonas et al. [263]. Figure 3.4B shows that NRG1β conferred complete resistance to lapatinib in L-HER2+ cells *in vivo* suggesting that NRG1β mediated resistance also occurs *in vivo*.

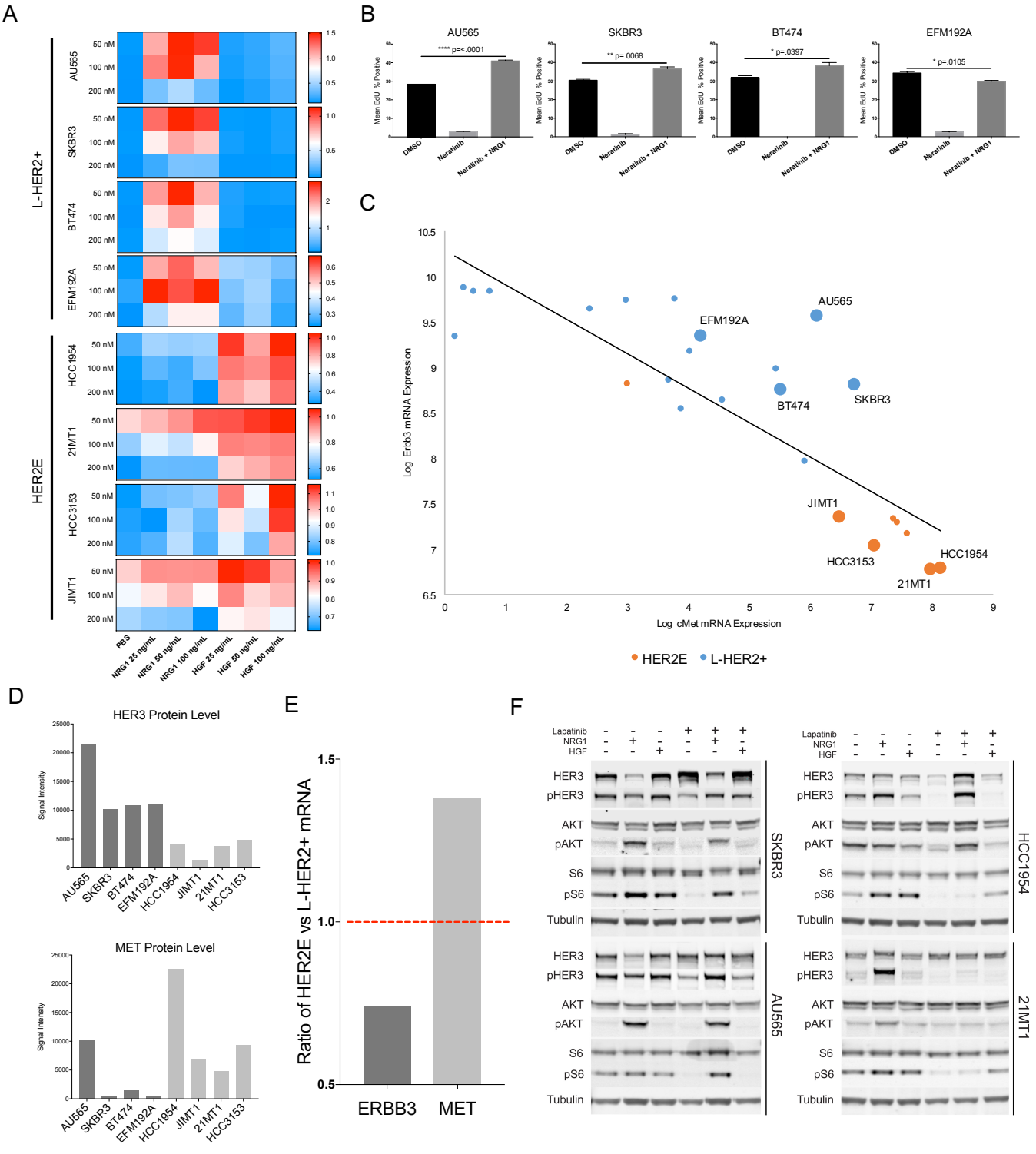
A
L-HER2+
HER2E
AU565
SKBR3
BT474
EFM192A
HCC1954
21MT1
HCC3153
JIMT1
50 nM
100 nM
200 nM
PBS
NRG1 25 ng/mL
NRG1 50 ng/mL
NRG1 100 ng/mL
HGF 25 ng/mL
HGF 50 ng/mL
HGF 100 ng/mL
B
AU565
SKBR3
BT474
EFM192A
**** p=<.0001
** p=.0068
* p=.0397
* p=.0105
Mean EdU % Positive
DMSO
Neratinib
Neratinib + NRG1
C
Log Erbb3 mRNA Expression
Log cMet mRNA Expression
AU565
EFM192A
BT474
SKBR3
JIMT1
HCC3153
HCC1954
21MT1
HER2E
L-HER2+
D
HER3 Protein Level
MET Protein Level
Signal Intensity
AU565
SKBR3
BT474
EFM192A
HCC1954
JIMT1
21MT1
HCC3153
E
Ratio of HER2E vs L-HER2+ mRNA
ERBB3
MET
F
Lapatinib
NRG1
HGF
HER3
pHER3
AKT
pAKT
S6
pS6
Tubulin
SKBR3
HCC1954
AU565
21MT1

Figure 3.3. HER2+ breast cancer cell lines exhibit a subtype intrinsic proliferative response to NRG1β and HGF when under lapatinib or neratinib treatment. (3.3A) Heatmap of mean cell count (n = 3, BR = 3) of 8 cell lines exposed to a dose range of neratinib and 3 concentrations of NRG1β and HGF, each value normalized to the mean cell count of the corresponding DMSO treated control. Scale to right indicates color grading relative to ratio; 1 being no change in cell count, less than 1 a decrease in cell count under drug treatment, and greater than 1 being an increase in cell count under drug treatment. (3.3B) Mean percentage of EdU positive cells and SEM (n = 3) in 4 L-HER2+ cell lines treated in 3.3A with DMSO, 100 nM neratinib, and 100 nM neratinib plus 25 ng/ml NRG1β. p-values show unpaired t-test of significance. (3.3C) Log-scale mRNA expression of *ERBB3* and *MET* in a panel of HER2+ cell lines. Enlarged spots indicate cell lines used in 3.3A. (3.3D) Quantification of Western blot protein analysis of HER3 and MET levels in a panel of 8 cell lines (BR = 3). (3.3E) Ratio of *ERBB3* and *MET* mRNA expression comparisons of human breast cancer tumors described as HER2E and L-HER2+. Data derived from ©TCGA 2012. Originally published in Nature Oct 2012, 490(7418):61-70. (3.3F) Western blot protein analysis of AU565, SKBR3, HCC-1954, and 21MT1 cell lines treated for 48 hours with combinations of DMSO, 500 nM lapatinib, and 50 ng/ml NRG1β (BR = 3).

3.3.5. *HER2+ subtypes have differential reliance on PI3K and MAPK pathways*

The microenvironment proteins HGF and FGF2, rather than NRG1β, mediate resistance to lapatinib and neratinib in HER2E cells. HGF has been previously shown to rescue HER2E HCC-1954 by activating MAPK signaling [255] under lapatinib treatment. We hypothesized that HER2E lines rely less on HER3 than L-HER2+ lines due to increased utilization of EGFR and the MAPK pathway [264]. This is supported by siRNA knockdown experiments that show that that HER2E cells do not depend as much on HER3 as do L-HER2+ lines (Supplemental Figure S3.3A). We further tested the hypothesis through a GSEA of RNAseq profiles measured for 8 L-HER2+ and 8 HER2E lines (Table 1). An unbiased query of the Hallmarks library of gene signatures showed that the "KRAS Signaling Up" gene set, which is a collection of genes upregulated by activity of KRAS, an oncogene upstream of the MAPK pathway, is enhanced in HER2E cells compared to L-HER2+ cells (Figure 3.4C). Additionally, one of the most significant sets upregulated in the reverse comparison of L-HER2+ vs HER2E was the "KRAS Signaling Down" gene set, indicating that this pathway is differentially regulated between the subtypes. We also observed that FOXA1, the inducible co-transcription factor that binds to the promoter region of HER3 [265] was markedly enhanced in L-HER2+ expression compared to HER2E. In addition, EGFR expression was significantly higher in HER2E expression than in L-HER2+ (Figure 3.4D).

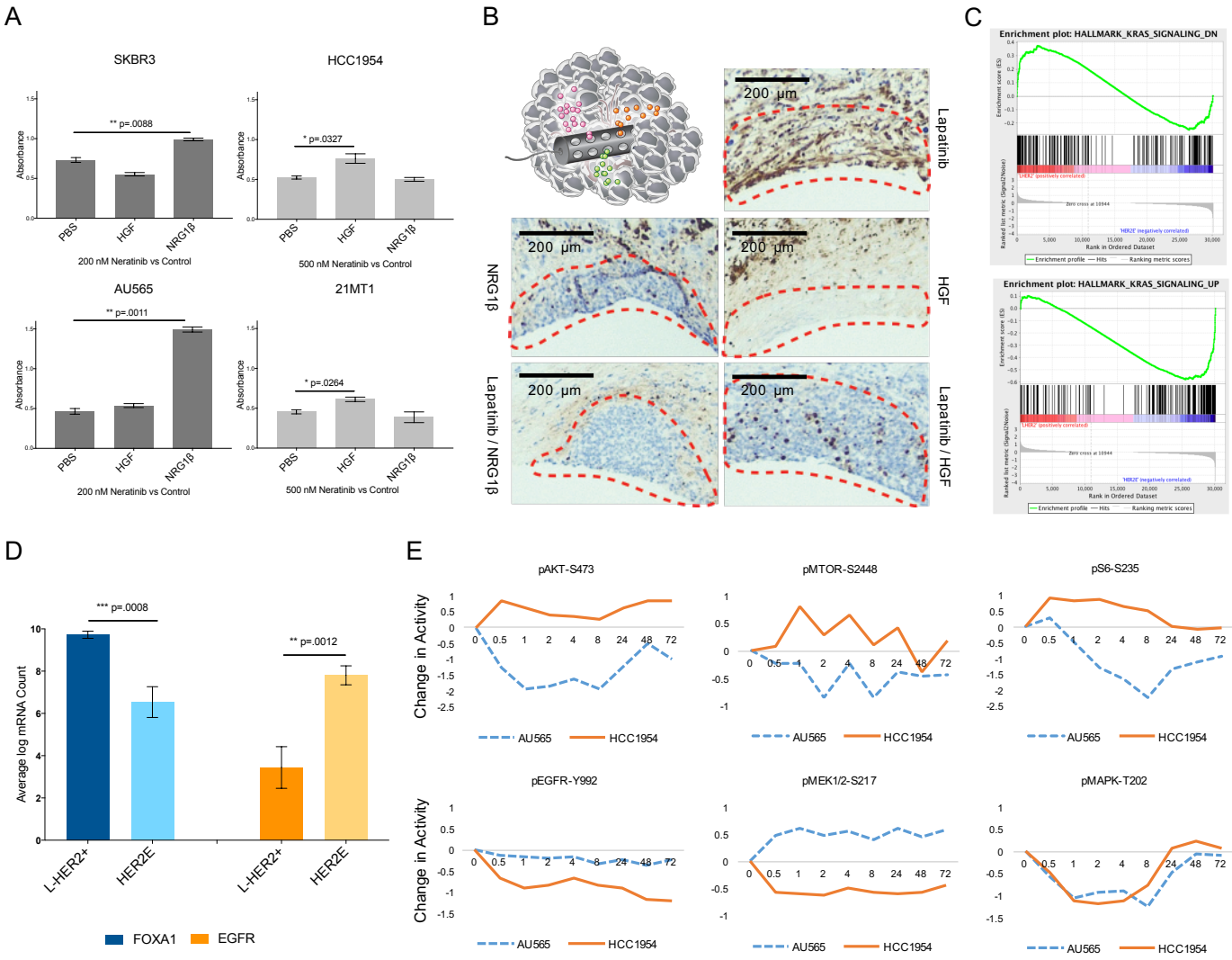
A
SKBR3
HCC1954
AU565
21MT1
Absorbance
** p=.0088
* p=.0327
** p=.0011
* p=.0264
PBS
HGF
NRG1β
200 nM Neratinib vs Control
500 nM Neratinib vs Control
B
200 μm
Lapatinib
NRG1β
HGF
Lapatinib / NRG1β
Lapatinib / HGF
C
Enrichment plot: HALLMARK_KRAS_SIGNALING_DN
Enrichment plot: HALLMARK_KRAS_SIGNALING_UP
Rank in Ordered Dataset
Enrichment profile
Hits
Ranking metric scores
D
*** p=.0008
** p=.0012
Average log mRNA Count
L-HER2+
HER2E
FOXA1
EGFR
E
pAKT-S473
pMTOR-S2448
pS6-S235
pEGFR-Y992
pMEK1/2-S217
pMAPK-T202
Change in Activity
AU565
HCC1954
F
HER2E
L-HER2+
JIMT1
21PT1
21MT1
HCC1954
HCC3153
AU565
SKBR3
BT474
EFM192A
MDAMB361
Cell Viability
log(Concentration)
Lapatinib
Trametinib
Lapatinib + Trametinib

Figure 3.4. L-HER2+ and HER2E lines differ in their resistance mechanisms to HER2 inhibition. (3.4A) Graphs of mean absorbance measurements and SEM (n = 2, BR = 3) of alamar blue stains of 4 cell lines in a 3D matrigel assay following 96 hour treatments of 200 or 500 nM neratinib, and exposure to 50 ng/ml NRG1β and HGF. p-value shows unpaired t-test of significance. Data provided by ©Moqing Liu, used with permission. (3.4B) Representative images from sectioned tissue surrounding domains of implantable microdevices delivering NRG1β, HGF, lapatinib, and combinations to BT474 xenografts on murine flanks. Apoptosis is shown by cleaved caspase-3 antibody staining, BT474 tumor tissue are highlighted in red. Data provided by ©Jonas et al., used with permission. (BR = 3) (3.4C) GSEA comparison plots of L-HER2+ (n = 8) and HER2E lines (n = 8). Top plot shows Hallmark gene set KRAS Down enrichment for L-HER2 vs HER2E (NOM p-val = .003, FDR q-val = .098), and bottom shows KRAS Up gene set enrichment for the reverse comparison (NOM p-val = 0, FDR q-val = 0). (3.4D) Mean log mRNA counts and SEM (n = 8) of 8 L-HER2+ cell lines, and 8 HER2 lines expression of FOXA1 and EGFR. p-value shows unpaired t-test of significance. (3.4E) RPPA time course of AU565 and HCC-1954 cells treated with 250 nM lapatinib. y-axis shows mean (n = 3) signal intensity of each phospho-protein vs its respective total protein, with each signal normalized to its DMSO treated control cohort at each time point, representing change in protein activity over 72 hours of treatment. Top 3 proteins are canonical constituents of the PI3K/MTOR pathway, bottom are canonical constituents of the MAPK pathway. Data provided by ©Mills et al., used with permission. (3.4F) GI50 graphs and SEM (n = 3) of CTG assays from HER2E and L-HER2+ cell lines treated for 72 hours with a dose range of lapatinib, trametinib, and the combination.

We previously performed reverse phase protein array (RPPA) analysis on HER2+ cell lines treated with 250 nM lapatinib over a timecourse, examining PIK3CA mutation effects on lapatinib response [196]. We re-examined this data in the context of HER2 subtype to identify the pathways primarily affected by lapatinib treatment. Figure 3.4E shows that lapatinib preferentially inhibited activity of PI3K-MTORC pathway constituents in AU565 compared to HCC-1954, and inhibited activity of EGFR and MEK in HCC-1954 compared to AU565. We also assessed pathway use in L-HER2+ and HER2E lines by measuring their responses to HER2 and MEK inhibitors. Specifically, we treated the HER2E cell lines JIMT1, HCC-1954, 21MT1, 21PT1, and HCC3153, and the L-HER2+ lines SKBR3, BT474, AU565, MDAMB361, and EFM192A with 9 different concentrations of lapatinib, the MEK inhibitor trametinib, and the combination. Figure 3.4F shows that the L-HER2+ lines were less sensitive to the MEK inhibitor, and more sensitive to lapatinib than HER2E lines. HER2E lines showed far more senstitivity to trametinib than L-HER2+ lines, and the combination of lapatinib and trametinib resulted in significantly decreased cell viability in comparison to each agent alone. This suggests that HER2E lines rely more on MAPK signaling than PI3K signaling compared to L-HER2+ lines.

3.3.6. *Countering microenvironment mediated resistance*

Our studies suggest that the HGF mediated attenuation of response of HER2E cells to lapatinib or neratinib is due to the constitutive high level expression of MET in HER2E cells. In environments where HGF is present, HGF activation of MET allows HER2E cells to escape lapatinib inhibition. This raised the possibility that combined treatment of HER2E cells (but not L-HER2+ cells) with lapatinib and the MET targeting TKI, crizotinib, to block signaling through MET would be effective. Figures 3.5A, and Supplemental Figure S3.4A shows this to be the case.

Table 3.1. L-HER2+ and HER2E cells lines exhibit differential regulation of MAPK and estrogen receptor pathways.

Gene Sets Enriched in L-HER2+ vs HER2E	Set Size	ES[a]	NES[b]	NOM p-val[c]	FDR q-val[d]	FWER p-val[e]	Rank at MAX
HALLMARK_ESTROGEN_RESPONSE_LATE	197	0.399	1.435	0.003	0.080	0.179	3989
HALLMARK_KRAS_SIGNALING_DN	196	0.376	1.340	0.003	0.098	0.375	3186
CHARAFE_BREAST_CANCER_LUMINAL_VS_MESENCHYMAL_UP	409	0.718	2.740	0.000	0.000	0	4656
CHARAFE_BREAST_CANCER_LUMINAL_VS_BASAL_UP	331	0.723	2.728	0.000	0.000	0	3968
DOANE_BREAST_CANCER_ESR1_UP	105	0.734	2.410	0.000	0.000	0	3184
SMID_BREAST_CANCER_ERBB2_UP	137	0.640	2.171	0.000	0.000	0	3999
LIM_MAMMARY_LUMINAL_MATURE_UP	112	0.585	1.948	0.000	0.004	0.108	4358
SMID_BREAST_CANCER_LUMINAL_B_UP	160	0.529	1.846	0.000	0.019	0.512	5542
Gene Sets Enriched in HER2E vs L-HER2+							
HALLMARK_EPITHELIAL_MESENCHYMAL_TRANSITION	196	-0.674	-2.265	0.000	0.000	0	4041
HALLMARK_TNFA_SIGNALING_VIA_NFKB	189	-0.671	-2.226	0.000	0.000	0	4687
HALLMARK_KRAS_SIGNALING_UP	195	-0.579	-1.932	0.000	0.000	0	4596
CHARAFE_BREAST_CANCER_LUMINAL_VS_BASAL_DN	421	-0.804	-2.875	0.000	0.000	0	3540
CHARAFE_BREAST_CANCER_LUMINAL_VS_MESENCHYMAL_DN	431	-0.793	-2.855	0.000	0.000	0	3662
WU_CELL_MIGRATION	175	-0.675	-2.230	0.000	0.000	0	3196
VANTVEER_BREAST_CANCER_ESR1_DN	228	-0.651	-2.191	0.000	0.000	0	5062
GO_EXTRACELLULAR_STRUCTURE_ORGANIZATION	297	-0.553	-1.934	0.000	0.040	0.062	3607

Legend: a = Enrichment Score, b = Normalized Enrichment Score, c = Nominal p-value, d = False Discover Rate q-value, e = Familywise error rate p-value

Table 3.1. L-HER2+ and HER2E cell lines exhibit differential regulation of MAPK and estrogen receptor pathways. Table of selected significantly enriched gene sets (false discovery rate q-value < 25%, and nominal p-value < .01) for GSEA comparisons of 8 L-HER2+ (AU565, SKBR3, BT474, EFM192A, EFM192B, EFM192C, UACC812, ZR7530) and 8 HER2 cell lines (JIMT1, 21MT1, 21MT2, 21PT, 21NT, HCC1954, HCC3153, HCC1569). Top table shows gene set enriched in comparison of L-HER2+ vs HER2E, bottom table depicts gene sets enriched in the reverse comparison.

Our studies also suggest the mechanisms by which NRG1β and lapatinib lead to immediate growth stimulation in L-HER2+ cells. This seems to be a multistep process that begins with lapatinib treatment triggering increased HER3 on the cell surface [125, 126], as a result of a feedback mechanism caused by loss of pAKT levels. This is then followed by NRG1β binding to HER3 thereby stabilizing HER2-HER3 heterodimers. We employed proximity ligation assays (PLAs) to assess lapatinib induced differences in HER2-HER3 dimerization on the cell surface of the L-HER2+ line SKBR3, and the HER2E line HCC-1954 treated with combinations of lapatinib, and NRG1β. This analysis revealed a significant increase in heterodimers on the cell surface in L-HER2+ lines under exposure to the combination of lapatinib and NRG1β following 48 hours of treatment (Figure 3.5B). No such increase was observed in HCC-1954 (Figure 3.5C). Structual studies of ErbB family kinase domains [100, 101] suggest that the HER2-HER3 heterodimerization mediated by NRG1β changes the conformation of the ATP binding pocket of HER2 [99] so that lapatinib and neratinib efficacy is reduced. With this insight, we reasoned that treatment of the NRG1β-HER2-HER3 complex with pertuzumab to disrupt HER2-HER3 dimerization might restore the conformation of the ATP binding pocket to increase lapatinib or neratinib binding efficacy. Figure 3.5D and Supplementary Figure S3.4B show this to be the case. Interestingly, in the absence of NRG1β, pertuzumab had no effect as a single agent and did not improve growth inhibition when combined with lapatinib in SKBR3. Pertuzumab also had no effect on HGF mediated resistance in HCC-1954.

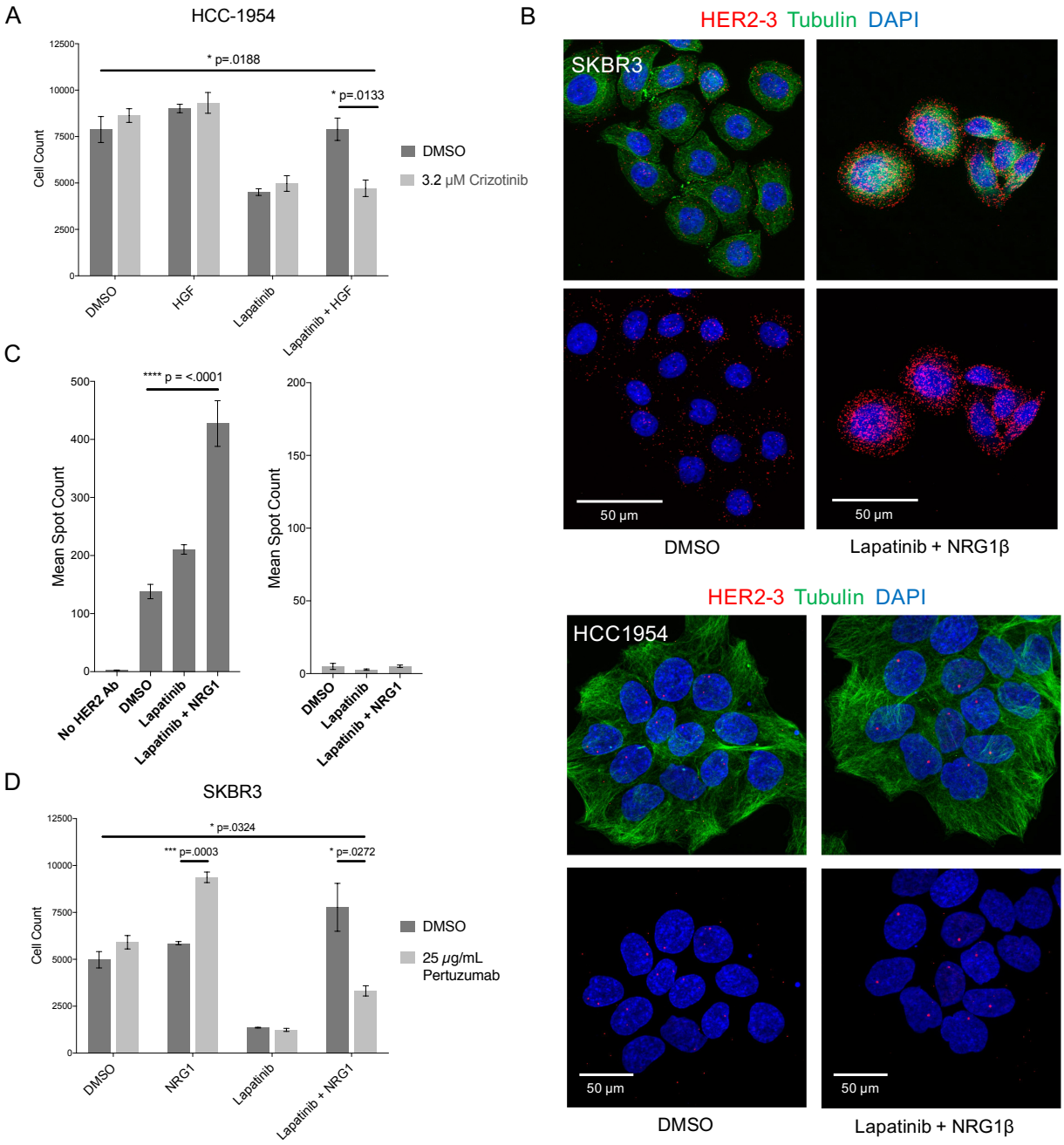

Figure 3.5. HER2E and L-HER2+ lines show differential reliance on MAPK and PI3K signaling. (3.5A) Mean cell count and SEM (n = 3, BR = 3) of HCC-1954 under 72 hours of exposure to combinations of 3.2 µM crizotinib, 500 nM lapatinib and 50 ng/ml HGF. p-value shows unpaired t-test of significance. (3.5B) Maximum projection fluorescent images of SKBR3 and HCC-1954 cells treated for 48 hours with combinations of 500 nM lapatinib and 12.5 ng/mL NRG1β. Cell nuclei imaged with DAPI (blue), β-tubulin (green), and HER2-HER3 heterodimers (red) imaged by PLA. Image data provided by © Koei Chin and ©Ting Zheng, used with permission. (3.5C) Mean and SEM of PLA spot counts for SKBR3 (n = 79, 93, 150, 54) and HCC-1954 (n = 52, 60, 54) treated for 48 hours with DSMO, 12.5 ng/ml NRG1β, 500 nM lapatinib, and the combination. p-value shows unpaired t-test of significance. Quantification provided by Michel Nederlof, used with permission. (3.5D) Graph of mean cell count and SEM (n = 3, BR = 3) of SKBR3 under 72 hours of exposure to combinations of 25 µg/ml pertuzumab, 500 nM lapatinib and 50 ng/ml NRG1β. p-value shows unpaired t-test of significance.

3.4. Discussion

This study shows the utility of MEMAs as a high throughput platform for identification of specific soluble and insoluble factors from the microenvironment that can significantly alter the responses of cancer cells to therapeutic agents. The power of the platform comes from its utility in quickly assessing the effects of thousands of different microenvironments in multiple cell lines. We assessed here the impact of >2500 microenvironments on responses of proliferative indicators of response to the TKI lapatinib. However, the platform is generally applicable to assessing the impacts of microenvironmental signals on any phenotype that can be revealed using fluorescent reporters or other indicators that can be quantified using imaging.

The present study reveals several important features of HER2+ breast cancer. First, our studies show that several soluble and insoluble proteins from the microenvironment alter the efficacy of the TKIs lapatinib and neratinib and that their effects differ between the HER2E and L-HER2+ subtypes of HER2+ breast cancer. We show that these differences derive primarily from preferential dependence of L-HER2+ cells on PI3K signaling and increased HER3 expression and preferential dependence of HER2E on MAPK signaling and increased MET expression. These subtype differences suggest that the HER2E and L-HER2+ subtypes should be treated biologically and clinically as separate diseases. On a more general level, this paper demonstrates that the behavior of cells grown *in vitro* are dependent on the exact composition of the culture environment and may provide some biological understanding of why experimental results are sometimes not reproducible between laboratories.

Remarkably, we found that L-HER2+ cells treated with lapatinib or neratinib grew faster than untreated control cells when microenvironmental factor, NRG1β was present. In other words, NRG1β converts lapatinib or neratinib into stimulatory drugs. We attribute this to a PI3K pathway mediated upregulation of HER3 in response to lapatinib coupled with a NRG1β mediated change in the conformation of the

HER2-HER3 complex that reduces the efficacy of the TKIs. This is a process that leaves the TKI treated cells with more HER2-HER3 heterodimers on the cells surface and alters the ATP binding pocket of HER2 so that the TKIs are less effective. We show that this NRG1β mediated resistance mechanism can be reversed by adding pertuzumab to defeat the NRG1β mediated conformational change that renders lapatinib ineffective. There are of course other strategies that might be deployed to defeat NRG1β mediated resistance including co-treatment with drugs to inhibit PI3K pathway feedback mediated upregulation of HER3, treatment with antibodies targeting NRG1β [130] or designing small molecule inhibitors that are effective against the HER2 kinase in the altered configuration as proposed by Shokat et al. [99].

We also show that HGF renders HER2E cells resistant to lapatinib and neratinib although the HGF does not convert the TKIs to stimulatory agents. We attribute the HGF mediated resistance to activation of signaling through MET that is constitutively expressed on the HER2E cells and we show that this can be blocked by cotreating with the TKI and crizotinib. This had been independently reported by Settleman et al. [255] in the HER2E line HCC-1954 for lapatinib response.

Taken as a whole, this study shows that HER2E and L-HER2+ tumors should be treated as different diseases that respond differently to treatment and to signals from the microenvironment. This difference in HER2 subtype biology is consistent with results from a recent clinical study from Perez et al [189] that showed that L–HER2+ tumors respond better to trastuzumab than HER2E tumors. Our study also suggests that the responses to treatment of L-HER2+ and HER2E tumors may vary between metastatic sites due to differential expression of microenvironmental proteins between these sites. For example, HGF and NRG1β are highly expressed by CAFs at the site of the primary tumor [79, 216]. Outside of mammary tissue HGF is highly expressed in the liver and lung [68], common sites of HER2+ ER- (HER2E) metastasis, while NRG1β is highly expressed at common sites of HER2+ ER+ (L-HER2+) metastasis including the lung, lymph node, and brain [68, 266].

Exact measurements of localized concentration of secreted HGF and NRG1β in human tissue is under-studied, but what data is available shows the concentration range we tested (3.125-200 ng/ml) to be relevant to *in vivo* human biology. The concentration of HGF secreted by patient derived bone marrow stem cells (BMSCs) was found to be in the range of 2-12 ng/ml [267]. The incidence rate of HER2E metastasizing to bone is 30.1% [152]. Pleural effusions from cancer patients found concentrations of HGF anywhere from 0.5 to 11 ng/ml [268], and the incidence rate of lung metastasis for HER2E is 24.1% [152]. Local concentrations of NRG1β is even less well studied, but serum levels have been found to be in the range of 5-700 ng/ml [269]. Assays on pulmonary fluid have found NRG1β concentrations in the range of 50 ng/ml up to 10,000 ng/ml in patients with acute lung injury [94]. L-HER2+ breast cancer has a lung metastasis incidence rate of 17.7% [152]. This data suggests that both HER2E and L-HER2+ cancer cells can encounter growth factor concentrations *in vivo* within the range we have tested *in vitro*, and that this can occur in common sites of HER2+ breast cancer metastasis.

Going forward, we suggest that treatment strategies for HER2+ tumors should be devised that take into account the biological differences between HER2E and L-HER2+ tumors as well as variations in the expression of microenvironmental signals that differ between metastatic sites.

3.5. Experimental Procedures

3.5.1. *Cell Lines*

Breast cancer cell lines AU565, SKBR3, HCC-1954, HCC-1569, HCC-202, HCC-2218, HCC-1419, MDA-MB-361, SUM190PT, ZR-75-30, BT474, UACC893, and MDA-MB-453 were obtained from American Type Culture Collection (ATCC), Manassas, VA. HCC-3153 was obtained from UT-Southwestern, SUM190P and SUM225CWN were provided by Steve Ethier at UCSF, and 21NT1,

21PT1, and 21MT1 were provided by Ruth Sager and Kornelia Polyak at the Dana-Farber Institute of Harvard, Cambridge MA. JIMT1, EFM192A, EFM192B, and EFM192C were obtained from DSMZ, Braunschweig Germany. Each cell line was genotyped to ensure accurate identity, and regularly screened for mycoplasma infection. The generation of SKBR3 and HCC-1954 cell lines expressing nuclear localized GFP has been previously described [270]. Cell lines were maintained in their respective medium as recommended by ATCC at 37°C in 5% CO2 in a humidified incubator and cultured according to ATCC recommendations.

3.5.2. *MicroEnvironment MicroArrays*

MEMAs were generated in 8-well cell culture plates. A manuscript detailing the preparation and use of the MEMA is underway. A detailed description of the methodology and protein library is currently available at the Synapse MEP-LINCs website (https://www.synapse.org/#!Synapse:syn2862345/wiki/72486). Briefly, $2.5x10^5$ cells of each cell line were added to replicate arrays for 15 minutes, after which unbound cells were removed with a medium wash. Arrays were cultured in RPMI medium with 10% FBS for 12 hours at 37°C in 5% CO2 in a humidified incubator. Following this, appropriate concentrations of soluble ligands were added to duplicate sets of arrays, one of which was treated with 750 nm lapatinib, and the other DMSO. Arrays were returned to incubator for 71 hours, following this 1uM EdU was added to the medium for 1 hour. Cells were then fixed in 2% PFA, and stored at 4^0C in PBS.

Array-bound cells were permeabilized by Triton X-100, and proliferation was assessed by detection of fluorescently labeled EdU incorporation into DNA during S phase (Click-It EdU Assay kits from ThermoFisher Scientific). Following this, cells were immunofluorescently stained for KRT14 (Abcam), KRT19 (Dako), and nucleic acids by DAPI. Arrays were imaged on an automated high content fluorescent microscope platform, and resulting image data was output to an OMERO image database.

Cells were segmented and intensity levels were calculated using CellProfiler. The resulting MEMA data was preprocessed and normalized using open source R software available from (https://www.synapse.org/#!Synapse:syn2862345/wiki/72486). The spot cell count was based on the DAPI stained nuclei. EdU intensity was auto-gated to label cells as EdU^+ and the proportion of EdU^+ cells in each spot was reported to measure proliferation. The per-cell intensity values for the CK14 and CK19 stains and the nuclear morphology measurements were median summarized to the spot level. Each intensity and morphology signal was independently RUV3 normalized in a series of matrices with arrays as the rows and spots as the columns. The RUV3 controls were the residuals created by subtracting the replicate median from each spot value. After RUV3 normalization, bivariate LOESS normalization was applied to the normalized residuals using the array row and array column as the independent variables. After normalization, the ~15 replicates of each condition were median summarized to the MEP level. Major findings from MEMA were recapitulated in at least 3 experimental replicates. Exact replicate count and standard error for each condition are available in supplemental MEMA files linked to in Data Availability.

3.5.3. *Cell Line Assays and Image Cytometry*

Lapatinib Ditosylate and neratinib were purchased from Selleckchem. Recombinant human nerugulin-1-beta-1 EGF domain, and recombinant human hepatocyte growth factor were purchased from R&D Systems. Pertuzumab was made available by the OHSU Pharmacy. Exposure of cells to immobilized ECM proteins, soluble ligands, and drug treatments were performed in medium containing the recommended concentration of serum for normal cell culture conditions. Biological response to treatment was assessed using immunofluorescent labeling and high content imaging. Cells were treated in multiwell plates with soluble drug and ligand combinations added to their medium, then fixed with 2% PFA, permeabalized with Triton X-100, and monoclonal antibody labeling was used to assess protein quantity and localization of KRT19 (clone RCK108, Dako), KRT14 (clone LL002, Abcam), HER2 (clone OP15),

and HER3 (clone D22C5). Proliferation was assessed by Click-It EdU detection kits (ThermoFisher). Well plates were imaged and analyzed on the GE InCell 6000 platform. Size gating of nuclei was used to exclude apoptotic cells, and EdU positivity was determined as nuclei having a mean fluorescent intensity above an experimentally consistent threshold (this threshold was defined using single cell parametric analysis plotting total DAPI intensity against mean EdU intensity). All fluorescent imaging studies were performed at consistent intensity and gain settings across experiments.

Live-cell imaging experiments were performed on the IncuCyte ZOOM platform with SKBR3 and HCC-1954 cells transfected with a nuclear located GFP. Cell cohorts exposed to varying concentrations of NRG1β or HGF had these factors added to their medium at time zero of the time course. At 24 hours from the start of the experiment cells were exposed to requisite doses of lapatinib. Cells were fluorescently imaged every 2 hours (4 images per well), and Incucyte proprietary image analysis software quantified detected nuclei (following size gating to exclude apoptotic bodies and un-segmentable clusters).

3D assays were performed using a previously described approach of coating well plates with matrigel matrix (Corning), plating cells, and adding medium with low density matrigel [271]. Cell quantity was assessed using absorbance measurements of alamar blue stains.

Drug combination studies and CTG assays were performed as previously reported [272 273] in randomized replicates.

3.5.4. *Murine Xenograft Implantable Microdevices*

Microdose drug delivery devices were manufactured and implanted as previously described [263]. Cylindrical microdevices 4mm in length and 820 μm in diameter were manufactured from medical-grade Delrin acetyl resin blocks (DuPont) by micromachining (CNC Micromachining Center) with 18

reservoirs 200 μm (diameter) x 250 μm (depth) on the outer surface. Reservoirs were packed with approximately 1 μg of drug mixed with polymer using a tapered metal needle (Electron Microscopy Science). Growth factors and proteins were lyophilized and packed into reservoirs in the same manner.

Devices were implanted into subcutaneous BT474 xenograft tumors grown on the flanks of three 6-8 week old female Crl:NU(NCr)-Foxn1^{nu} mice (purchased from Charles River Laboratories) using a 19-gauge spinal biopsy needle (Angiotech) using a retractable needle obturator to push the device into tissue. Tumors were excised 48 hours after device implantation, fixed for 24 hours in 10% formalin, then perfused with paraffin. Specimens were sectioned using a standard microtome and sections were collected from each reservoir. Sections were then antibody stained by standard IHC using cleaved caspase-3 antibody (Cell Signaling Technology). All animal studies were conducted in accordance with protocols approved by MIT's Committee on Animal Care (CAC).

3.5.5. *Statistics and Analytics*

The reported statistics used sample means, standard error of the mean (SEM), and p-values obtained from un-paired *t*-tests of sample sizes of equivalent variance. All reported cell assays had at least 3 experimental replicates unless otherwise stated.

Clustering analysis of RNAseq data was performed using open source R statistical software and the 'gplots' library. Genes found by TCGA [260] to be differentially expressed between patient tumors identified as HER2+ and expressing the HER2E PAM50 gene signature, and those identified as HER2+ but lacking the HER2E signature, were used to cluster RNAseq data obtained on a panel of human HER2+ breast cancer cell lines. Following measurement of expression variance, the top 10% variable of the gene set were used to cluster the cell lines by Euclidean distance.

Unbiased GSEA comparisons were performed between 8 L-HER2+ cell lines (AU565, BT474, SKBR3, ZR-75-30, UACC812, EFM192A, EFM192B, EFM-192C), and 8 HER2E cell lines (JIMT1, 21MT1, 21MT2, 21NT, 21PT, HCC1569, HCC-1954, HCC3153) using the javaGSEA Desktop Application available from the Broad Institute (http://software.broadinstitute.org/gsea/index.jsp). Gene sets with nominal p-values of less than 0.001, and false discovery rate q-values of less than 25% were considered significantly enriched.

3.5.6. *Proximity Ligation Assays (PLA)*

We performed PLA to detect the interactions between the c-terminal domains of HER2 and HER3 with the Duolink PLA kit (Sigma-Aldrich) according to the manufacturer's recommendations with at least 2 biological replicates per sample, and 3 experimental replicates. Cells were exposed to growth factors and drug combinations as previously described, then fixed in 4% PFA, permeabilized with Triton X-100, and the Duolink PLA protocol was followed using HER2 (clone OP15) and HER3 (clone D22C5) antibodies purchased from Cell Signaling Technology. Because of the abundance of HER2-HER3 heterodimers, the assay was slightly modified to reduce detection of total HER2-HER3 dimers for the purpose of more accurate quantification. HER2-HER3 heterodimers were detected as single fluorescent dots in z-series of cells imaged with confocal microscopy. Additionally, cell nuclei were fluorescently stained with DAPI, and cellular cytoskeletons were labeled with tubulin antibody staining. The image analysis software CellProfiler (http://www.cellprofiler.org) was used to quantify the PLA signal.

3.5.7. *Liposomal siRNA Transfection*

siRNA transfection into breast cancer cell lines in 96-well plates (AU565 7,000/well, SKBR3 7,000/well, BT474 7000/well, HCC-1954 4000/well, JIMT1 2000/well, 21MT1 1000/well, and HCC3153 2000/well)

was performed by reverse transfection by using Dharmafect (Dharmacon) as previously described [274]. Four single siRNA oligos (Dharmacon HER3 J-003127-10, J-003127-11, J-003127-12, and J-003127-13, 12 nM each) were used for HER3, and non-targeting siRNA (Dharmacon siCONTROL) was used as a control. Following 96 hours of treatment with siRNA, cells were assayed for viable cell count as described above and the average cell count resulting from treatment with the 4 HER3 oligos was reported.

3.5.8. *Immunoblot Assays*

Cell lysates were collected using Nonidet-P40 lysis buffer, supplemented with Halt protease and phosphatase inhibitor cocktail (Thermo Scientific) and immunodetection of proteins was carried out using standard protocols. The antibodies HER2 (clone 29D8), pHER2 (Y1221/1222, clone 6B12), HER3 (clone D22C5), pHER3 (Y1298, clone 21D3), panAKT (clone C67E7), pAKT (S473, clone D9E), S6 (clone 54D2), pS6 (S235/236, clone D57.2.2E), ERK1/2 (clone 137FS), and pERK1/2 (T202/Y204, clone D13.14.4E) were all purchased from Cell Signaling Technologies.

3.5.9. *Reverse Phase Protein Arrays*

RPPA and analysis were performed as previously described [275] on cell lysates obtained from HCC-1954 and AU565 cells treated for 0.5, 2, 4, 8, 24, 48, and 72 hours with 250 nM lapatinib in full serum medium.

3.5.10. *RNAseq*

RNAseq analysis of purified mRNA from cell lysate was performed by our group as previously described [261].

3.6. Supplemental Figures

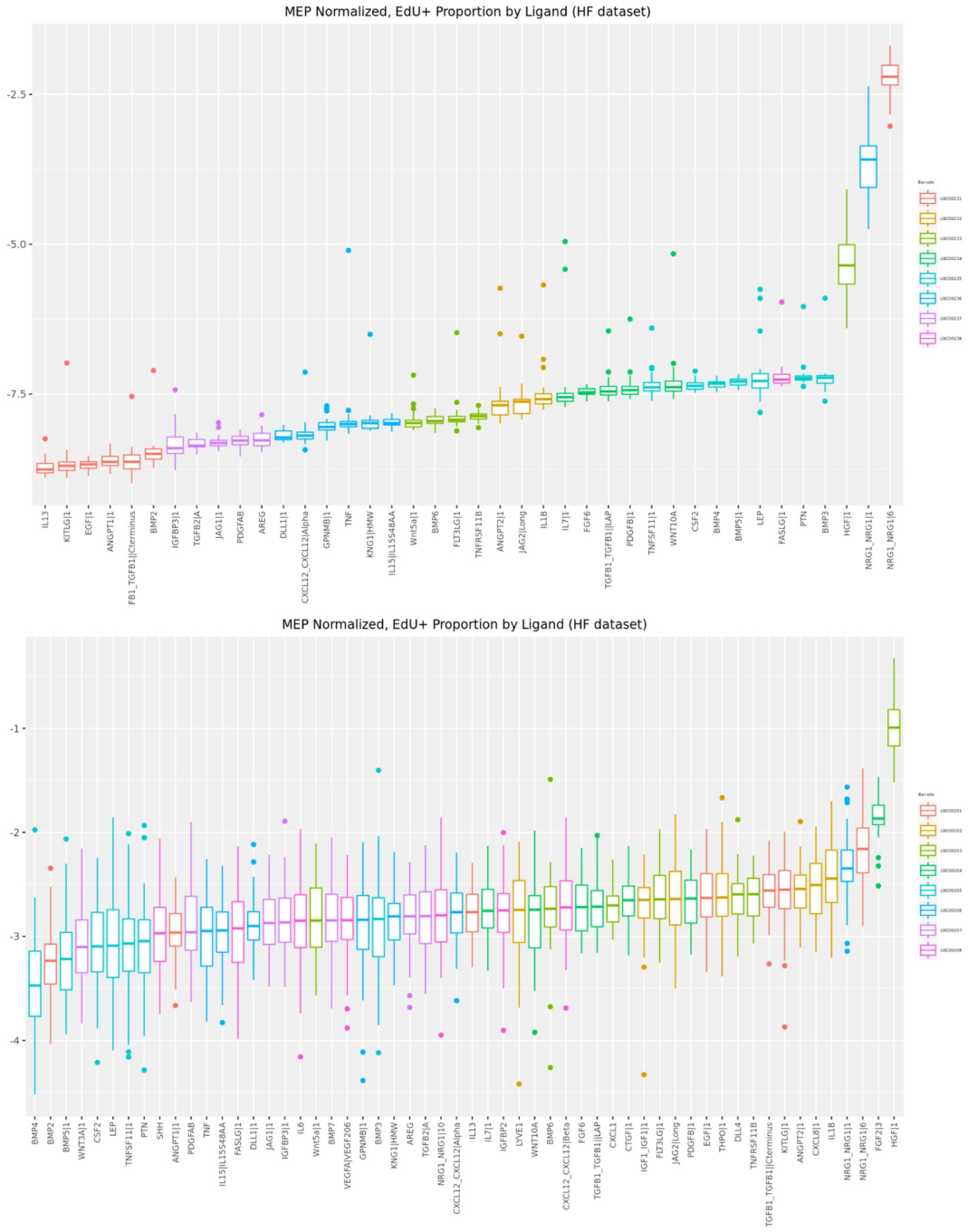

Supplemental Figure S3.1. MEMA analysis and validations reveal small subset of mutually exclusive ligands that rescue HER2+ subtypes from lapatinib treatment, and ECM/ligand combinations that modulate these effects. Box plots of normalized EdU+ proportion (n = 15, mean, upper & lower quartile, min & max, with outliers) of AU565 and HCC-1954 following 72 hours of lapatinib exposure on MEMAs. Data analysis provided by ©Mark Dane, used with permission.

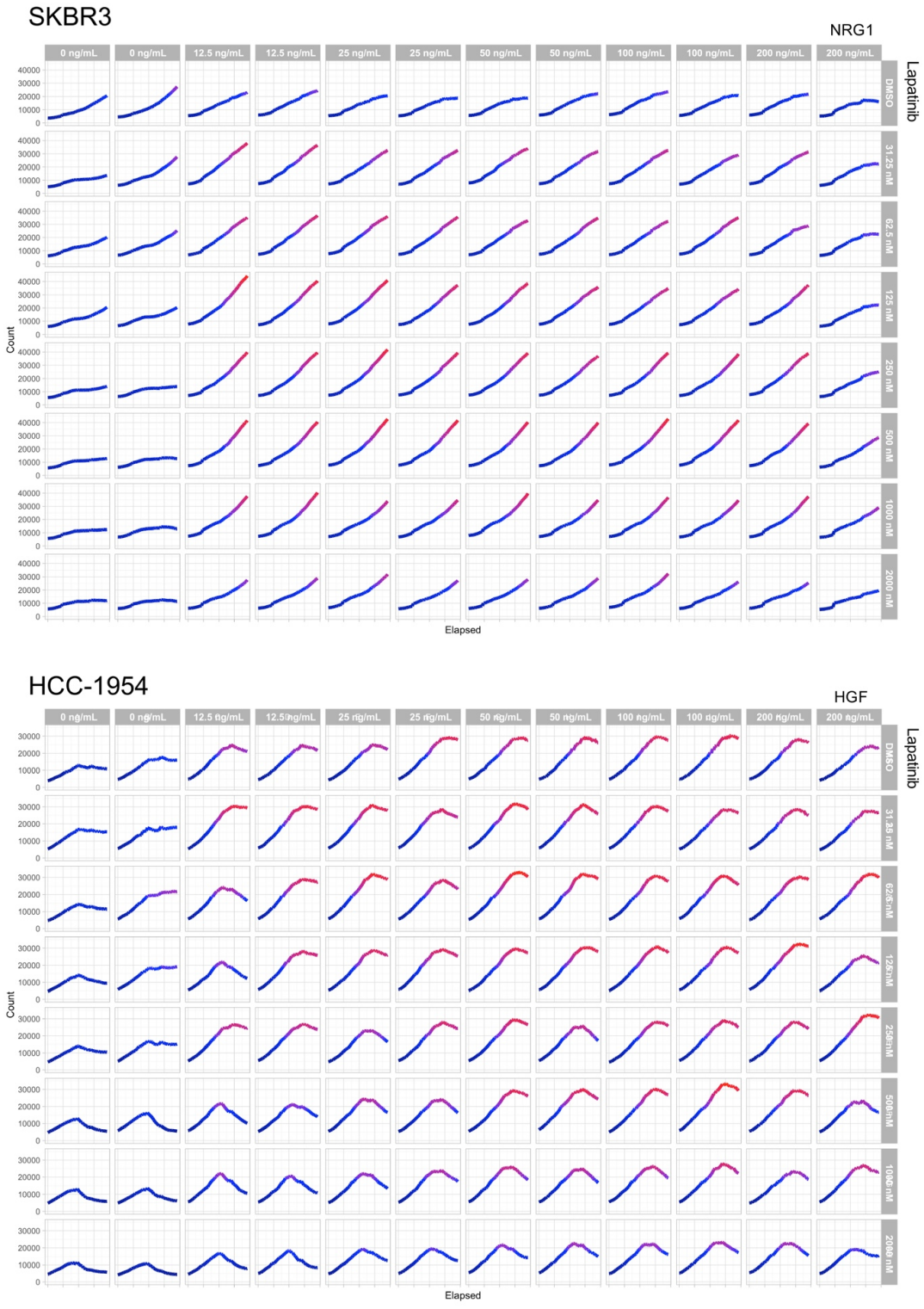

Supplemental Figure S3.2. Live-cell Imaging reveals a range of concentrations of lapatinib and NRG1β or HGF that either restore proliferation, or enhance it over DMSO treated controls. Line graphs of cell count over 96 hours taken every 2 hours for a dose range of lapatinib versus a concentration range of NRG1β (for SKBR3), or HGF (for HCC-1954). Cohorts exposed to NRG1β or HGF had ligand added from the start of the experiment. For drug treated cohorts in both cell lines lapatinib was added 24 hours from the start of the experiment. Red indicates cell count in excess of untreated controls.

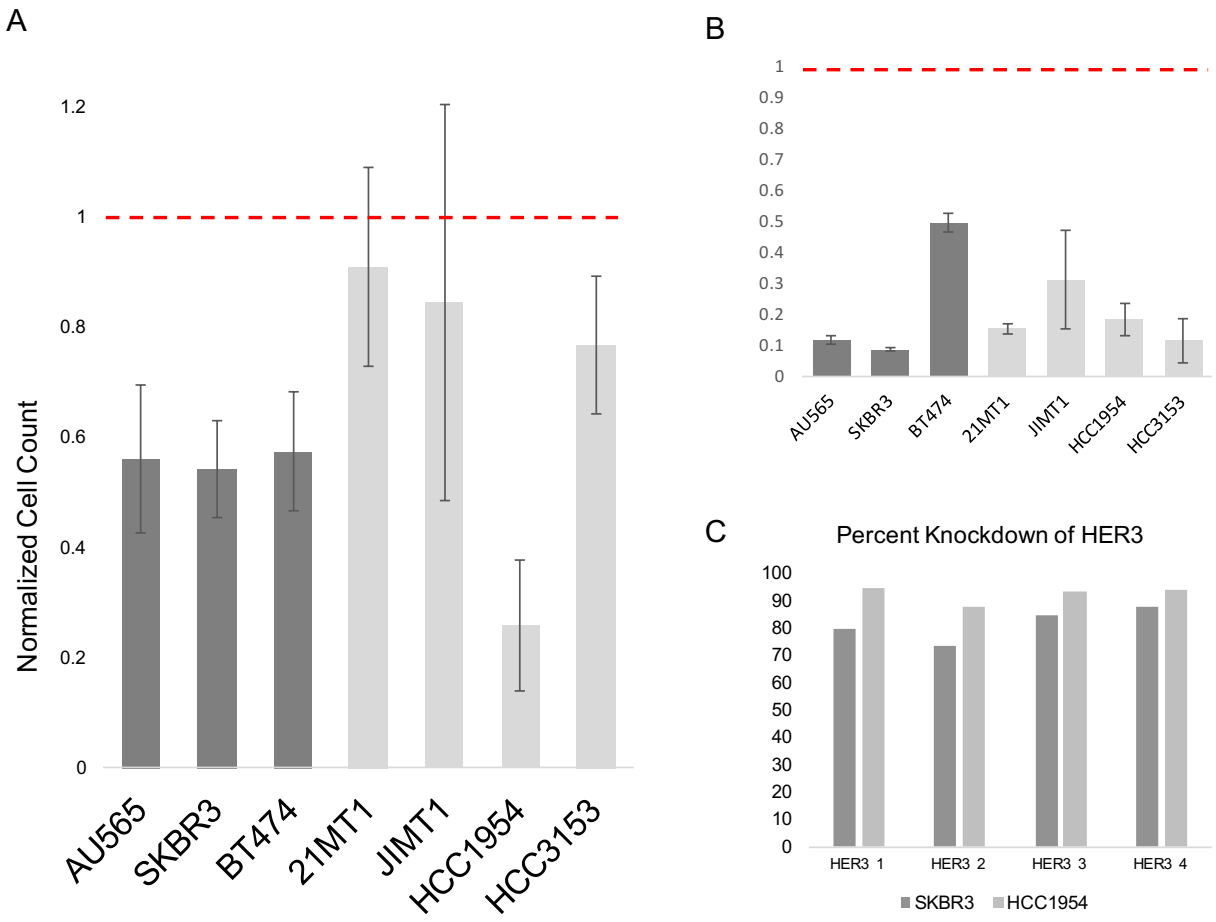

Supplemental Figure S3.3. HER2E cell lines are less sensitive to HER3 siRNA knockdown than L-HER2+ lines. (S3.3A) Ratio of mean cell count and SEM (n = 3) of cell lines following 96 hours of HER3 knockdown, normalized to cohorts treated with scrambled siRNA control. Red line indicates baseline cell count. (S3.3B) Mean cell count and SEM (n = 3) of cell lines following 96 hours of HER2 knockdown, normalized to cohorts treated with scrambled siRNA control. Red line indicates baseline cell count. (S3.3C) Quantification of Western blot analysis of HER3 protein level in SKBR3 and HCC-1954 cell lysate following 48 hours of HER3 siRNA knockdown compared to scrambled siRNA controls.

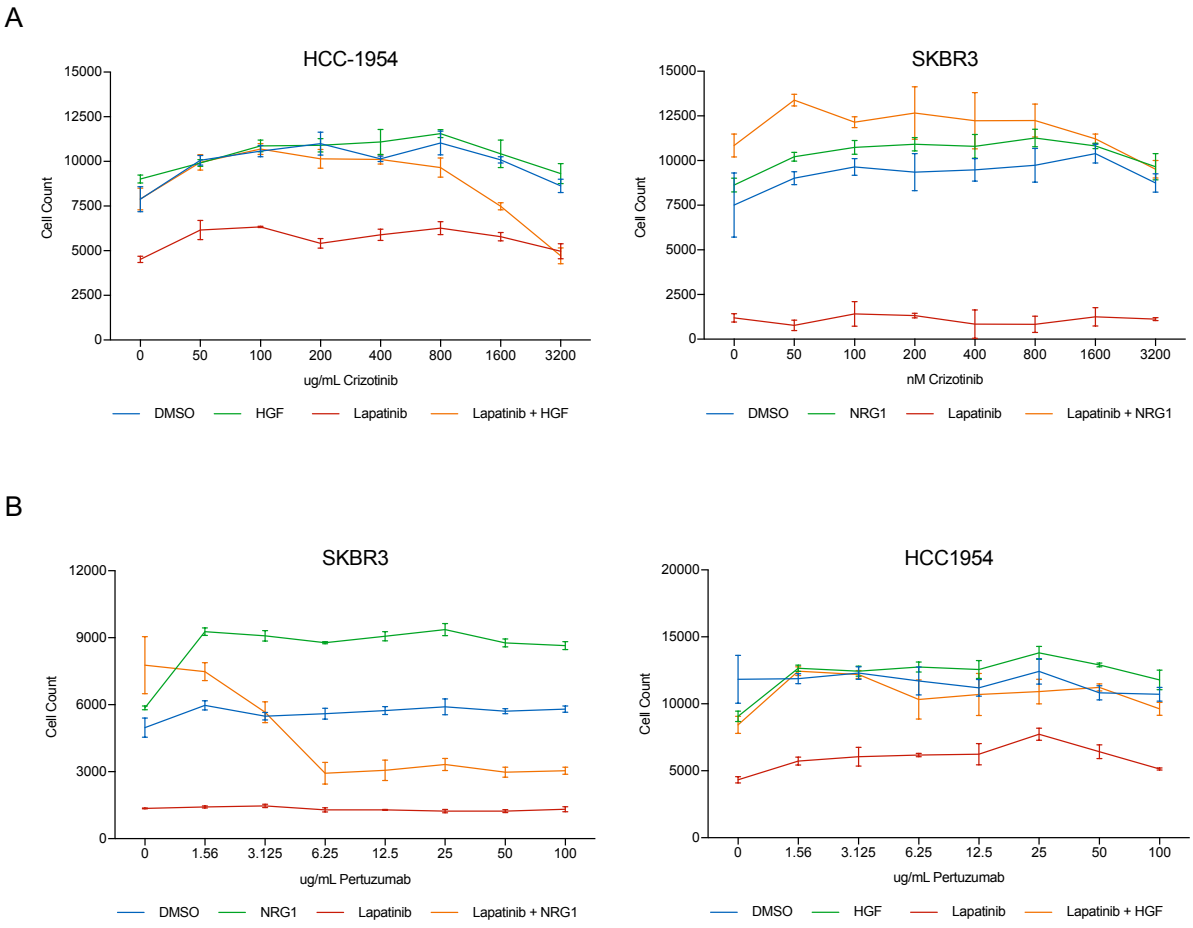

Supplemental Figure S3.4. HER2+ subtype specific resistance mechanisms can be ablated by combination treatment with either pertuzumab or crizotinib. (S3.4A) Line graphs of mean cell count and SEM (n = 3) of SKBR3 and HCC-1954 cells treated for 72 hours with combinations of 500 nM lapatinib, 50 ng/mL NRG1β of HGF, and a dose range of crizotinib. (S3.4B) Line graphs of mean cell count and SEM (n=3) of HCC-1954 and SKBR3 cells treated for 72 hours with combinations of 500 nM lapatinib, 50 ng/mL HGF or NRG1β, and a dose range of pertuzumab.

Chapter 4. Supporting Evidence and Additional Findings

The experimental studies in this work support the findings and concepts of the thesis, but are not currently in press

4.1. Mechanistic Summary

The study in Chapter 3 provides strong evidence for the mechanistic model depicted in Figure 4.1. This model shows a prototypical HER2+ breast cancer cell with overexpression of HER2 on the cell surface, resulting in increased HER2 homodimer or HER2/EGFR heterodimer mitogenic signaling. Previous studies of HER2 amplified cells have shown that the most common ErbB pairing at baseline conditions is the HER2 homodimer, followed by the HER2/EGFR heterodimer [124]. HER2-HER3 heterodimers, or HER3-EGFR heterodimers appear to be far less prevalent, likely because HER3 is predominantly maintained the in endosomal compartment of the cytoplasm [124, 126]. The most common mitogenic pathways utilized by these receptor pairs are the PI3K/AKT/mTOR or MAPK pathways, and pathway analysis in Figure 3.3F suggests that the ribosomal protein S6 appears to be a major downstream regulator of proliferative signaling for both. Treatment with the TKIs lapatinib or neratinib inhibits the kinase activity of both HER2 and EGFR, which inhibits the mTOR and MAPK pathways, resulting in cessation of proliferation or cell death. However, while this model of signaling and inhibition may hold true for a single cell in a plastic dish, it does not account for microenvironmental influences found *in vivo*, nor the heterogeneity of HER2+ cancer cells. As the study in Chapter 3 suggests, HER2+ cancers comprise at least two biologically distinct diseases that respond differently to their surrounding environments. Our data indicates that a HER2E cancer cell in an environment high in HGF can utilize MET signaling to

bypass lapatinib or neratinib inhibition, and restore proliferation in the presence of the drug. Conversely, a L-HER2+ cancer cell in a high NRG1β environment can form HER2-HER3 heterodimers, which greatly decreases the binding affinity of lapatinib, and renders the drug ineffective at inhibiting HER2. By targeting these resistance mechanisms specifically with crizotinib to inhibit MET, or pertuzumab to alter HER2-HER3 dimerization, sensitivity to lapatinib or neratinib in each specific HER2+ subtype can be restored.

The mechanistic model of drug resistance proposed in this thesis involves the interconnected mechanisms of cell extrinsic signaling proteins, cell intrinsic processing of those signals, mammary lineage differentiation, recapitulation of cell-of-origin expression patterns by cancer cells, and response of all these features to drug treatment. The study in Chapter 3 did not address all of these factors, and instead focused specifically on the mechanisms of response to NRG1β and HGF between the subtypes of HER2+ breast cancer. However, the project produced additional data not included in the narrative of Chapter 3 that further supports the above mechanistic model. Chapter 2 addressed how the MEMA experiment influenced expression of differentiation markers in representatives of luminal and basal HER2+ breast cancer cell lines. The following sections of this chapter will discuss additional findings related to the interconnected mechanisms involved in drug resistance.

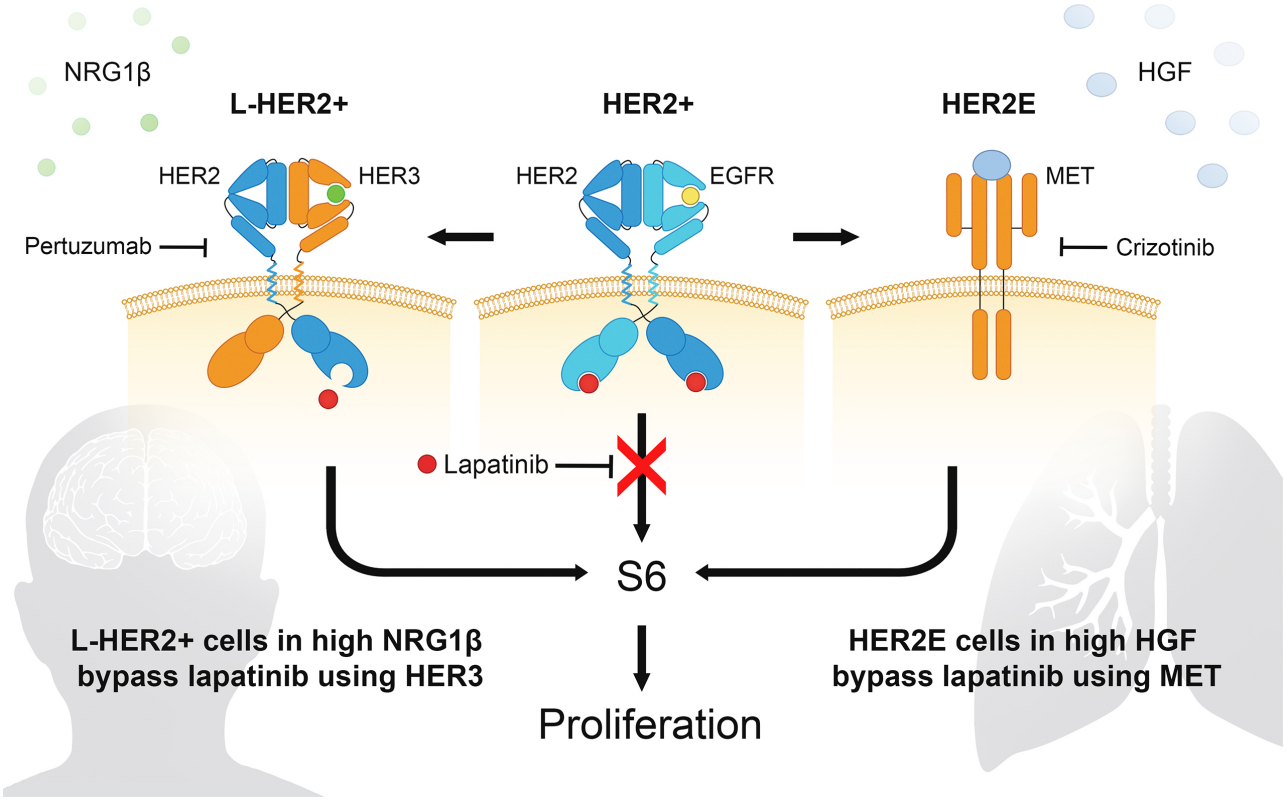

Figure 4.1. Proposed model of microenvironment mediated resistance in HER2+ subtypes. Graphic depicts how the normal mechanism of targeted HER2 inhibition is complicated by the interplay of subtype heterogeneity and microenviornmental conditions in HER2+ breast cancer. L-HER2+ cells are resistant to lapatinib in high NRG1 environments, and HER2E cells are resistant in high HGF environments. These mechanisms can be specifically blocked by the addition of pertuzumab to target HER-HER3 dimers, or crizotinib to target MET signaling.

4.2. Cell Adhesion Proteins Enhance Growth Factor Mediated Drug Resistance

Data from the lapatinib MEMA study demonstrated that multiple immobilized proteins present in the printed spots were capable of modulating the drug resistance effects of the soluble ligands for cell lines AU565 and HCC-1954. In particular, nidogen protein prevented both cellular adhesion and proliferation, even in the absence of drug treatment, potentially recapitulating its previously discussed biological role in the basement membrane as a barrier to stromal invasion. The mechanisms behind these effects could not be fully characterized during the study. However, validation studies yielded an interesting result. The follow up studies on how ECM and cell adhesion proteins influenced ligand-mediated drug resistance focused on 4 different immobilized proteins, and the soluble growth factors NRG1β and HGF. The immobilized proteins included 2 ECM proteins (collagen I and laminin), and 2 cell adhesion proteins (desmoglein II (DSG2) and E-cadherin), which were coated to the surface of 96-well cell culture plates at identical concentrations to that used in the MEMA. AU565 and HCC-1954 cells were seeded in replicate wells, and combinations of NRG1β and HGF were added to the medium. This experimental approach served as a more traditional cell culture validation assay by scaling up the protein conditions of individual MEMA spots, by allowing for more cell growth and expansion than the MEMA spots provide.

Replicate cell cohorts exposed to each protein combination were treated for 72 hours with either 500 nM lapatinib, or a DMSO control in both cell lines. Figure 4.2 shows the cell count of each condition at the end of the experiment. Remarkably, the ability of NRG1β to convert lapatinib to a stimulant of proliferation was greatly enhanced by DSG2 in AU565 compared to uncoated plastic conditions. E-cadherin also enhanced this effect, however, both collagen I and laminin moderately abrogated the resistance effect of NRG1β. This was also observed in the HCC-1954 cell line, except that the modulatory effect is not on NRG1β signaling but on HGF. However, ECM proteins did not abrogate HGF mediated resistance as they did with NRG1β. In collagen I and laminin coated wells, cells treated with lapatinib and NRG1β outgrew untreated controls.

This experiment suggests that cell adhesion proteins enhance the effect of ligand-mediated drug resistance in both cell lines, while exposure to ECM proteins appears to reduce it. This again shows differential response to the environment between representatives of L-HER2+ and HER2E. However, the sample size of immobilized proteins in this follow-up study were too small to suggest this response was universal in juxtacrine signaling, and interrogation of the MEMA data to support this finding was inconclusive.

How proteins such as DSG2 or E-cadherin enhance NRG1β or HGF signaling remains unclear. Their roles in cell-cell adhesion and juxtacrine signaling is presently well understood, but nothing in their reported biology pertains to HER2/HER3 or MET signaling. One possibility is that they influence cell type differentiation patterns that increase expression or localization of cell surface receptors. Cellular differentiation in the mammary duct is driven by local context, and the expression of E-cadherin and DSG2 tends to be highly specific in mammary epithelial cell types. Desmogleins, along with desmocollins, are integral components of desmosomes that link cellular membranes in an epithelial layer. However, luminal mammary cells exclusively connect to each other with DSG2, while basal cells connect to each other with DSG3, and this polarity of expression has been found to be integral to mammary duct formation and cellular orientation [276]. E-cadherin, which creates adherins junctions between epithelial cells, is also highly specific to luminal cell types in the normal mammary duct and luminal-like breast cancers.

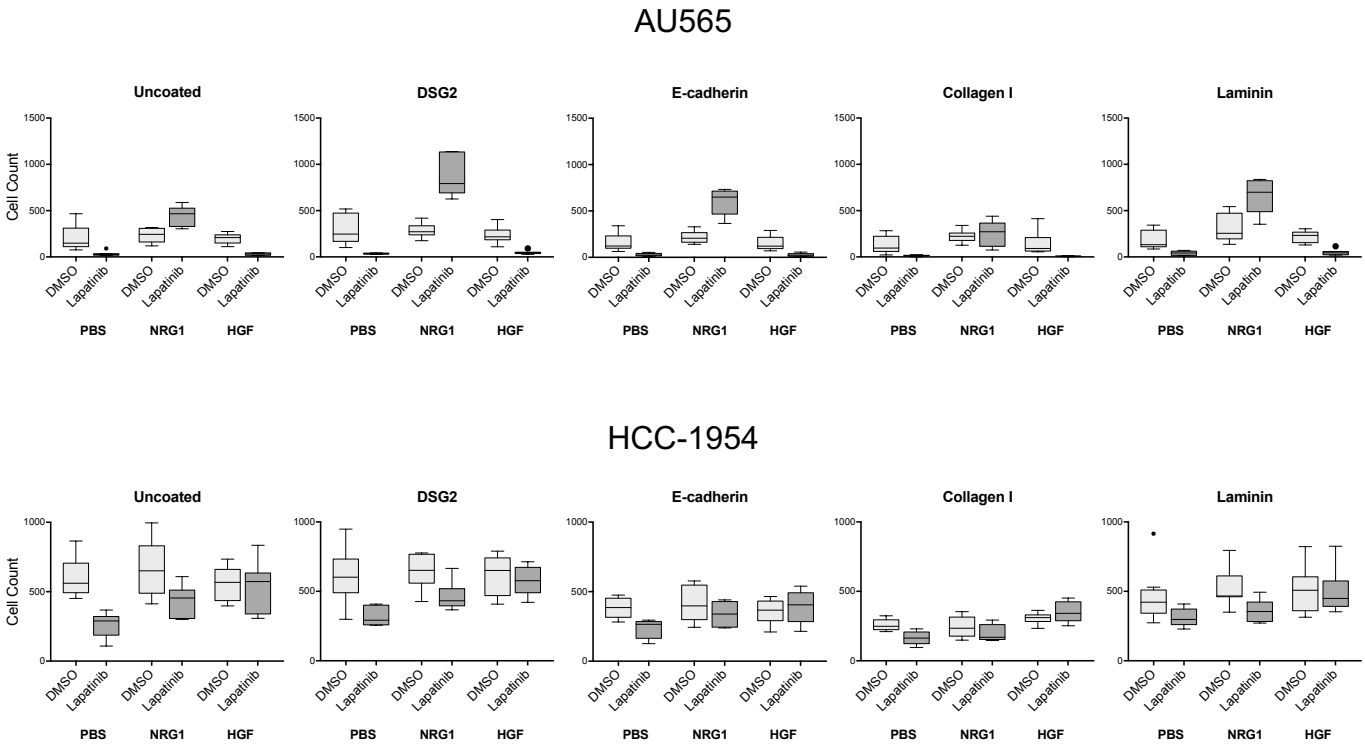

Figure 4.2. Cell adhesion proteins enhance growth factor mediated drug resistance. Boxplots show range of AU565 (top) and HCC-1954 (bottom) cell counts for replicate wells (n = 8, mean, upper & lower quartile, max & min, with outliers) coated with E-cadherin, DSG2, collagen I, laminin, or uncoated control. 50 ng/ml NRG1, 50 ng/ml HGF, or PBS control were added to cohort wells, and replicates of each condition combination were treated with 500 nM lapatinib or DMSO for 72 hours.

It may then be possible that cell-cell junction proteins like DSG2 and E-cadherin provide contextual signals that influence or reinforce cell type expression patterns, and that these have profound effects on the expression or activity of HER2/HER3 and MET signaling. However, there are other possible explanations, such as these membrane adhesion structures stabilizing cell surface signaling complexes, or activating other mitogenic pathways such as FAK signaling. These represent several intriguing and novel possibilities for drug resistance mechanisms that warrant further investigation.

4.3. Kinome Adaptation in Response to Lapatinib and NRG1β

The lapatinib MEMA study identified HER2/HER3 heterodimers and the RTK MET as mediators of NRG1β and HGF driven drug resistance respectively. However, this does not preclude the possibility of other compensatory kinases playing significant roles in resistance. Kinase expression and activity experiments on AU565 and BT474 L-HER2+ cell lines by Johnson et al. found extensive kinome adaptation in response to lapatinib treatment [202]. If kinome adaptation is playing a role in NRG1β mediated resistance, a possible explanation for the enhanced proliferation observed when L-HER2+ cells were treated with NRG1β and lapatinib is that the combined treatments could be abrogating pathway inhibition by increasing the expression of other kinases that stimulated enhanced proliferation. In this two-step model, NRG1β mediated resistance could represent an initial rescue mechanism, and later kinome adaptation stimulated by lapatinib would result in increased proliferative signaling.

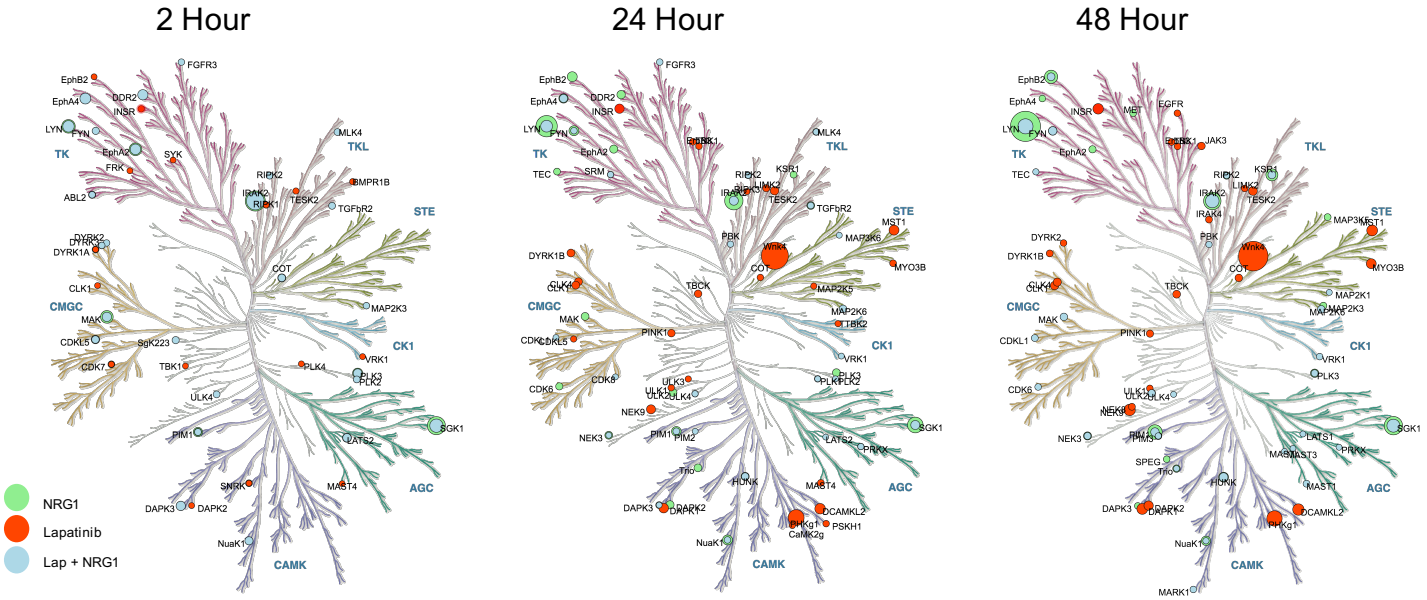

Figure 4.3. Lapatinib and NRG1 increase expression of divergent sets of kinases. KinMap diagrams of the top 15 most enhanced kinases by treatment compared to untreated controls for each time point. Mean expression of treatment at time-point (n = 3) divided by mean expression at time-zero (n = 3). Size of dot indicates relative scale of increase. 50 ng/ml NRG1β (green) and 500 nM Lapatinib plus NRG1β (blue) enhance a similar set of kinases, while lapatinib alone (red) enhances a divergent kinase set. RNAseq data analysis provided by ©Kami Chiotti, used with permission.

To put this in the context of our working model; L-HER2+ cells have several responses to lapatinib, including increased expression and surface localization of HER3, DDR1, MET, IGF-1R, and others [202]. However, these increases were observed after at least 48 hours of lapatinib treatment, and time course treatments from Chapter 3 (Figure 3.1F) showed that the increase in proliferation following lapatinib and NRG1β treatment was nearly immediate, with increased cell count observable after 2 hours. This suggests that any changes in kinase expression that are responsible for increased proliferation would need to occur in a similar time frame.

If this hypothesis were correct, identification of kinases with increased expression under both lapatinib and lapatinib plus NRG1β treatment at early and late time points would provide druggable targets that could block enhanced proliferation, and potentially abrogate NRG1β mediated resistance. We performed RNAseq experiments on triplicate samples of AU565 cells following 48 hours of treatment with 500 nM lapatinib, 50 ng/ml NRG1β, and the combination to identify kinases with increased expression under drug treatment. We obtained samples at 2, 24, and 48 hours of treatment, and compared these to an untreated time-zero control to track how gene expression changed during the course of the experiment, and to identify potentially early changes that endured through the treatment time course.

mRNA from sample lysates were purified and sequenced on the Illumina platform by the OHSU Massively Parallel Sequencing Shared Resource, and the quality control and processing of the resulting data was done by Laura Heiser, and Kami Chiotti, and I. We found extensive changes in the kinome fraction expressed in AU565 between the treatment conditions at each time point. Figure 4.3 maps the top 15 most increased kinases for each treatment condition at each time point onto the kinome tree map. The size of each dot indicates the scale of the increase over untreated controls. Kinases implicated in breast cancer progression and drug resistance and enhanced by NRG1β included EphA2, SGK1, LYN, and IRAK2. Surprisingly, some of these already had greatly increased expression after only 2 hours of exposure, such as EPHA2. Treatment with lapatinib increased a largely divergent set of kinases, similar to

those found by Johnson et al., including INSR, WNK4, EGFR, HER3, and PIK3CA [202]. The addition of NRG1β to lapatinib completely abrogated the increases seen under lapatinib alone, and instead increased the expression of kinases most similar to NRG1β alone.

The kinome adaptation data did not reveal any strong candidate kinases that showed enhanced expression under the combination of NRG1β and lapatinib. The kinases increased by this treatment were similar to NRG1β treatment alone, which does stimulate increased proliferation in this cell line. Nevertheless, we set out to target the most enhanced kinases with small molecule kinase inhibitors to test the hypothesis that they could underlie enhanced proliferation. Figure 4.4 shows AU565 cell count data following 72 hours of treatment with a range of doses for these inhibitors alone, in combination with lapatinib, NRG1β, or lapatinib and NRG1β. The inhibitors and their targets are summarized in Table 4.1. We focused on kinases that showed enhanced expression under NRG1β and lapatinib treatment at the 2-hour time point in the RNAseq data, and were maintained at an elevated level for 48 hours. We tested several agents that target downstream pathway components to determine their ability to abrogate NRG1β mediated resistance. These included mTOR inhibitors, everolimus and INK-128, the glycolysis inhibitor 2-Deoxy-D-glucose (2DG), and epigenetic modification inhibitors trichostatin A (TSA), JQ-1, panobinostat, and vorinostat.

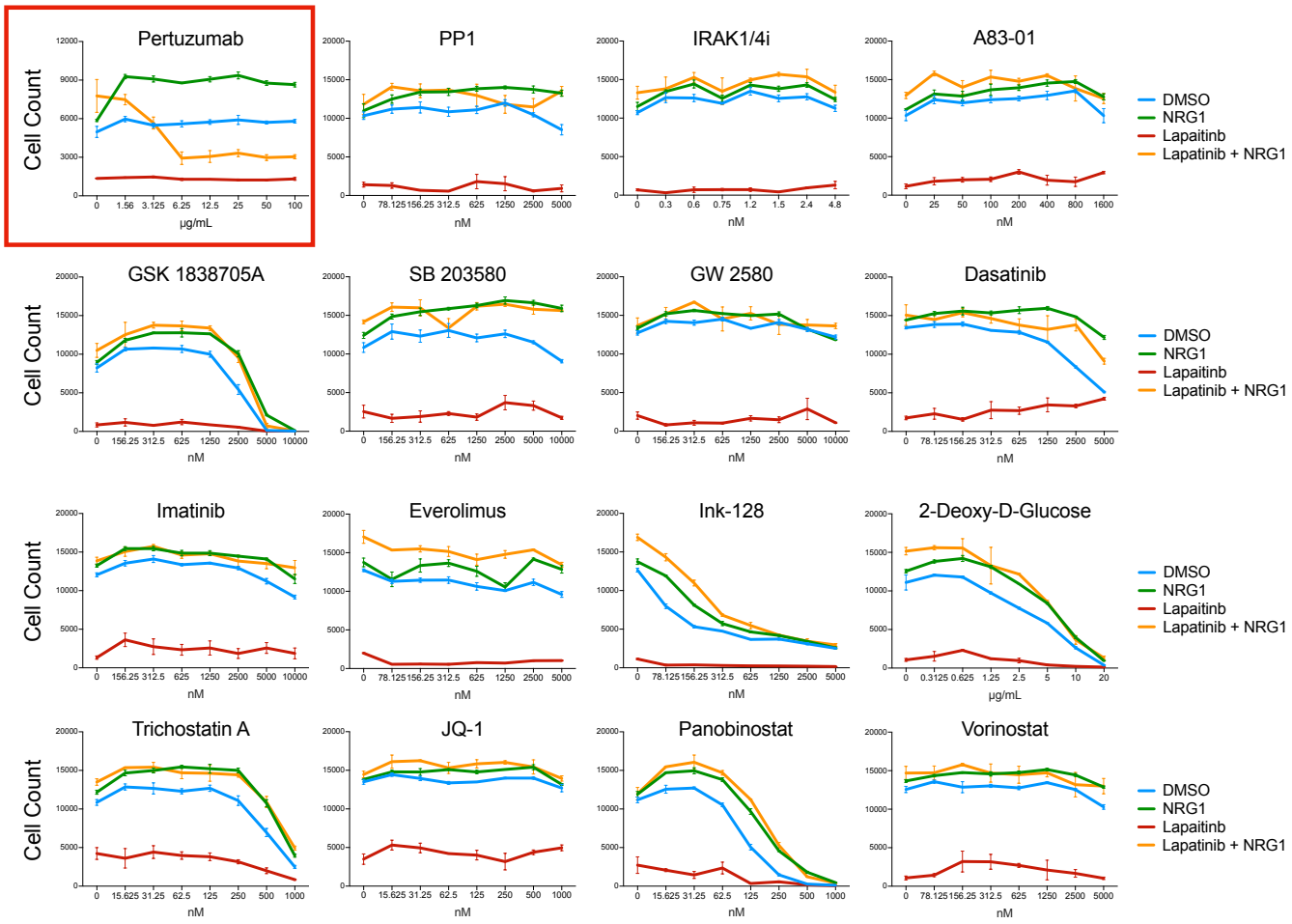

Figure 4.4. Inhibition of enhanced kinases fails to restore sensitivity to lapatinib in the presence of NRG1. Graphs show mean cell count and SEM (n = 3) graphs over a range of 7 doses for 16 inhibitors targeting kinases enhanced in kinome adaptation study, along with drugs targeting other metabolic and epigenomic response mechanisms. Replicate treatments were performed in the presence of 500 nM lapatinib, 50 ng/ml NRG1, and the combination. The top left chart for pertuzumab (from S3.4A) treatment in SKBR3 cells indicates the theoretical response for successful inhibition of NRG1 mediated resistance in AU565 cells. BR = 3.

The goal of this resistance ablation study was to find agents that were specific to NRG1β mediated resistance. Specificity is defined as agents that have no significant effect as monotherapies, but decrease the cell count of cohorts treated with lapatinib and NRG1β. As shown in Chapter 3, pertuzumab successfully met this criteria, having no effect on its own, not increasing sensitivity to lapatinib, but significantly decreasing the rescue effect of NRG1β (Figure 4.4). However, none of the other agents tested in this study could abrogate NRG1β mediated drug resistance without having a commensurate inhibitory effect on control cohorts.

The failure of targeting compensatory kinases in this study, along with the almost immediate stimulatory response seen in live-cell experiments, suggests that epigenomic mechanisms of acquired resistance are not involved in the initial stages of NRG1β mediated resistance. However, it remains a possibility that epigenetic responses, such as kinome adaptation, may play a later role. The above data further suggests that efforts to block resistance in patients with combination trials involving epigenomic remodeling inhibitors like JQ-1 may still fail in environments high in NRG1β. However, they may be successful in abrogating later kinome adaptations if the initial NRG1β mediated resistance is insufficient to block therapeutic response.

Table 4.1. Targeted agents against compensatory kinases and other biological mechanisms of NRG1 mediated resistance

Inhibitor	Class of agent	Target	Dose Range	Inhibitory	NMR Specific
Pertuzumab	mAb	HER2	1.56-100 µg/mL	No	Yes
PP1	TKI	Src	.78-5 µM	No	No
IRAK-1/4 Inhibitor I	TKI	IRAK 1/4	.3-4.8 µM	No	No
A83-01	TKI	TGF- βR, ALK 4/5	.25-1.6 µM	No	No
GSK 1838705A	TKI	IGF-1R	.16-10 µM	Yes	No
SB 203580	TKI	p83 MAPK	.16-10 µM	No	No
GW2580	TKI	CSF-1R	.16-10 µM	No	No
Dasatinib	TKI	Src, Abl	.78-5 µM	Yes	No
Imatinib	TKI	PDGF-R	.16-10 µM	No	No
Everolimus	TKI	mTORC1	.78-5 µM	No	No
Ink-128	TKI	mTORC1/2	.78-5 µM	Yes	No
2-Deoxy-D-glucose	Metaboloite	Glycolysis	.3-20 µg/mL	Yes	No
Trichostatin A	Epigenomic	HDAC Class I/II	.16-10 µM	Ye	No
JQ-1	Epigenomic	BET BRD2/3/4	.16-10 µM	No	No
Panobinostat	Epigenomic	HDAC Class I/II/IV	.16-10 µM	Yes	No
Vorinostat	Epigenomic	HDAC Class I/II	.78-5 µM	No	No

Legend: mAb = Monoclonal Antibody, TKI = Tyrosine Kinase Inhibitor, HDAC = Histone Deacetylase, NMR = NRG1 Mediated Resistance

4.4. NRG1 Exposure Results in EMT-like Differentiation in L-HER2+ Cells

We performed GSEA comparisons between samples from the above RNAseq study to identify other biological processes that might be underlying resistance. Interestingly, the most enhanced gene sets in comparisons between NRG1β treatment and control at 48-hours was the 'luminal vs basal down' gene set, indicating differentiation from the luminal phenotype to basal (Figure 4.5A). This is surprising, given that the normal role of NRG1β signaling in luminal cells is to promote luminal differentiation [48]. One of the other most significantly enhanced gene sets in this comparison was the 'luminal vs mesenchymal down' gene set, indicating a simultaneous shift towards a mesenchymal phenotype. The concordance of these two gene sets share similarities with the expression pattern of EMT.

Previous studies have shown that NRG1 can stimulate parts of the EMT expression pattern in some breast cancer cell lines, and normal luminal duct cells have an enhanced capacity for EMT [60]. Data from Chapter 3 demonstrated that NRG1β treatment alone resulted in decreased proliferation compared to controls (Figure S3.2), which may have resulted from cells undergoing EMT or otherwise differentiating into a less proliferative cell state. However, treatment with lapatinib and NRG1β resulted in the exact same gene set enrichments as NRG1β alone, but instead showed enhanced proliferation (Figure 4.5B). This suggests that epigenomic changes caused by NRG1β is unlikely to be driving changes in proliferative rate under drug treatment.

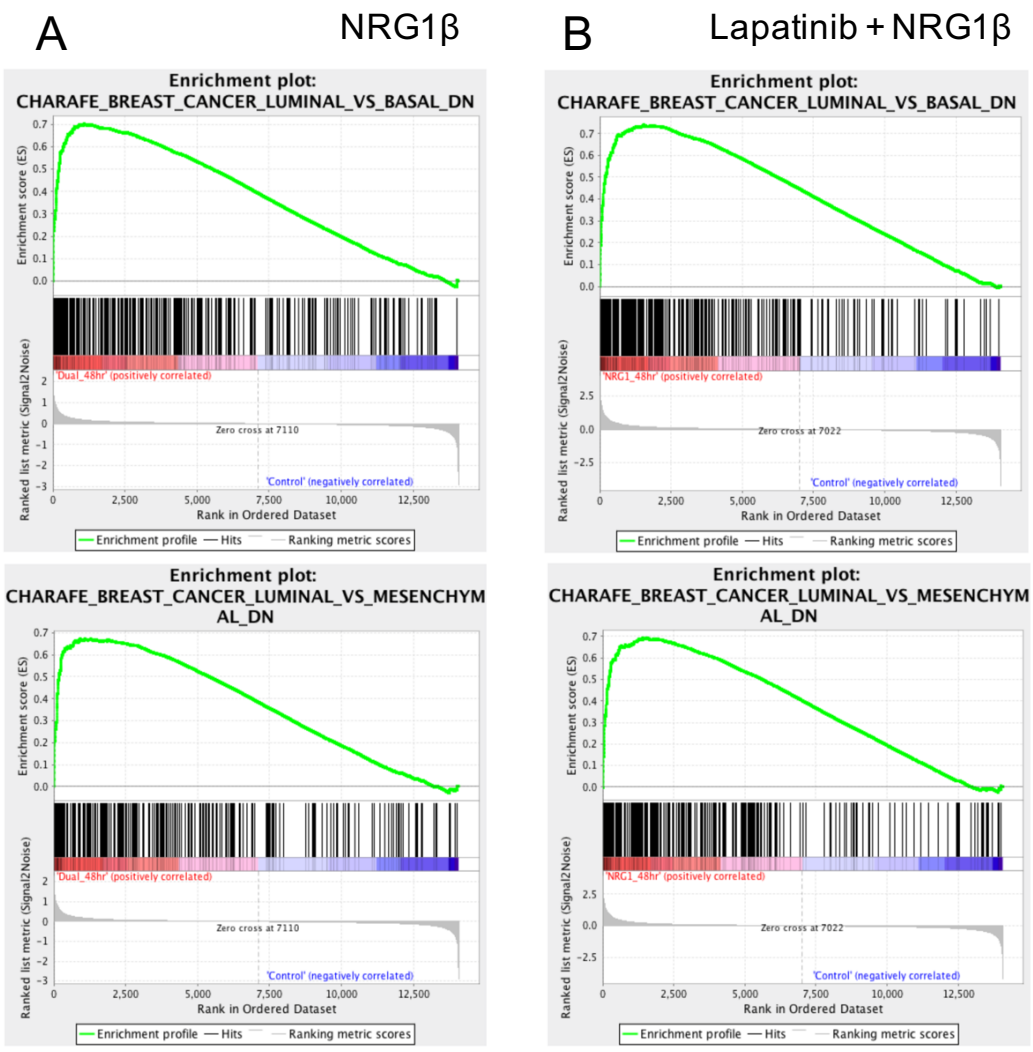

Figure 4.5. NRG1 treatment drives basal and mesenchymal differentiation in L-HER2+ cells. (4.5A&B) Most significant GSEA plots of unbiased comparisons between NRG1 treatment at 48 hours and untreated control (n = 3) and NRG1 plus lapatinib at 48 hours compared to untreated control (n = 3). Each treatment resulted in significant enhancement of the 'luminal vs basal down gene set', and the 'luminal vs mesenchymal down' gene set. (NOM p-val = 0, FDR q-val = 0).

These data implicate a potentially interesting interplay between cell state and drug resistance, where NRG1β is driving an EMT-like expression pattern, resulting in a cell state that shows little proliferation normally, but has a massive capacity for expansion if exposed to HER2 targeting drugs. How much this differentiation effect actually influences drug response is still unknown, but identification of tumor cells bearing the NRG1β-treatment expression pattern could be a strong prognostic indicator of resistance to lapatinib and other HER2 TKIs. How NRG1β actually causes differentiation, and what transcription factors it works through is also unknown, but there are still parts of this large RNAseq data set left unexplored. It could still hold relevant data for future projects investigating the interplay of cellular differentiation and drug resistance.

4.5. Paracrine Signaling Protein Secretion Increased by Lapatinib and NRG1 Treatment

Several of the other most significantly enhanced genes in the RNAseq data set were for cell extrinsic paracrine signaling ligands. However, there are multiple regulatory steps between gene expression, translation, post-translational processing, trafficking, and secretion into the extracellular space. We assayed cell culture medium with antibody arrays to investigate actual protein changes in growth factor and cytokine secretion in response to treatment. AU565 cells were treated for 48 hours with combinations of 500 nM lapatinib, 50 ng/ml NRG1, and DMSO or PBS controls. Following treatment, the medium was collected, filtered, and applied to growth factor antibody arrays. Figure 4.6 shows quantification of array results for each treatment condition as a differential to untreated controls.

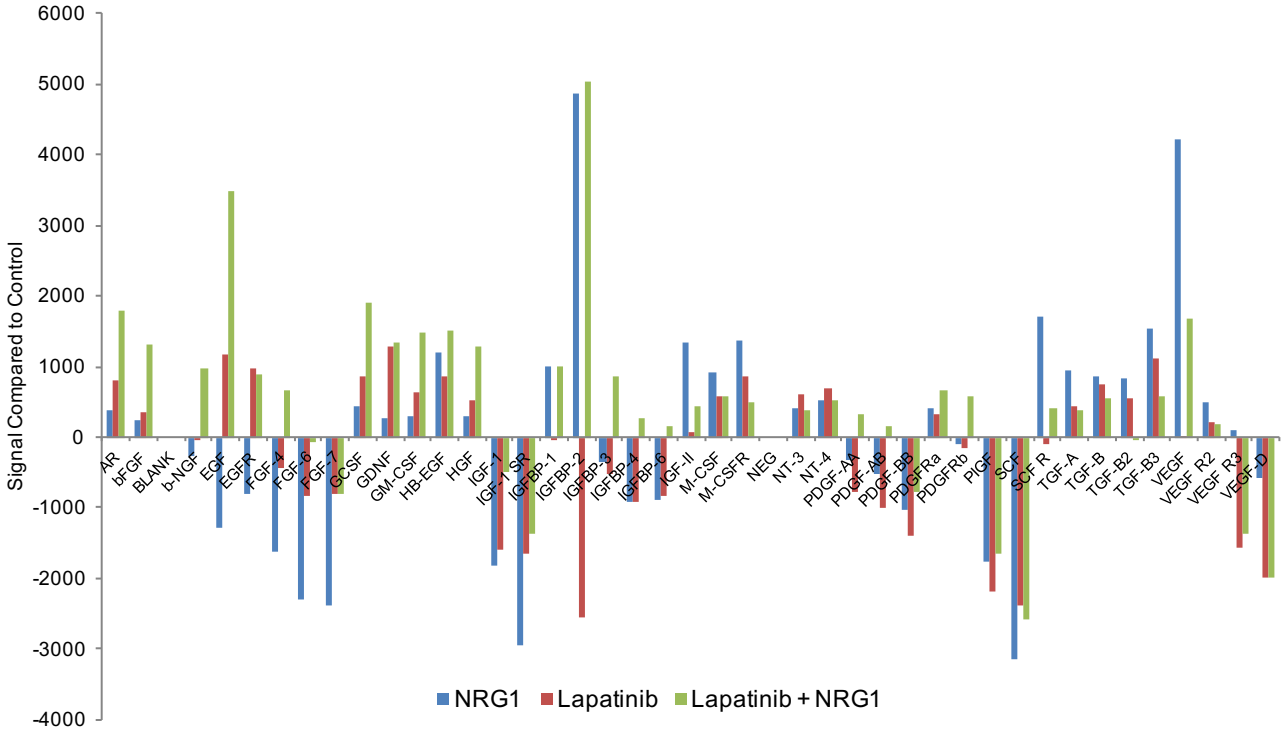

Figure 4.6. Lapatinib and NRG1 treatments differentially regulate the secretome in AU565 HER2+ cells. Bar graph shows pixel intensity of antibody array spots exposed to pooled biological replicates (n = 3) of filtered medium from AU565 cells recovered following 48 hours of treatment with combinations of 500 nM lapatinib, 50 ng/ml NRG1β, and controls. Intensity is presented as a differential compared to spot intensity of arrays exposed to medium from untreated control.

Lapatinib increased secretion of several growth factors such as EGF, GDNF, and TGF-β3, and decreased several others such as IGF Binding Protein 2 (IGFBP-2), SCF, and PIGF. However, these changes were modest compared to the differential expression seen in treatment with NRG1β, particularly in the cases of IGFBP-2 and VEGF, which saw dramatic increases under NRG1β treatment. Interestingly, IGFBP-2 was the most decreased in lapatinib treatment, the most increased in NRG1β treatment, and the combination of both treatments resulted in the greatest observed differential secretion on the array.

This experiment demonstrates the extensive potential for both autocrine loops, and cellular communications in response to treatment. Many of these are still poorly understood, and are often ignored in *in vitro* cellular drug assays, with most experiments focusing only on intercellular responses. However, these results suggest the ability of secreted factors and autocrine loops to drive resistance. IGFBP-2 in particular seems to be highly influenced by lapatinib and NRG1β, and its potential role in drug resistance is largely unknown. IGFBP-2 is known as a negative regulator of IGF-1 and 2, which binds to these ligands in the extracellular space and prevents them from signaling to IGF-1R. However, there is some evidence to suggest that IGFBP-2 can signal on its own through integrin receptors, and that this results in decreased levels of PTEN, a phosphatase responsible for negatively regulating PI3K signaling [277]. This has led several groups to classify IGFBP-2 as an oncogenic signal of proliferation, with the ability to increase PI3K and MAPK pathway activity [278].

Protein analysis in L-HER2+ cell lines AU565 and SKBR3 treated with NRG1β alone and NRG1β plus lapatinib did show decreased expression of PTEN, but the results were modest, and did not seem to account for the large increase in proliferation previously observed (data not shown). This possible mechanism has not been fully explored, nor has its potential connection to the NRG1β mediated differentiation. Another possibility is that IGFBP-2 may not be directly involved in an *in vitro* drug resistance mechanism, but may play several roles *in vivo*. IGFBP-2 has been found to be overexpressed in breast cancers, and is closely correlated with tumor grade ($p < .05$) [279]. IGFBP-2 has also been found to

play a role in immune surveillance as a tumor antigen that elicits both antibody and T-cell immunity in breast cancer [280]. Because of this, IGFBP-2 is a promising vaccine target for immunomodulation of breast cancer [281]. Because of this, IGFBP-2 is a promising vaccine target for immunomodulation of breast cancer [281]. However, there is still very little evidence for its involvement in resistance to HER2 targeted agents, and so represents another compelling direction for future research.

4.6. Higher Order Complexes with HER2-HER3 and IGF-1R

During the course of project presented in Chapter 3 there were two competing hypotheses for how NRG1β was restoring pathway activity in the presence of lapatinib. The first model postulated that lapatinib inhibited HER2 when in HER2-HER3 heterodimers, and that the conformation change of the HER2 kinase did not block lapatinib binding. This model raised the question as to what was phosphorylating HER3 in the presence of NRG1β and lapatinib, if HER2 kinase activity was effectively inhibited. The above finding that treatment conditions led to enhanced secretion of several growth factors led us to the possibility that other RTKs may be playing a more direct role in phosphorylating HER3. Previous studies have shown that other receptors, such as MET, were capable of binding to and activating HER3 [282].

This led us to perform immunoprecipitation pull downs of HER2 and HER3 following treatment with 500 nM lapatinib, 50 ng/ml NRG1β, and the combination, in L-HER2+ SKBR3 and HER2E HCC-1954. The hypothesis was that under lapatinib and NRG1β treatment, NRG1β would facilitate the dimerization of HER2 and HER3, and lapatinib would inhibit HER2 kinase activity. This also resulted in stabilized but inactive structures that could allow for a third RTK to hetero-trimerize with HER2-HER3, and phosphorylate HER3. If this heterotrimer were more active than HER2-HER3 dimers normally, then it would explain the higher observed proliferation in these conditions. Additionally, for this to fit our model, an RTK must be present in the pulldown of HER2 or HER3 in the NRG1β plus lapatinib treatment in the

L-HER2+ cell line, but not the HER2E cell line, explaining why L-HER2+ lines were rescued by NRG1β, but HER2E were not.

We assayed for overexpressed RTKs in HER2 and HER3 pulldowns, focusing on those whose own ligands were found to be increased by treatment conditions in the antibody array experiment in Figure 4.6, including MET and FGFR. However, the only RTK that fit our hypothetical model was the IGF-1 receptor IGF-1R. Western blot analysis of IGF-1R levels in HER2 pull downs showed a band in both samples treated with lapatinib, but this band was only detectable in HER3 pull downs treated with both lapatinib and NRG1β (Figure 4.7). Additionally, this IGF-1R band in the HER3 pulldown was only detectable in SKBR3 lysates, and not HCC-1954. This suggests that under lapatinib treatment IGF1-R binds to HER2, and if NRG1β is also present this facilitates the binding of HER2 to HER3, resulting in a heterotrimer of HER2, HER3, and IGF-1R that could potentially restore PI3K signaling. The observation that this band was found in SKBR3 but not HCC-1954 fits with the observed lack of HER2-HER3 heterodimerization seen in HCC-1954 in the PLA experiments in Chapter 3.

Previous studies provided support for this model, including protein-protein interaction studies that predicted HER2 and IGF-1R binding [283], and another finding of HER2-HER3-IGF-1R heterotimers being involved with trastuzumab resistance [284]. This also fit into the context of how pertuzumab could abrogate NRG1β mediated resistance, by blocking formation of this higher-order structure to restore lapatinib sensitivity. However, if these heterotrimers were solely responsible for NRG1β mediated resistance, then kinase inhibitors targeting IGF-1R should successfully restore lapatinib sensitivity in a similar manner to pertuzumab. As seen previously in Figure 4.4, the IGF-1R inhibitor GSK1838705A was not capable of restoring lapatinib sensitivity, suggesting that if these heterotrimers do play a role in resistance, they are not dominant drivers in NRG1β-mediated drug resistance.

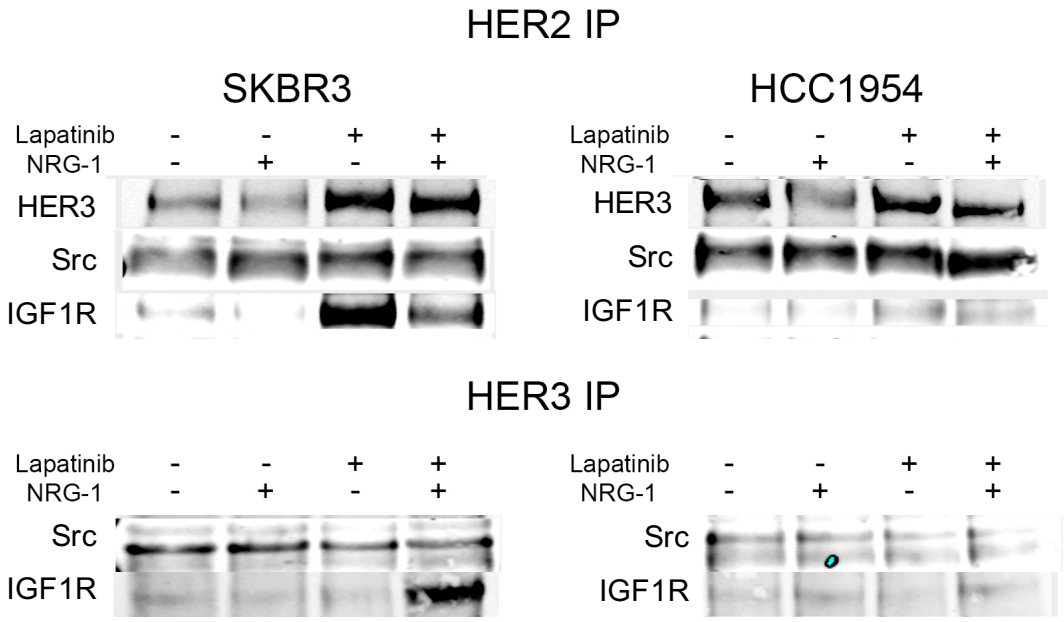

Figure 4.7. IGF-1R associates with HER2 and HER3 under exposure to NRG1 and lapatinib. Western blot analysis of IGF-1R and HER3 in immunoprecipitation pull downs of HER2 and HER3 from AU565 and HCC-1954 lysates following treatment with combinations of 500 nM lapatinib and 50 ng/ml NRG1, with Src used as a ubiquitous association control. IGF-1R was only found to associate with HER3 in SKBR3 cells exposed to both lapatinib and NRG1. (TR = 4, BR = 3).

Higher-order heterogeneous RTK structures are an interesting avenue for future studies, but they did not fully explain our observed data, due largely to the failure of IGF-1R inhibitors to abrogate resistance. Pertuzumab remained the most effective agent against NRG1β mediated resistance following our attempts with other TKIs in Figure 4.6, so we sought to determine its mode of action in this resistance mechanism. The following experiments, along with several studies focused on HER3 biology, ErbB kinase domain structure, and new data from Kevan Shokat's group, provided a more complete model that fit our experimental observations on NRG1β mediated resistance, and the ability of pertuzumab to ablate it.

4.7. The HER3 Feedback Response and Pertuzumab

Cell surface levels of HER3 can be enhanced as part of an adaptive feedback loop in response to decreased pAKT levels [126]. Based on this data, drug response, and PLA data from Figure 3.5B, it was determined that a cell intrinsic HER3 feedback response was most likely a major component of the NRG1β mediated resistance mechanism. Figure 3.5D demonstrated that pertuzumab could abrogate this resistance mechanism, but had no effect as a single agent on cellular proliferation or pathway activity in L-HER2+ cells, and even increased proliferation when in combination with NRG1β.

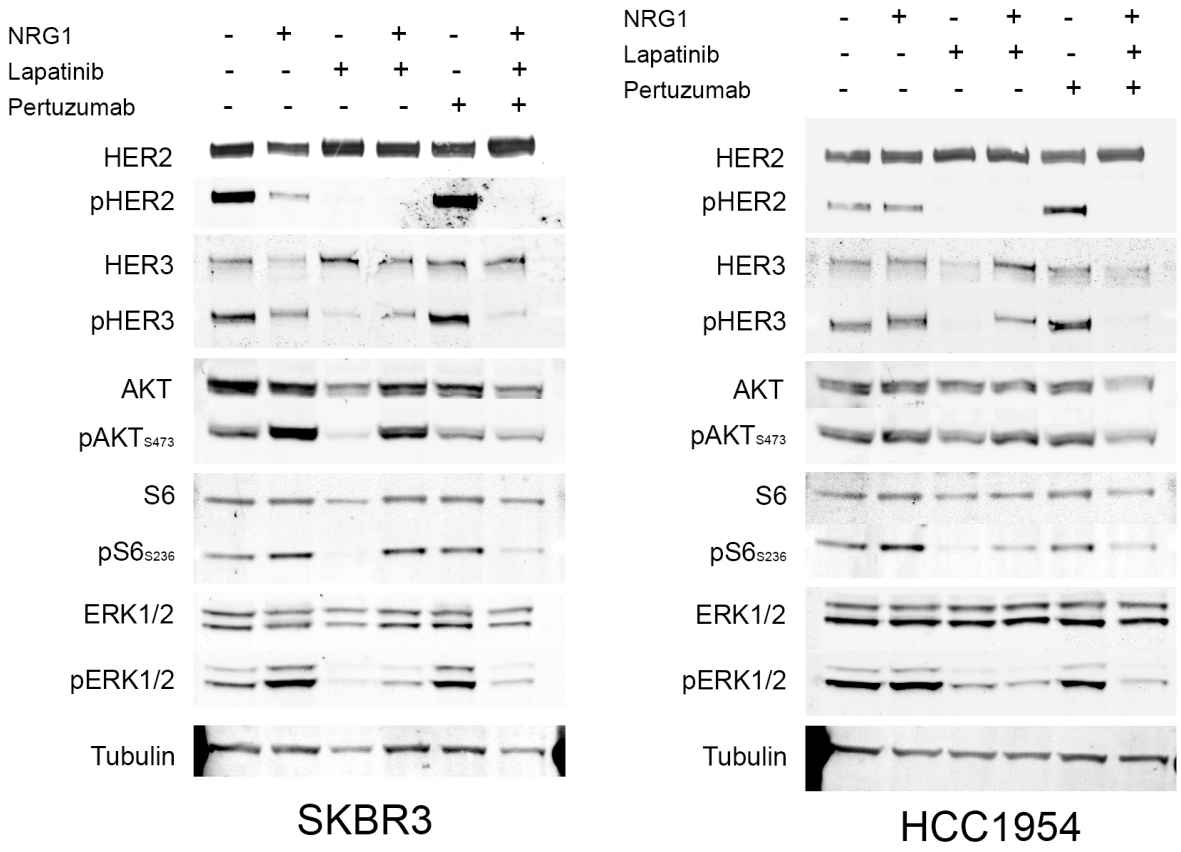

Figure 4.8. Pertuzumab restores mitogenic pathway sensitivity to lapatinib in the presence of NRG1. Western blot analysis of AU565 and HCC-1954 cell lysates following treatment with combinations of 500 nM lapatinib, 50 ng/mL NRG1β, and 25 μg/mL pertuzumab for 48 hours. Levels of pHER2, pHER3, pAKT, pS6, and pERK were all decreased by lapatinib and restored by addition of NRG1β. Further addition of pertuzumab restored pathway sensitivity to lapatinib, but had no effect as a single agent (TR = 2, BR = 3).

Western blot analysis of cells treated with combinations of 500 nM lapatinib, 50 ng/ml NRG1β, and 20 μg/ml pertuzumab are shown in Figure 4.8. Activity of several protein components of HER2 signaling are shown to be reduced by treatment with lapatinib, and restored by combination with NRG1. Pertuzumab on the other hand had no such inhibitory effect, despite showing the ability to abrogate the NRG1β-mediated rescue of pathway activity. The suggested mode of action of pertuzumab is that it binds to the extracellular domain II of HER2, and that this blocks association with other HER2 molecules, EGFR, or HER3 through steric hindrance, and so should be inhibitory of HER2 signaling as a single agent [285]. We hypothesized that this mode of inaction was incomplete in this context, and that a more detailed understanding of protein interactions would explain why pertuzumab was failing to inhibit HER2 signaling in L-HER2+ cells.

With the aid of Larry David and the OHSU Proteomics Shared Resource core we performed tandem mass spectrometry proteomic analysis on immunoprecipitation pull downs of HER3 from lysate samples obtained from AU565 cells treated with combinations of lapatinib, NRG1β, and pertuzumab (Figure 4.9). HER2 phosphorylation of the p85 binding site on HER3 recruits PI3K. As expected, inhibition of phosphorylation with lapatinib resulted in decreased presence of PI3K subunits in HER3 pulldowns. These levels were in turn restored by combination with NRG1β, and decreased again by further combination with pertuzumab, similar to what was observed in Western blot pathway analysis. Surprisingly, this was true for all the detected HER3 binding proteins except HER2, which was instead found to have a large increase in HER3 association under pertuzumab treatment. This suggested that pertuzumab was not blocking association between HER2 and HER3, but somehow binding them together in such a way that it did not stimulate or inhibit proliferation as a single agent, yet still abrogated the effect of NRG1β on lapatinib inhibition.

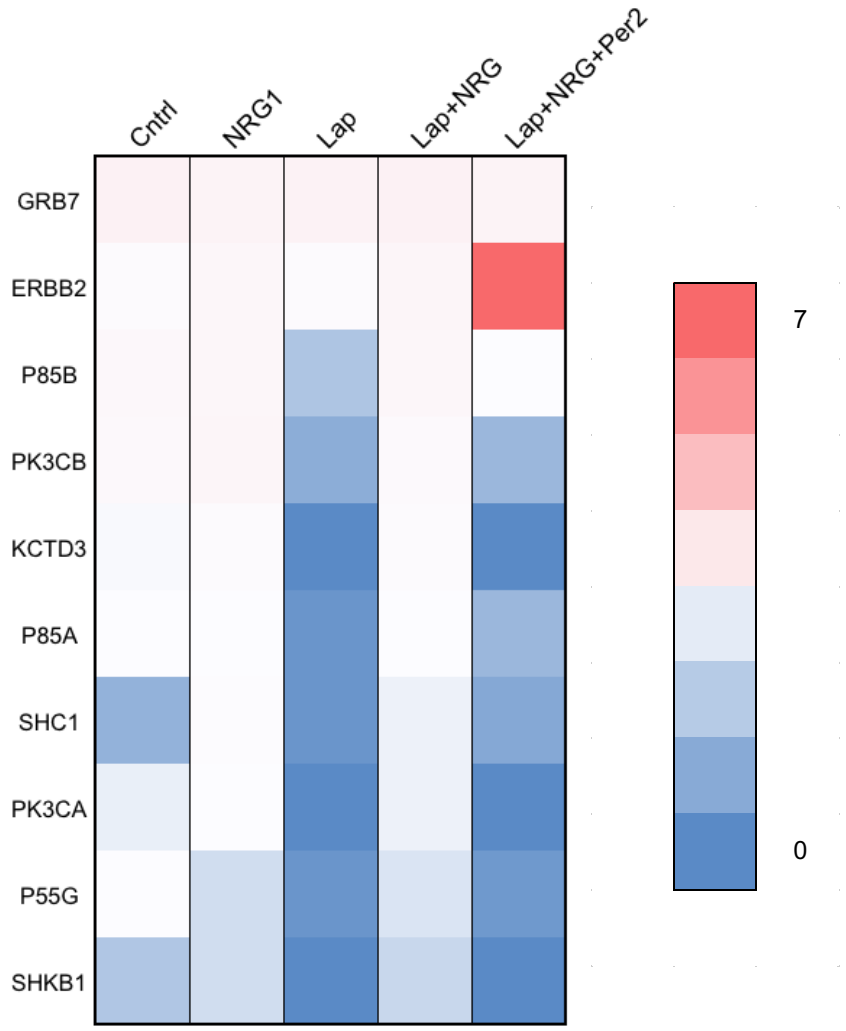

Figure 4.9. Association of PI3K subunits with HER3 regulated by NRG1 and HER2 targeting drugs. Heatmap depicts detection counts from tandem mass spec proteomic analysis of HER3 immunoprecipitation from AU565 cell lysate following 48 hours of treatment with 500 nM lapatinib, 50 ng/ml NRG1β, 25 µg /ml pertuzumab, and selected combinations. Each count is normalized to the detected quantity of HER3 in each treatment sample. Scale shows ratio of individual protein count to HER3 count. Pooled biological replicates (n = 3).

A more nuanced model of the mechanism of pertuzumab was needed that could combine the observed experimental evidence. The questions that needed to be addressed by this model were as follows: If pertuzumab is inhibiting HER2 homodimerization, and heterodimerization with HER3 or EGFR, why is this not sufficient to inhibit proliferation when used as a single agent? How can pertuzumab restore lapatinib sensitivity under NRG1 exposure but have no effect as a single agent? If the mode of action of pertuzmab is steric hinderance blocking association with dimer partners, why is this resulting in increased HER2 protein in HER3 pulldowns?

Previously reported structural analysis of HER2-HER3 complexes and the SELEX-derived RNA aptamer A30 provided a useful insight into the nature of the RTK structures [286]. They found that HER2 not only activates HER3 proteins it is directly dimerized with (termed direct or cis-activation), but can also activate HER3 proteins of other dimers (termed proxy or trans-activation) in higher-order RTK complexes when both proteins are overexpressed.

Trans-activation suggets a model that explains our mass spec data, and why pertuzumab has no efficacy in cells with high HER3 expression. Pertuzumab treatment blocks complete dimerization of HER2 and HER3, but appears to bind to both proteins, locking them into an inactive complex where HER2 cannot cis-activate HER3. However, when both of these proteins are highly expressed on the cell surface they can mass into higher-order complexes, allowing HER2 to trans-phosphorylate the HER3 of other dimers, restoring pathway activity (Figure 4.9A). This means that if cells high in HER2 and HER3 are exposed to high levels of NRG1β, then pertuzumab treatment would not only be ineffective, but could actually lead to enhanced pathway activity and proliferation. In fact, this is exactly what we see in the project presented in Chapter 3.

The other factor this model needs to address is the question of how pertuzumab is effective in restoring lapatinib sensitivity if it is not effective as a single agent. As discussed previously, complete HER2-HER3

dimerization, which is facilitated by NRG1β, causes a conformational shift in the activation loop of the ATP-pocket of HER2, rendering it inaccessible to lapatinib, and thus blocks cis-activation of HER3 [99]. However, if pertuzumab disrupts this structure, then the kinase domains remain separate, and the ATP-binding pocket of HER2 is accessible by lapatinib. Figure 4.9B depicts a model where trans-activation in higher-order structures overcome inhibition by pertuzumab as a single agent, and NRG1β restores cis-activation to overcome lapatinib inhibition as a single agent, but the combination of lapatinib and pertuzumab is needed to overcome both cis and trans activation to inhibit HER2-HER3 heterodimers.

The combination of the mechanisms of state-specific HER2 kinase conformations, and higher order trans-activation of HER3 creates a mechanistic model which both fits our experimental observations, and answers our remaining questions about pertuzumab's lack of efficacy as a single agent in these cell lines. The model also provides new research directions into the binding dynamics of higher order structures, as well as potential new targets to eliminate this resistance mechanism. Specifically, targeted agents rapid endosomal recycling, or pathways upregulated by AKT inhibition, could block HER3 localization to the cell surface, and increase the efficacy of lapatinib and pertuzumab.

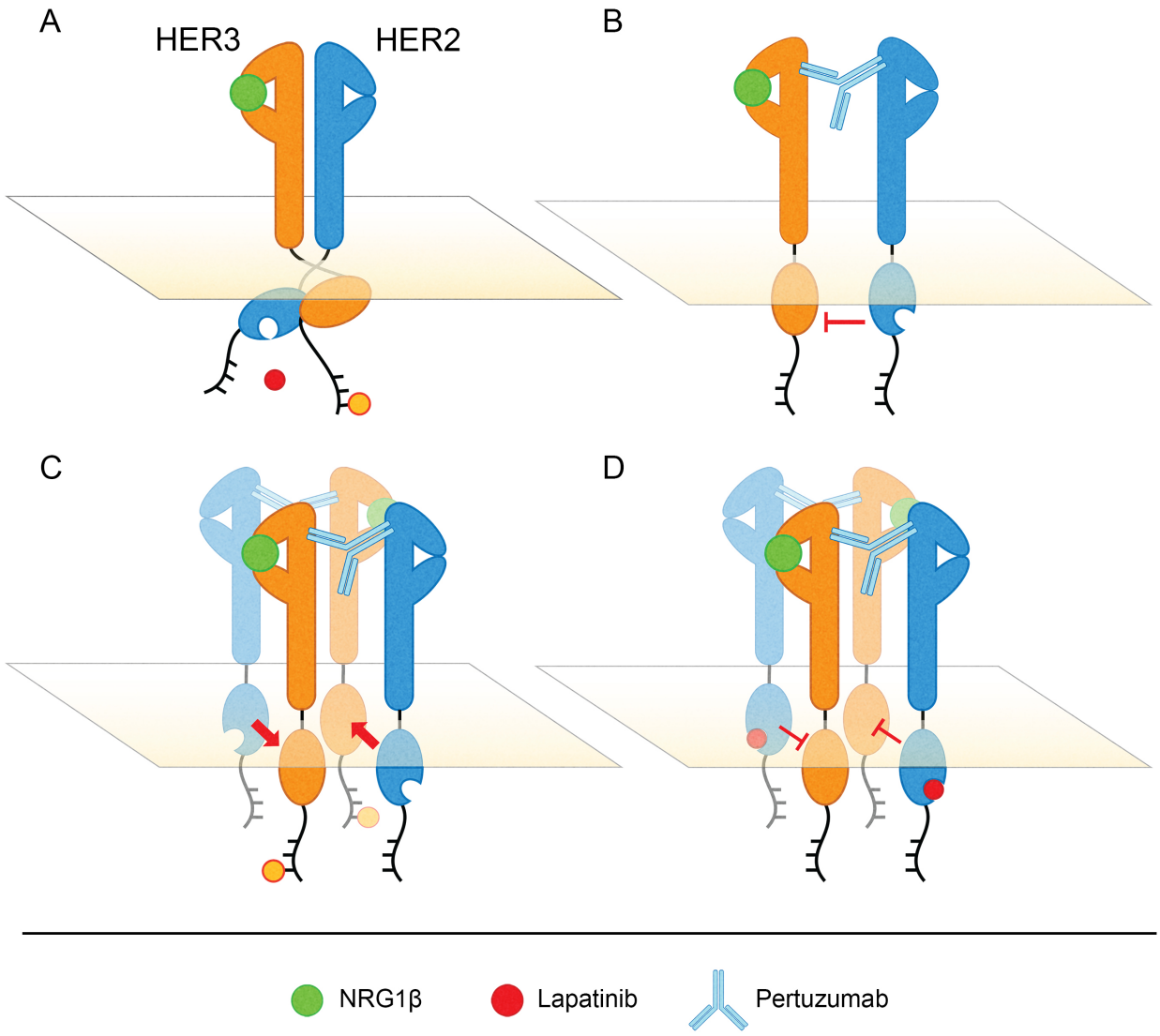

Figure 4.10. Lapatinib and Pertuzumab are required to inhibit cis and trans HER3 phosphorylation. High levels of NRG1β in the micorenvironment cause lapatinib and pertuzumab to be ineffective as single agents in breast cancer cells overexpressing HER2 and HER3. 4.10A Depicts a simplified graphic model of HER2 and HER3 dimerization on the cell surface when activated by NRG1β. This structure changes the conformation of the ATP binding pocket on the HER2 cytoplasmic kinase domain to one which lapatinib cannot readily bind. 4.10B shows how pertuzumab inhibits cis-phosphorylation of HER3 via separation of the cytoplasmic kinase domains. This structure returns the HER2 kinase domain conformation to one which lapatinib can bind. Note that receptors remain linked under pertuzumab treatment. 4.10C shows how higher-order receptor structures overcome inhibition by pertuzumab via trans-phosphorylation of HER3. 4.10D depicts the proposed mechanism for how pertuzumab and lapatinib combine to overcome cis and trans phosphorylation of HER3 respectively. Figure based on data from ©Novotny et al. 2016, originally published in Nature Chem Bio 2016, and ©Zhang et al. Sep 2012 12(11), 923-930, originally published in PNAS Aug 2012 109(33): 13237–13242.

4.8. Experimental Procedures

4.8.1. *Cell lines*

Breast cancer cell lines AU565, SKBR3, HCC-1954were obtained from American Type Culture Collection (ATCC), Manassas, VA. Each cell line was genotyped to ensure accurate identity, and continuously screened for mycoplasma infection. Cell lines were maintained in their respective media as recommended by ATCC at 37°C in 5% CO2 in a humidified incubator and cultured according to ATCC recommendations.

4.8.2. *ECM immobilization*

DSG2 and E-Cadherin were purchased from R&D System. Collagen I and laminin were purchased from Abcam. Proteins were diluted in PBS to achieve similar $\mu g/cm^2$ in 96-well plate surfaces as used in the MEMA assay. 100 µL of diluted proteins were added to 96-well cell culture treated plates on ice, and then left at 4^0 C overnight. Remaining liquid was aspirated off the following day, and plates were dried at RT for 4 hours. 8,000 SKBR3 and 2,000 HCC-1954 cells were plated in respective ECM-coated wells at the start of the experiment. Following 48-hour treatment with 500 nM lapatinib or DMSO control, medium was removed, cells were fixed in 2% PFA for 15 mins at RT, and immunofluorescently stained as previously described.

4.8.3. *RNAseq time course*

RNA was extacted from cell lysate of 3 biological replicates using Qiagen RNEasy kit. mRNA was purified, and cDNA library was created using Illumina TruSeq Stranded mRNA Library Prep Kit, and

sequenced on the Illumina HiSeq 2500 platform. Paired-end 100-bp RNA-seq reads were aligned to the GRCh38 human reference genome and raw gene expression counts calculated using STAR (v2.4.2a) [287].

Through implementation of the edgeR software package [288], raw counts were normalized using the TMM (trimmed mean of M-values) method [289], to adjust for compositional differences between the libraries. Further full quantile normalization [290] was carried out utilizing the 'betweenLaneNormalization' feature of the EDASeq package [291] to account for between-lane distributional differences, such as sequencing depth. Determination of differential expression was conducted within edgeR using a generalized linear model likelihood ratio test [292], with significance based on q-value less than 0.05 and log fold change in expression greater than 1.5 fold.

4.8.4. *Gene set enrichment analysis*

Unbiased GSEA comparisons were performed between AU565 RNAseq data sets from samples treated with 50 ng/mL NRG1, 500 nM lapatinib, or the combination for 2, 24, and 48 hours (n = 3). An additional untreated sample was used as a time-zero control. GSEA comparisons between each sample at each time point to the untreated control were performed using the javaGSEA Desktop Application available from the Broad Institute (http://software.broadinstitute.org/gsea/index.jsp). Gene sets with nominal p-values of less than 0.001, and false discovery rate q-values of less than 25% were considered significantly enriched.

4.8.5. *Antibody arrays*

Human growth factor antibody arrays (41 targets) were purchased from Abcam. 8,000 AU565 were plated in 96-well cell culture plates, and treated for 48 hours with 50 ng/mL NRG1, 500 nM lapatinib, the combination, and a DMSO control. Medium was recovered from each condition following treatment, sterile filtered, and combined with biological replicates (n = 3). 1 mL of medium was applied to antibody

array membranes overnight at 4^0C with gentle rocking. Following detection protocol membranes were imaged for chemiluminescence, and intensity of each antibody spot was assessed by ImageJ.

4.8.6. *Immunoprecipitation mass spectrometry*

Immunoprecipitated fractions from whole cell lysate were applied to NuPAGE 10% Bis-Tris SDS-PAGE gels (NP0301BOX), electrophoresed for 6 min at 200 V to remove impurities, and stained for 30 min with Imperial Blue protein stain (purchased from Thermo Scientific) to assess sample concentration and quality. Gels were washed in water and the entire top of each lane, from the bottom of the loading well to the tracking dye, was excised. Gel slices were then cut into 1 mm pieces, processed, reduced/alkylated, and digested with trypsin for one hour at 50°C in the presence of 0.01% ProteaseMax detergent (ProMega) using the method recommended from the manufacturer. Recovered peptides were then dried by vacuum centrifugation then dissolved in 5% formic acid in preparation for LC/MS analysis. Digests were loaded onto an Acclaim PepMap 0.1 x 20 mm NanoViper C18 peptide trap (Thermo Scientific) for 5 min at a 5 µl/min flow rate in a 0.1% formic acid mobile phase. Peptides were then separated using a PepMap RSLC C18, 2 µm particle, 75 µm x 25 cm EasySpray column (Thermo Scientific) and 7.5–30% acetonitrile gradient over 60 min in mobile phase containing 0.1% formic acid at a 300 nl/min flow rate using a Dionex NCS-3500RS UltiMate RSLCnano UPLC system. Tandem mass spectrometry data was collected using an Orbitrap Fusion Tribrid mass spectrometer configured with an EasySpray NanoSource (Thermo Scientific). Survey scans were performed in the Orbitrap mass analyzer at 120,000 resolution, and data-dependent MS2 scans in the linear ion trap using HCD following isolation with the instrument's quadrupole.

Sequest (version 28, revision 12; Thermo Scientific) was used to search MS2 spectra against a June 2016 version of the Sprot human FASTA protein database, with added concatenated sequence-reversed entries to estimate error thresholds, and 179 common contaminant sequences and their reversed forms. The

database processing was performed with Python scripts that have been described previously 1. Searches for all samples were performed with trypsin enzyme specificity. The monoisotopic parent and fragment ion mass tolerances were 1.25 and 1.0 Da, respectively. A static modification of +57.02 Da was added to all cysteine residues. A variable modification of +16 Da on methionine residues was also allowed, with a maximum of 3 modifications per peptide. A linear discriminant transformation was used to improve the identification sensitivity from the SEQUEST analysis 1,2. SEQUEST scores were combined into linear discriminant function scores, and discriminant score histograms were created separately for each peptide charge state (1+, 2+, and 3+). Separate histograms were created for matches to forward sequences and for matches to reversed sequences for all peptides of 7 amino acids or longer. Scores of histograms for reversed matches were used to estimate peptide false-discovery rates (FDR) and set score thresholds for each peptide class and a minimum of at least two unique peptide assignments to a protein entry was required across samples. This achieved a final protein FDR of 1.1%.

Chapter 5. Final Comments and Future Directions

5.1. Conclusions

Our experimental evidence supports the following conclusions. HER2+ breast cancer is not a single heterogeneous disease, but at least two biologically distinct diseases with unique common mutations, divergent responses to the tumor microenvironment, mitogenic pathway utilization, and drug sensitivities. The basal-like HER2E subtype can bypass HER2 inhibition in environments high in HGF due to its high expression of the HGF receptor MET, which has very low expression in L-HER2+ cells. The luminal-like L-HER2+ subtype can overcome HER2 targeting TKIs in environments high in NRG1β by trafficking HER3 to its cell surface to form HER2-HER3 heterodimers, which render lapatinib ineffective by blocking the lapatinib binding site [99].

The HER3 adaptive feedback response in L-HER2+ cells is rapid, occurring in less than 2 hours, and requires no changes in gene or protein expression. HER2 is reported to be resistant to negative regulation from internalization due to its selective expression on cellular protrusions in human HER2+ cells [111]. This likely endows internalization resistance to dimer partners, resulting in HER2-HER3 heterodimers that form rapidly in response to lapatinib and NRG1β, and persist on cell surface even after they have restored pathway activity. This combination of events leads to greatly enhanced and enduring mitogenic signaling, converting lapatinib treatment into a stimulant of proliferation in the presence of high NRG1β.

The NRG1β and HGF resistance mechanisms can be directly targeted by combination therapy. Lapatinib sensitivity can be restored in HER2E cells exposed to HGF by targeting MET kinase activity with crizotinib. NRG1β mediated resistance in L-HER2+ cells can be abrogated with pertuzumab, which acts in conjunction with lapatinib to block both cis and trans phosphorylation of HER3.

Drug treatment experiments with trametinib and GSEA comparisons between L-HER2+ and HER2E lines revealed that L-HER2+ cells rely on PI3K/AKT signaling more than MAPK signaling, and the inverse was observed for HER2E cells. Interestingly, L-HER2+ cell lines have significantly more HER2 homodimers at baseline culture conditions compared to HER2-HER3 dimers, and more HER2 homodimers than HER2E cells [107, 124]. HER2 homodimers primarily signal through MAPK [107], but GSEA data showed that the genes downstream of MAPK signaling have decreased expression in L-HER2+ lines compared to HER2E lines. These data appear to be contradictory. Possible explanations for this discrepency in are; i) HER2 homodimers are signaling through PI3K via adapter proteins such as GAB1 in L-HER2+ cells, ii) the smaller fraction of HER2-HER3 dimers are more active in terms of propagating sigaling cascades compared to the more numberous HER2 homodimers, iii) differential epigenomic regulation of genes downstream of MAPK siglaning results in lower expression in L-HER2+ cells compared to HER2E cells. There is currently insuficient data to determine which possibility is correct, so this represents an interesting direction for future investigation.

Another factor in L-HER2+ resistance to MAPK inhibition is that MEK inhibitors also trigger the HER3 feedback response [128]. This indicates that the PI3K/AKT pathway is an essential fallback pathway following loss of HER2 or MAPK signaling in L-HER2+ cells. L-HER2+ cells also require HER3 to survive in the absence of drug treatment (Figure S3.3), likely due to its role in supporting both PI3K/AKT and MAPK pathways. HER2E cells appear to lack any HER3 feedback response to HER2 inhibition. The HER3 feedback response in L-HER2+ cells likely represents the first line of defense in a two-step adaptive resistance response, following which epigenomic kinome adaptation can increase expression of compensatory RTKs if HER2-HER3 dimers fail to restore pathway activity.

While this mechanistic model and supporting evidence is compelling, there are several obstacles to applying it translationally to HER2+ breast cancer patients. Currently there is a lack of patient data to

unequivocally prove this resistance mechanism occurs in patients, despite the strong indications presented in this thesis. This is largely due to three factors; first, there are few large studies that include both targeted HER2 agents, and intrinsic molecular subtyping to reliably identify the HER2E and L-HER2+ subtypes. Second, while we can identify anatomic sites high in NRG1 and HGF, clinical trials do not consistently report on local responses of individual tumors in patients with metastatic disease at these anatomic locations. And finally, large scale proteomic assessment of the tumor stroma by mass spectrometry or ELISA arrays has never been done in HER2 targeting drug trials, and few other approaches would provide accurate data on local concentrations of potentially resistance causing secreted growth factors.

***

There remain some mechanistic and clinical questions not fully explored following the studies presented in Chapter 3 that can serve as new avenues for investigation to advance our conclusions. The work of Shokat et al. on the resistance conferring conformation change in the HER2 ATP binding pocket following HER2-HER3 dimerization supports our suggested mechanism. However, it is lacking in structural evidence [99]. The following proposed experiments could be used to provide further evidence for the hypothesis that HER2-HER3 heterodimerization results in a conformation change in HER2 that blocks lapatinib binding.

i. Cryo-EM structural studies of the HER2 kinase domain when in HER2 homodimers, or in combination with HER3, EGFR, or HER4 could provide more robust evidence that the lapatinib binding site is being concealed by a conformation change. Gold-nanoparticle labeling of HIS-tagged HER2 kinase domains would allow for determination of which kinase position HER2 takes in each pairing, and how much ‘kinase-switching’ occurs. Structural analysis of each

pairing in the presence or absence of pertuzumab would provide strong support for our proposed model. This approach could also identify state-agnostic inhibition sites for rational drug design.

ii. Another informative and novel experiment would be cell-free ATP-binding assays to measure lapatinib binding when HER2 is in each ErbB pairing and in combination with pertuzumab. Cell-free kinase assays like these typically only utilize the active kinase domain of the protein, which would not be sufficient to investigate HER2 conformation changes in transmembrane dimers. However, Wei He et al. described a method for producing cell-free full length and active ErbB proteins using apolipoprotein A-I based nanolipoprotein particles [293]. ATP-binding kinase activity experiments with this model would allow for the interrogation of lapatinib binding rates under NRG1β and pertuzumab treatments when HER2 is in each ErbB pairing.

iii. Site specific mutagenesis experiments could be performed on the HER2 kinase domain to identify which residues are sufficient and necessary for the conformation change caused by dimerization with HER3. These experiments could use the above cell-free lapatinib binding assay as a read out of conformation change, and/or employ Cryo-EM for more precise analysis. CRISPR knock-in of mutations that ablate the conformation change in L-HER2+ lines treated with lapatinib and NRG1β would then serve as validation.

The above experiments would provide convincing data to support the hypothesis that HER2 becomes lapatinib insensitive as a direct result of binding with HER3 following activation by NRG1β. Another question not fully addressed in Chapter 3 is; does endosomal recycling play a role the dynamics of HER2-HER3 signaling? Live-cell super resolution microscopy, or Cryo-EM of labeled NRG1β and HER2 can quantify the effects of combinations of lapatinib, pertuzumab, and NRG1β have on the dynamics of dimerization, as well as how rapid-endosomal recycling factors into the mechanism of drug resistance.

siRNA knockdown studies of known RAB proteins involved in rapid-endosomal-recycling could then determine targetable components of HER3 trafficking [294].

And finally, mass spectrometry analysis of Multiplexed kinase Inhibitor Bead (MIBs) assays with lapatinib and neratinib can reveal the binding dynamics of these agents to HER2 under stimulation by NRG1β, EGF, or the HER4 ligand NRG2, across a range of cell lines. This could better reveal the role different ErbB family dimer combinations have on HER2 TKI response in HER2+ breast cancer cells.

***

Future clinical directions will require providing convincing evidence that HER2+ patients would benefit from molecular subtyping and assessment of their tumor microenvironment. At present there is a lack of appreciation that HER2 could be at least two distinct diseases, and that L-HER2+ and HER2E tumors have different responses to targeted treatments and their local environment. We propose to address this through a collaborative clinical trial design with clinicians treating HER2+ patients with HER2 targeting TKIs such as neratinib.

Three hypotheses are outlined in the following section to investigate in a clinical trial setting, using neratinib as an example HER2 TKI. The proposed trial will compare neratinib treatment to neratinib plus pertuzumab in L-HER2+ patients, or neratinib plus trametinib in HER2E patient. We used crizotinib in our *in vitro* assays to overcome HGF-mediated neratinib resistance in HER2E cells, but data suggests that crizotinib treatment could abrogate the anti-tumor effect of neutrophils in patients, and so trametinib is likely a better combinatorial agent with neratinib [295]. Trametinib targets MEK downstream of MET activation, and our data showed synergy between lapatinib and trametinib in HER2E cell lines (Figure 3.4F).

Identification of high concentrations of growth factors like NRG1β or HGF in primary or metastatic tumor sites, and correlation with poor response to targeted therapeutics like lapatinib or neratinib, would provide substantial evidence that these microenvironment-mediated resistance mechanisms are indeed playing a substantial role in localized therapeutic response in patients. We are currently investigating using HER2+ patient subtype information (either by our own gene set, the PAM50 gene sets, or by simple ER status) to stratify HER2+ patients in upcoming clinical trials. Our hope is to improve patient response to neratinib treatment by combination treatment with pertuzumab in L-HER2+ (ER+) patients, and MEK inhibitors in HER2E (ER-) patients. Further characterization of their tumors for NRG1β or HGF, and assessment of localized response to treatment in metastatic patients would support our hypothesis that these growth factors are not simply predictors of poor prognosis, but targetable mechanisms of resistance.

5.2. Proposed Clinical Trail Design

The goal of this proposed clinical trial is to investigate the following hypotheses. The first hypothesis is that stratification of post-standard-of-care HER2+ patients into L-HER2+ and HER2E cohorts will reveal differential responsiveness to the HER2 targeting TKI neratinib, specifically that L-HER2+ patients will respond better than HER2E patients. The second hypothesis is that L-HER2+ patients will derive additional benefit in terms of progression-free survival from the combination of neratinib and pertuzumab, compared to neratinib alone. The final hypothesis is that HER2E patients will derive additional benefit in terms of progression-free survival from the combination of neratinib and trametinib, compared to neratinib alone.

The combinations of neratinib plus pertuzumab, and neratinib plus trametinib have not yet cleared phase I trials. Two placebo-controlled, double-blind phase I dose escalation trials will determine the Maximum Tolerated Dose (MTD) for each drug combination. The sample size for each trial will be 20-25 patients, based on biostatistics recommendations from O'Quigley et al. for the continual reassessment method [296].

Patients will be randomly assigned to placebo or drug combination cohorts. The criteria for patient inclusion in these trials are that they are females over the age of 18. Patients with stage II to stage III HER2+ breast cancer are preferred, but not essential for phase I. The criteria for patient exclusion are that they have a history of heart disease, a corrected QT interval (QTc) of >.45 (as an indicator of cardiovascular disease), or have a history of severe diarrhea linked to gastrointestinal disease. Each patient will also receive anti-diarrheal prophylactic treatment with loperamide and budesonide.

The next phase will be a partially-randomized, placebo-controlled, double-blind phase II study with three cohorts of HER2+ breast cancer patients. This design will be required to test all three hypotheses of the proposed trial. The criteria for patient inclusion in the phase II trial are that they are females over the age of 18, have stage II to stage III breast carcinoma, are +3 HER2+ by IHC, show *ERBB2* amplification by FISH (HER2-CEP17 ratio > 2.2), and have progressed on chemotherapy plus trastuzumab. Because patients with luminal HER2+ tumors have shown preferential benefit from trastuzumab compared to basal HER2+ tumors, this may limit the L-HER2+ sample size [189]. The criteria for patient exclusion are that they have a history of heart disease, a QTc interval of >.45, or have a history of severe diarrhea linked to gastrointestinal disease.

This enrichment trial design will have 2 arms (L-HER2+ and HER2E) that compare a combination regimen to neratinib alone, requiring 3 cohorts in total. Each of the 3 cohorts in the trial (Control, L-HER2+, HER2E) will require a minimum of 98 patients, 294 in all. This assumes a relative hazard ratio of .67, and provides sufficient total events for statistical power of .8, a 0.05 type I error rate (significance level), and a type II error rate of 0.2 for each arm of the trial. Assuming a potential patient dropout of 30%, the proposed clinical trial will require 140 patients in each cohort to prove or disprove all three hypotheses, 420 in total.

Primary tumors and any available metastases will be biopsied at the outset of the trial, and assessed by transcriptomics. This data will inform which arm patients are enrolled in to test the hypothesis that L-HER2+ tumors will respond better to neratinib than HER2E tumors. Spatially separated biopsies from the same tumor should be pooled or individually assessed by transcriptomics to account for subclonal heterogeneity within the tumor. Gene expression profiling will employ the TCGA HER2-diff gene set (302 genes differentially expressed between L-HER2+ and HER2E patients [46]) to assign patients to either the L-HER2+ or HER2E cohorts. Additionally, tumor samples from available sites with peripheral stromal involvement will be fresh frozen and prepared for tandem-mass spectrometry proteomics. If fresh frozen tissue is unavailable, Formalin-Fixed Paraffin Embedded (FFPE) tissue microarrays will be provided for highly-multiplexed immunofluorescent assessment of markers for stromal-derived proteins previously identified as involved in drug resistance (NRG1β, HGF, FGF2, etc.).

Patients will be assigned to each arm based on gene expression profiles. L-HER2+ and HER2E patients will be randomly assigned to either the control group that receives the 24 months of the neratinib plus placebo at MTD, or their respective experimental cohort. This results in a mixed population control group that can be compared to the experimental cohorts as a whole, or stratified based on expression profile. Comparisons within the control group will test the hypothesis that L-HER2+ patients derive more benefit from neratinib than HER2E patients. The L-HER2+ cohort will receive 24 months of neratinib plus pertuzumab at the MTD. This will test the hypothesis that L-HER2+ patients will receive greater benefit from neratinib plus pertuzumab than from neratinib alone. The HER2E cohort will receive 24 months of neratinib plus trametinib at the MTD. This will test the hypothesis that HER2E patients will receive greater benefit from neratinib plus trametinib than from neratinib alone. Regular assessments of response should be scheduled every 2 months. Each patient in all 3 cohorts will also receive anti-diarrheal prophylactic treatment with loperamide and budesonide.

Local assessment of known metastases should be individually measured by CT or PET imaging at each assessment period if well tolerated, especially in anatomically distinct locations such as the lung, liver, or brain. Final reporting for each patient in the 4 arms should include:

Primary Outcome Measures:

i. Disease free survival (24 months)
ii. Tumor transcriptomics
iii. Any available proteomics (with special attention given to pan-NRG and HGF levels in the tumor and periphery)

Secondary Outcome Measures:

i. Anatomically localized response
ii. Overall survival (5 years)
iii. Time to distant recurrence (2-5 years)
iv. Adverse effects and complications

5.3. Final Comments

Future directions to translate our findings into improved patient outcomes will require new clinical trial designs, such as that outlined above, to provide the necessary tumor subtype and microenvironment composition data. Despite the challenges, this aim is aided by a growing movement in clinical circles to treat HER2+ breast cancer as at least two unique diseases, either by stratifying them by ER status, or by aspects of their intrinsic subtype. Some clinicians have found increased efficacy in adding tamoxifen to trastuzumab in HER2+ ER+ patients, and Perez et al. employed the Prosigna (PAM50) algorithm to show that luminal-like HER2+ tumors respond better to trastuzumab than basal-like, as previously discussed. However, these classifications may not be as exact as our gene signature derived from TCGA patient data.

Our hope is that this study will lead to increased scrutiny of gene expression profiles and the tumor microenvironment in patients. The studies presented in this thesis have demonstrated that the intersection of these two factors have a profound influence on drug sensitivity in HER2+ breast cancer models that are otherwise responsive to treatment. Proper identification of the combination of risk factors we have outlined in this study can better inform targeted therapy regimen design, and potentially vastly increase the efficacy of existing front and second line treatments. We believe there is a strong potential for these rationally designed regimens to abrogate major drivers of drug resistance, resulting in lasting responses to treatment and dramatically improved long-term outcomes.

References

1. Cunha, F. The Edwin Smith surgical papyrus. *Am J Surg* **78**, 277 (1949).
2. Bloom, H. *Homer's The Iliad*, (Chelsea House, New York, 1987).
3. Lakhtakia, R. A Brief History of Breast Cancer: Part I: Surgical domination reinvented. *Sultan Qaboos Univ Med J* **14**, e166-169 (2014).
4. Wilmanns, J.C. [Surgical treatment of breast carcinoma since Hippocrates of Cos]. *Gynakol Geburtshilfliche Rundsch* **35**, 103-111 (1995).
5. Loukas, M.*, et al.* The history of mastectomy. *Am Surg* **77**, 566-571 (2011).
6. Boveri, T. *Concerning the origin of malignant tumours*, (The Company of Biologists ; Cold Spring Harbor Laboratory Press, Cambridge, England Woodbury, N.Y., 2008).
7. Sutton, W.S. The chromosomes in heredity. *The Biological Bulletin* **4**, 231-250 (1903).
8. Morgan, T.H. Sex Limited Inheritance in Drosophila. *Science* **32**, 120-122 (1910).
9. Baltimore, D. RNA-dependent DNA polymerase in virions of RNA tumour viruses. *Nature* **226**, 1209-1211 (1970).
10. Rous, P. A Sarcoma of the Fowl Transmissible by an Agent Separable from the Tumor Cells. *J Exp Med* **13**, 397-411 (1911).
11. Temin, H.M. & Rubin, H. Characteristics of an assay for Rous sarcoma virus and Rous sarcoma cells in tissue culture. *Virology* **6**, 669-688 (1958).
12. Shih, C., Padhy, L.C., Murray, M. & Weinberg, R.A. Transforming genes of carcinomas and neuroblastomas introduced into mouse fibroblasts. *Nature* **290**, 261-264 (1981).
13. Hanafusa, H., Hanafusa, T. & Rubin, H. Analysis of the Defectiveness of Rous Sarcoma Virus. I. Characterization of the Helper Virus. *Virology* **22**, 591-601 (1964).
14. Hanafusa, H., Hanafusa, T. & Rubin, H. Analysis of the Defectiveness of Rous Sarcoma Virus, Ii. Specification of Rsv Antigenicity by Helper Virus. *Proc Natl Acad Sci U S A* **51**, 41-48 (1964).
15. Martin, G.S. The road to Src. *Oncogene* **23**, 7910-7917 (2004).
16. Stehelin, D., Varmus, H.E., Bishop, J.M. & Vogt, P.K. DNA related to the transforming gene(s) of avian sarcoma viruses is present in normal avian DNA. *Nature* **260**, 170-173 (1976).
17. Pawson, T. Specificity in signal transduction: from phosphotyrosine-SH2 domain interactions to complex cellular systems. *Cell* **116**, 191-203 (2004).
18. Xu, W., Doshi, A., Lei, M., Eck, M.J. & Harrison, S.C. Crystal structures of c-Src reveal features of its autoinhibitory mechanism. *Mol Cell* **3**, 629-638 (1999).
19. Vogt, P.K. Retroviral oncogenes: a historical primer. *Nat Rev Cancer* **12**, 639-648 (2012).
20. Slamon, D.J.*, et al.* Studies of the HER-2/neu proto-oncogene in human breast and ovarian cancer. *Science* **244**, 707-712 (1989).
21. Phillips, W.A., St Clair, F., Munday, A.D., Thomas, R.J. & Mitchell, C.A. Increased levels of phosphatidylinositol 3-kinase activity in colorectal tumors. *Cancer* **83**, 41-47 (1998).
22. Schwab, M.*, et al.* Enhanced expression of the human gene N-myc consequent to amplification of DNA may contribute to malignant progression of neuroblastoma. *Proc Natl Acad Sci U S A* **81**, 4940-4944 (1984).
23. Ben-Neriah, Y., Daley, G.Q., Mes-Masson, A.M., Witte, O.N. & Baltimore, D. The chronic myelogenous leukemia-specific P210 protein is the product of the bcr/abl hybrid gene. *Science* **233**, 212-214 (1986).
24. Der, C.J., Krontiris, T.G. & Cooper, G.M. Transforming genes of human bladder and lung carcinoma cell lines are homologous to the ras genes of Harvey and Kirsten sarcoma viruses. *Proc Natl Acad Sci U S A* **79**, 3637-3640 (1982).

25. Hihara, H., Yamamoto, H., Shimohira, H., Arai, K. & Shimizu, T. Avian erythroblastosis virus isolated from chick erythroblastosis induced by lymphatic leukemia virus subgroup A. *J Natl Cancer Inst* **70**, 891-897 (1983).
26. Ullrich, A.*, et al.* Human epidermal growth factor receptor cDNA sequence and aberrant expression of the amplified gene in A431 epidermoid carcinoma cells. *Nature* **309**, 418-425 (1984).
27. Schechter, A.L.*, et al.* The neu gene: an erbB-homologous gene distinct from and unlinked to the gene encoding the EGF receptor. *Science* **229**, 976-978 (1985).
28. Coussens, L.*, et al.* Tyrosine kinase receptor with extensive homology to EGF receptor shares chromosomal location with neu oncogene. *Science* **230**, 1132-1139 (1985).
29. King, C.R., Kraus, M.H. & Aaronson, S.A. Amplification of a novel v-erbB-related gene in a human mammary carcinoma. *Science* **229**, 974-976 (1985).
30. Brennan, P.J., Kumagai, T., Berezov, A., Murali, R. & Greene, M.I. HER2/Neu: mechanisms of dimerization/oligomerization. *Oncogene* **21**, 328 (2002).
31. Bargmann, C.I., Hung, M.C. & Weinberg, R.A. Multiple independent activations of the neu oncogene by a point mutation altering the transmembrane domain of p185. *Cell* **45**, 649-657 (1986).
32. Hudziak, R.M., Schlessinger, J. & Ullrich, A. Increased expression of the putative growth factor receptor p185HER2 causes transformation and tumorigenesis of NIH 3T3 cells. *Proc Natl Acad Sci U S A* **84**, 7159-7163 (1987).
33. Farber, S. & Diamond, L.K. Temporary remissions in acute leukemia in children produced by folic acid antagonist, 4-aminopteroyl-glutamic acid. *N Engl J Med* **238**, 787-793 (1948).
34. Hertz, R., Bergenstal, D.M., Lipsett, M.B., Price, E.B. & Hilbish, T.F. Chemotherapy of choriocarcinoma and related trophoblastic tumors in women. *J Am Med Assoc* **168**, 845-854 (1958).
35. Knight, W.A., Livingston, R.B., Gregory, E.J. & McGuire, W.L. Estrogen receptor as an independent prognostic factor for early recurrence in breast cancer. *Cancer Res* **37**, 4669-4671 (1977).
36. Colditz, G.A., Rosner, B.A., Chen, W.Y., Holmes, M.D. & Hankinson, S.E. Risk factors for breast cancer according to estrogen and progesterone receptor status. *J Natl Cancer Inst* **96**, 218-228 (2004).
37. Parise, C.A. & Caggiano, V. Breast Cancer Survival Defined by the ER/PR/HER2 Subtypes and a Surrogate Classification according to Tumor Grade and Immunohistochemical Biomarkers. *J Cancer Epidemiol* **2014**, 469251 (2014).
38. Cole, M.P., Jones, C.T. & Todd, I.D. A new anti-oestrogenic agent in late breast cancer. An early clinical appraisal of ICI46474. *Br J Cancer* **25**, 270-275 (1971).
39. Gnant, M., Harbeck, N. & Thomssen, C. St. Gallen 2011: Summary of the Consensus Discussion. *Breast Care (Basel)* **6**, 136-141 (2011).
40. Harbeck, N., Thomssen, C. & Gnant, M. St. Gallen 2013: brief preliminary summary of the consensus discussion. *Breast Care (Basel)* **8**, 102-109 (2013).
41. Wolff, A.C.*, et al.* American Society of Clinical Oncology/College of American Pathologists guideline recommendations for human epidermal growth factor receptor 2 testing in breast cancer. *J Clin Oncol* **25**, 118-145 (2007).
42. Prat, A. & Baselga, J. The role of hormonal therapy in the management of hormonal-receptor-positive breast cancer with co-expression of HER2. *Nat Clin Pract Oncol* **5**, 531-542 (2008).
43. Perou, C.M.*, et al.* Molecular portraits of human breast tumours. *Nature* **406**, 747-752 (2000).
44. Rivenbark, A.G., O'Connor, S.M. & Coleman, W.B. Molecular and cellular heterogeneity in breast cancer: challenges for personalized medicine. *Am J Pathol* **183**, 1113-1124 (2013).
45. Ali, H.R.*, et al.* Genome-driven integrated classification of breast cancer validated in over 7,500 samples. *Genome Biol* **15**, 431 (2014).

46. Cancer Genome Atlas, N. Comprehensive molecular portraits of human breast tumours. *Nature* **490**, 61-70 (2012).
47. Gudjonsson, T., Adriance, M.C., Sternlicht, M.D., Petersen, O.W. & Bissell, M.J. Myoepithelial cells: their origin and function in breast morphogenesis and neoplasia. *J Mammary Gland Biol Neoplasia* **10**, 261-272 (2005).
48. Forster, N.*, et al.* Basal cell signaling by p63 controls luminal progenitor function and lactation via NRG1. *Dev Cell* **28**, 147-160 (2014).
49. Mallepell, S., Krust, A., Chambon, P. & Brisken, C. Paracrine signaling through the epithelial estrogen receptor alpha is required for proliferation and morphogenesis in the mammary gland. *Proc Natl Acad Sci U S A* **103**, 2196-2201 (2006).
50. Ye, X.*, et al.* Distinct EMT programs control normal mammary stem cells and tumour-initiating cells. *Nature* **525**, 256-260 (2015).
51. Santagata, S.*, et al.* Taxonomy of breast cancer based on normal cell phenotype predicts outcome. *J Clin Invest* **124**, 859-870 (2014).
52. Petersen, O.W., Hoyer, P.E. & van Deurs, B. Frequency and distribution of estrogen receptor-positive cells in normal, nonlactating human breast tissue. *Cancer Res* **47**, 5748-5751 (1987).
53. Sternlicht, M.D.*, et al.* Mammary ductal morphogenesis requires paracrine activation of stromal EGFR via ADAM17-dependent shedding of epithelial amphiregulin. *Development* **132**, 3923-3933 (2005).
54. Lu, P., Ewald, A.J., Martin, G.R. & Werb, Z. Genetic mosaic analysis reveals FGF receptor 2 function in terminal end buds during mammary gland branching morphogenesis. *Dev Biol* **321**, 77-87 (2008).
55. Shackleton, M.*, et al.* Generation of a functional mammary gland from a single stem cell. *Nature* **439**, 84-88 (2006).
56. Stingl, J.*, et al.* Purification and unique properties of mammary epithelial stem cells. *Nature* **439**, 993-997 (2006).
57. Asselin-Labat, M.L.*, et al.* Control of mammary stem cell function by steroid hormone signalling. *Nature* **465**, 798-802 (2010).
58. Visvader, J.E. & Lindeman, G.J. Mammary stem cells and mammopoiesis. *Cancer Res* **66**, 9798-9801 (2006).
59. Visvader, J.E. Keeping abreast of the mammary epithelial hierarchy and breast tumorigenesis. *Genes Dev* **23**, 2563-2577 (2009).
60. Kim, J.*, et al.* HRG-beta1-driven ErbB3 signaling induces epithelial-mesenchymal transition in breast cancer cells. *BMC Cancer* **13**, 383 (2013).
61. Skibinski, A.*, et al.* The Hippo transducer TAZ interacts with the SWI/SNF complex to regulate breast epithelial lineage commitment. *Cell Rep* **6**, 1059-1072 (2014).
62. Van Nguyen, A. & Pollard, J.W. Colony stimulating factor-1 is required to recruit macrophages into the mammary gland to facilitate mammary ductal outgrowth. *Dev Biol* **247**, 11-25 (2002).
63. Mukhopadhyay, C., Zhao, X., Maroni, D., Band, V. & Naramura, M. Distinct effects of EGFR ligands on human mammary epithelial cell differentiation. *PLoS One* **8**, e75907 (2013).
64. Jones, J.T., Akita, R.W. & Sliwkowski, M.X. Binding specificities and affinities of egf domains for ErbB receptors. *FEBS Lett* **447**, 227-231 (1999).
65. Luo, X.*, et al.* Cleavage of neuregulin-1 by BACE1 or ADAM10 protein produces differential effects on myelination. *J Biol Chem* **286**, 23967-23974 (2011).
66. Ieguchi, K.*, et al.* Direct binding of the EGF-like domain of neuregulin-1 to integrins ({alpha}v{beta}3 and {alpha}6{beta}4) is involved in neuregulin-1/ErbB signaling. *J Biol Chem* **285**, 31388-31398 (2010).
67. Consortium, G.T. The Genotype-Tissue Expression (GTEx) project. *Nat Genet* **45**, 580-585 (2013).
68. Uhlen, M.*, et al.* Proteomics. Tissue-based map of the human proteome. *Science* **347**, 1260419 (2015).

69. Gonzalez, L.*, et al.* Gene expression profile of normal and cancer-associated fibroblasts according to intratumoral inflammatory cells phenotype from breast cancer tissue. *Mol Carcinog* **55**, 1489-1502 (2016).
70. Leung, W.Y.*, et al.* Combining lapatinib and pertuzumab to overcome lapatinib resistance due to NRG1-mediated signalling in HER2-amplified breast cancer. *Oncotarget* **6**, 5678-5694 (2015).
71. Jarde, T.*, et al.* Wnt and Neuregulin1/ErbB signalling extends 3D culture of hormone responsive mammary organoids. *Nat Commun* **7**, 13207 (2016).
72. Niemann, C.*, et al.* Reconstitution of mammary gland development in vitro: requirement of c-met and c-erbB2 signaling for branching and alveolar morphogenesis. *J Cell Biol* **143**, 533-545 (1998).
73. Park, J., Sarode, V.R., Euhus, D., Kittler, R. & Scherer, P.E. Neuregulin 1-HER axis as a key mediator of hyperglycemic memory effects in breast cancer. *Proc Natl Acad Sci U S A* **109**, 21058-21063 (2012).
74. Tidcombe, H.*, et al.* Neural and mammary gland defects in ErbB4 knockout mice genetically rescued from embryonic lethality. *Proc Natl Acad Sci U S A* **100**, 8281-8286 (2003).
75. Weidner, K.M.*, et al.* Evidence for the identity of human scatter factor and human hepatocyte growth factor. *Proc Natl Acad Sci U S A* **88**, 7001-7005 (1991).
76. Nakamura, T. Structure and function of hepatocyte growth factor. *Prog Growth Factor Res* **3**, 67-85 (1991).
77. Naldini, L.*, et al.* Biological activation of pro-HGF (hepatocyte growth factor) by urokinase is controlled by a stoichiometric reaction. *J Biol Chem* **270**, 603-611 (1995).
78. Schaeper, U.*, et al.* Coupling of Gab1 to c-Met, Grb2, and Shp2 mediates biological responses. *J Cell Biol* **149**, 1419-1432 (2000).
79. Tyan, S.W.*, et al.* Breast cancer cells induce cancer-associated fibroblasts to secrete hepatocyte growth factor to enhance breast tumorigenesis. *PLoS One* **6**, e15313 (2011).
80. Zhang, H.Z., Bennett, J.M., Smith, K.T., Sunil, N. & Haslam, S.Z. Estrogen mediates mammary epithelial cell proliferation in serum-free culture indirectly via mammary stroma-derived hepatocyte growth factor. *Endocrinology* **143**, 3427-3434 (2002).
81. Niranjan, B.*, et al.* HGF/SF: a potent cytokine for mammary growth, morphogenesis and development. *Development* **121**, 2897-2908 (1995).
82. Kitajima, Y., Ide, T., Ohtsuka, T. & Miyazaki, K. Induction of hepatocyte growth factor activator gene expression under hypoxia activates the hepatocyte growth factor/c-Met system via hypoxia inducible factor-1 in pancreatic cancer. *Cancer Sci* **99**, 1341-1347 (2008).
83. Miyazawa, K., Shimomura, T. & Kitamura, N. Activation of hepatocyte growth factor in the injured tissues is mediated by hepatocyte growth factor activator. *J Biol Chem* **271**, 3615-3618 (1996).
84. Parr, C., Watkins, G., Mansel, R.E. & Jiang, W.G. The hepatocyte growth factor regulatory factors in human breast cancer. *Clin Cancer Res* **10**, 202-211 (2004).
85. Veenstra, C.*, et al.* Met and its ligand HGF are associated with clinical outcome in breast cancer. *Oncotarget* **7**, 37145-37159 (2016).
86. Cho, H.S.*, et al.* Structure of the extracellular region of HER2 alone and in complex with the Herceptin Fab. *Nature* **421**, 756-760 (2003).
87. Garrett, T.P.*, et al.* The crystal structure of a truncated ErbB2 ectodomain reveals an active conformation, poised to interact with other ErbB receptors. *Mol Cell* **11**, 495-505 (2003).
88. Mitra, D.*, et al.* An oncogenic isoform of HER2 associated with locally disseminated breast cancer and trastuzumab resistance. *Mol Cancer Ther* **8**, 2152-2162 (2009).
89. Press, M.F., Cordon-Cardo, C. & Slamon, D.J. Expression of the HER-2/neu proto-oncogene in normal human adult and fetal tissues. *Oncogene* **5**, 953-962 (1990).
90. Andrechek, E.R., White, D. & Muller, W.J. Targeted disruption of ErbB2/Neu in the mammary epithelium results in impaired ductal outgrowth. *Oncogene* **24**, 932-937 (2005).

91. Negro, A., Brar, B.K. & Lee, K.F. Essential roles of Her2/erbB2 in cardiac development and function. *Recent Prog Horm Res* **59**, 1-12 (2004).
92. Keefe, D.L. Trastuzumab-associated cardiotoxicity. *Cancer* **95**, 1592-1600 (2002).
93. Bonifazi, M.*, et al.* Trastuzumab-related cardiotoxicity in early breast cancer: a cohort study. *Oncologist* **18**, 795-801 (2013).
94. Finigan, J.H.*, et al.* Neuregulin-1-human epidermal receptor-2 signaling is a central regulator of pulmonary epithelial permeability and acute lung injury. *J Biol Chem* **286**, 10660-10670 (2011).
95. Ferguson, K.M.*, et al.* EGF activates its receptor by removing interactions that autoinhibit ectodomain dimerization. *Mol Cell* **11**, 507-517 (2003).
96. Witton, C.J., Reeves, J.R., Going, J.J., Cooke, T.G. & Bartlett, J.M. Expression of the HER1-4 family of receptor tyrosine kinases in breast cancer. *J Pathol* **200**, 290-297 (2003).
97. Ferguson, K.M. Structure-based view of epidermal growth factor receptor regulation. *Annu Rev Biophys* **37**, 353-373 (2008).
98. Ward, M.D. & Leahy, D.J. Kinase activator-receiver preference in ErbB heterodimers is determined by intracellular regions and is not coupled to extracellular asymmetry. *J Biol Chem* **290**, 1570-1579 (2015).
99. Novotny, C.J.*, et al.* Overcoming resistance to HER2 inhibitors through state-specific kinase binding. *Nat Chem Biol* **12**, 923-930 (2016).
100. Wood, E.R.*, et al.* A unique structure for epidermal growth factor receptor bound to GW572016 (Lapatinib): relationships among protein conformation, inhibitor off-rate, and receptor activity in tumor cells. *Cancer Res* **64**, 6652-6659 (2004).
101. Aertgeerts, K.*, et al.* Structural analysis of the mechanism of inhibition and allosteric activation of the kinase domain of HER2 protein. *J Biol Chem* **286**, 18756-18765 (2011).
102. Zhang, X., Gureasko, J., Shen, K., Cole, P.A. & Kuriyan, J. An allosteric mechanism for activation of the kinase domain of epidermal growth factor receptor. *Cell* **125**, 1137-1149 (2006).
103. Bose, R.*, et al.* Phosphoproteomic analysis of Her2/neu signaling and inhibition. *Proc Natl Acad Sci U S A* **103**, 9773-9778 (2006).
104. Wang, H.M.*, et al.* The catalytic region and PEST domain of PTPN18 distinctly regulate the HER2 phosphorylation and ubiquitination barcodes. *Cell Res* **24**, 1067-1090 (2014).
105. Janes, P.W.*, et al.* Structural determinants of the interaction between the erbB2 receptor and the Src homology 2 domain of Grb7. *J Biol Chem* **272**, 8490-8497 (1997).
106. Hazan, R.*, et al.* Identification of autophosphorylation sites of HER2/neu. *Cell Growth Differ* **1**, 3-7 (1990).
107. Ghosh, R.*, et al.* Trastuzumab has preferential activity against breast cancers driven by HER2 homodimers. *Cancer Res* **71**, 1871-1882 (2011).
108. Schulze, W.X., Deng, L. & Mann, M. Phosphotyrosine interactome of the ErbB-receptor kinase family. *Mol Syst Biol* **1**, 2005 0008 (2005).
109. Muthuswamy, S.K., Gilman, M. & Brugge, J.S. Controlled dimerization of ErbB receptors provides evidence for differential signaling by homo- and heterodimers. *Mol Cell Biol* **19**, 6845-6857 (1999).
110. Hartman, Z., Zhao, H. & Agazie, Y.M. HER2 stabilizes EGFR and itself by altering autophosphorylation patterns in a manner that overcomes regulatory mechanisms and promotes proliferative and transformation signaling. *Oncogene* **32**, 4169-4180 (2013).
111. Hommelgaard, A.M., Lerdrup, M. & van Deurs, B. Association with membrane protrusions makes ErbB2 an internalization-resistant receptor. *Mol Biol Cell* **15**, 1557-1567 (2004).
112. Henriksen, L., Grandal, M.V., Knudsen, S.L., van Deurs, B. & Grovdal, L.M. Internalization mechanisms of the epidermal growth factor receptor after activation with different ligands. *PLoS One* **8**, e58148 (2013).
113. Chung, I.*, et al.* High cell-surface density of HER2 deforms cell membranes. *Nat Commun* **7**, 12742 (2016).

114. Prince, T.L., *et al.* Client Proteins and Small Molecule Inhibitors Display Distinct Binding Preferences for Constitutive and Stress-Induced HSP90 Isoforms and Their Conformationally Restricted Mutants. *PLoS One* **10**, e0141786 (2015).
115. Pust, S., *et al.* Flotillins as regulators of ErbB2 levels in breast cancer. *Oncogene* **32**, 3443-3451 (2013).
116. Jeong, J., *et al.* PMCA2 regulates HER2 protein kinase localization and signaling and promotes HER2-mediated breast cancer. *Proc Natl Acad Sci U S A* **113**, E282-290 (2016).
117. Austin, C.D., *et al.* Endocytosis and sorting of ErbB2 and the site of action of cancer therapeutics trastuzumab and geldanamycin. *Mol Biol Cell* **15**, 5268-5282 (2004).
118. Gostring, L., Lindegren, S. & Gedda, L. 17AAG-induced internalisation of HER2-specific Affibody molecules. *Oncol Lett* **12**, 2574-2580 (2016).
119. Naidu, R., Yadav, M., Nair, S. & Kutty, M.K. Expression of c-erbB3 protein in primary breast carcinomas. *Br J Cancer* **78**, 1385-1390 (1998).
120. Lemoine, N.R., *et al.* Expression of the ERBB3 gene product in breast cancer. *Br J Cancer* **66**, 1116-1121 (1992).
121. Jura, N., Shan, Y., Cao, X., Shaw, D.E. & Kuriyan, J. Structural analysis of the catalytically inactive kinase domain of the human EGF receptor 3. *Proc Natl Acad Sci U S A* **106**, 21608-21613 (2009).
122. Tzahar, E., *et al.* A hierarchical network of interreceptor interactions determines signal transduction by Neu differentiation factor/neuregulin and epidermal growth factor. *Mol Cell Biol* **16**, 5276-5287 (1996).
123. Pinkas-Kramarski, R., *et al.* Diversification of Neu differentiation factor and epidermal growth factor signaling by combinatorial receptor interactions. *The EMBO journal* **15**, 2452-2467 (1996).
124. Yang, S., *et al.* Mapping ErbB receptors on breast cancer cell membranes during signal transduction. *J Cell Sci* **120**, 2763-2773 (2007).
125. Amin, D.N., *et al.* Resiliency and vulnerability in the HER2-HER3 tumorigenic driver. *Sci Transl Med* **2**, 16ra17 (2010).
126. Amin, D.N., Sergina, N., Lim, L., Goga, A. & Moasser, M.M. HER3 signalling is regulated through a multitude of redundant mechanisms in HER2-driven tumour cells. *Biochem J* **447**, 417-425 (2012).
127. Garrett, J.T., *et al.* Transcriptional and posttranslational up-regulation of HER3 (ErbB3) compensates for inhibition of the HER2 tyrosine kinase. *Proc Natl Acad Sci U S A* **108**, 5021-5026 (2011).
128. Turke, A.B., *et al.* MEK inhibition leads to PI3K/AKT activation by relieving a negative feedback on ERBB receptors. *Cancer Res* **72**, 3228-3237 (2012).
129. Yonesaka, K., *et al.* Anti-HER3 monoclonal antibody patritumab sensitizes refractory non-small cell lung cancer to the epidermal growth factor receptor inhibitor erlotinib. *Oncogene* **35**, 878-886 (2016).
130. Hegde, G.V., *et al.* Blocking NRG1 and other ligand-mediated Her4 signaling enhances the magnitude and duration of the chemotherapeutic response of non-small cell lung cancer. *Sci Transl Med* **5**, 171ra118 (2013).
131. Downward, J., *et al.* Close similarity of epidermal growth factor receptor and v-erb-B oncogene protein sequences. *Nature* **307**, 521-527 (1984).
132. Schechter, A.L., *et al.* The neu oncogene: an erb-B-related gene encoding a 185,000-Mr tumour antigen. *Nature* **312**, 513-516 (1984).
133. Muller, W.J., Sinn, E., Pattengale, P.K., Wallace, R. & Leder, P. Single-step induction of mammary adenocarcinoma in transgenic mice bearing the activated c-neu oncogene. *Cell* **54**, 105-115 (1988).
134. Bouchard, L., Lamarre, L., Tremblay, P.J. & Jolicoeur, P. Stochastic appearance of mammary tumors in transgenic mice carrying the MMTV/c-neu oncogene. *Cell* **57**, 931-936 (1989).

135. Di Fiore, P.P.*, et al.* erbB-2 is a potent oncogene when overexpressed in NIH/3T3 cells. *Science* **237**, 178-182 (1987).
136. Chazin, V.R., Kaleko, M., Miller, A.D. & Slamon, D.J. Transformation mediated by the human HER-2 gene independent of the epidermal growth factor receptor. *Oncogene* **7**, 1859-1866 (1992).
137. Finkle, D.*, et al.* HER2-targeted therapy reduces incidence and progression of midlife mammary tumors in female murine mammary tumor virus huHER2-transgenic mice. *Clin Cancer Res* **10**, 2499-2511 (2004).
138. Park, J.W., Neve, R.M., Szollosi, J. & Benz, C.C. Unraveling the biologic and clinical complexities of HER2. *Clin Breast Cancer* **8**, 392-401 (2008).
139. Kallioniemi, O.P.*, et al.* ERBB2 amplification in breast cancer analyzed by fluorescence in situ hybridization. *Proc Natl Acad Sci U S A* **89**, 5321-5325 (1992).
140. Staaf, J.*, et al.* High-resolution genomic and expression analyses of copy number alterations in HER2-amplified breast cancer. *Breast Cancer Res* **12**, R25 (2010).
141. Ng, C.K., Schultheis, A.M., Bidard, F.C., Weigelt, B. & Reis-Filho, J.S. Breast cancer genomics from microarrays to massively parallel sequencing: paradigms and new insights. *J Natl Cancer Inst* **107**(2015).
142. Sahlberg, K.K.*, et al.* The HER2 amplicon includes several genes required for the growth and survival of HER2 positive breast cancer cells. *Mol Oncol* **7**, 392-401 (2013).
143. Bose, R.*, et al.* Activating HER2 mutations in HER2 gene amplification negative breast cancer. *Cancer discovery* **3**, 224-237 (2013).
144. Wilson, T.R., Lee, D.Y., Berry, L., Shames, D.S. & Settleman, J. Neuregulin-1-mediated autocrine signaling underlies sensitivity to HER2 kinase inhibitors in a subset of human cancers. *Cancer Cell* **20**, 158-172 (2011).
145. Wang, T.*, et al.* HER2 somatic mutations are associated with poor survival in HER2-negative breast cancers. *Cancer Sci* (2017).
146. Dumay, A.*, et al.* Distinct tumor protein p53 mutants in breast cancer subgroups. *Int J Cancer* **132**, 1227-1231 (2013).
147. Vicario, R.*, et al.* Patterns of HER2 Gene Amplification and Response to Anti-HER2 Therapies. *PLoS One* **10**, e0129876 (2015).
148. Nuciforo, P.*, et al.* High HER2 protein levels correlate with increased survival in breast cancer patients treated with anti-HER2 therapy. *Mol Oncol* **10**, 138-147 (2016).
149. Matsui, A., Ihara, T., Suda, H., Mikami, H. & Semba, K. Gene amplification: mechanisms and involvement in cancer. *Biomol Concepts* **4**, 567-582 (2013).
150. McClintock, B. The Stability of Broken Ends of Chromosomes in Zea Mays. *Genetics* **26**, 234-282 (1941).
151. McClintock, B. The Production of Homozygous Deficient Tissues with Mutant Characteristics by Means of the Aberrant Mitotic Behavior of Ring-Shaped Chromosomes. *Genetics* **23**, 315-376 (1938).
152. Kennecke, H.*, et al.* Metastatic behavior of breast cancer subtypes. *J Clin Oncol* **28**, 3271-3277 (2010).
153. Sharma, S.V. & Settleman, J. Oncogene addiction: setting the stage for molecularly targeted cancer therapy. *Genes Dev* **21**, 3214-3231 (2007).
154. Sorlie, T.*, et al.* Gene expression patterns of breast carcinomas distinguish tumor subclasses with clinical implications. *Proc Natl Acad Sci U S A* **98**, 10869-10874 (2001).
155. Sorlie, T.*, et al.* Repeated observation of breast tumor subtypes in independent gene expression data sets. *Proc Natl Acad Sci U S A* **100**, 8418-8423 (2003).
156. Wu, Z. & Irizarry, R.A. Preprocessing of oligonucleotide array data. *Nature biotechnology* **22**, 656-658; author reply 658 (2004).
157. Petranyi, G. [The 1984 Nobel Prize for physiology and medicine]. *Orv Hetil* **126**, 1485-1487 (1985).

158. Fendly, B.M., *et al.* Characterization of murine monoclonal antibodies reactive to either the human epidermal growth factor receptor or HER2/neu gene product. *Cancer Res* **50**, 1550-1558 (1990).
159. Carter, P., *et al.* Humanization of an anti-p185HER2 antibody for human cancer therapy. *Proc Natl Acad Sci U S A* **89**, 4285-4289 (1992).
160. Perez, E.A., *et al.* Trastuzumab plus adjuvant chemotherapy for human epidermal growth factor receptor 2-positive breast cancer: planned joint analysis of overall survival from NSABP B-31 and NCCTG N9831. *J Clin Oncol* **32**, 3744-3752 (2014).
161. Geyer, C.E., *et al.* Lapatinib plus capecitabine for HER2-positive advanced breast cancer. *N Engl J Med* **355**, 2733-2743 (2006).
162. Blackwell, K.L., *et al.* Single-agent lapatinib for HER2-overexpressing advanced or metastatic breast cancer that progressed on first- or second-line trastuzumab-containing regimens. *Ann Oncol* **20**, 1026-1031 (2009).
163. Kaufman, B., *et al.* Lapatinib monotherapy in patients with HER2-overexpressing relapsed or refractory inflammatory breast cancer: final results and survival of the expanded HER2+ cohort in EGF103009, a phase II study. *Lancet Oncol* **10**, 581-588 (2009).
164. Longva, K.E., Pedersen, N.M., Haslekas, C., Stang, E. & Madshus, I.H. Herceptin-induced inhibition of ErbB2 signaling involves reduced phosphorylation of Akt but not endocytic down-regulation of ErbB2. *Int J Cancer* **116**, 359-367 (2005).
165. Miller, K., *et al.* HERMIONE: a randomized Phase 2 trial of MM-302 plus trastuzumab versus chemotherapy of physician's choice plus trastuzumab in patients with previously treated, anthracycline-naive, HER2-positive, locally advanced/metastatic breast cancer. *BMC Cancer* **16**, 352 (2016).
166. Baselga, J., *et al.* Pertuzumab plus trastuzumab plus docetaxel for metastatic breast cancer. *N Engl J Med* **366**, 109-119 (2012).
167. Schuler, M., *et al.* A phase II trial to assess efficacy and safety of afatinib in extensively pretreated patients with HER2-negative metastatic breast cancer. *Breast Cancer Res Treat* **134**, 1149-1159 (2012).
168. Blackwell, K.L., *et al.* Randomized study of Lapatinib alone or in combination with trastuzumab in women with ErbB2-positive, trastuzumab-refractory metastatic breast cancer. *J Clin Oncol* **28**, 1124-1130 (2010).
169. Saura, C., *et al.* Safety and efficacy of neratinib in combination with capecitabine in patients with metastatic human epidermal growth factor receptor 2-positive breast cancer. *J Clin Oncol* **32**, 3626-3633 (2014).
170. Chan, A., *et al.* Neratinib after trastuzumab-based adjuvant therapy in patients with HER2-positive breast cancer (ExteNET): a multicentre, randomised, double-blind, placebo-controlled, phase 3 trial. *Lancet Oncol* **17**, 367-377 (2016).
171. Eriksson, J.E., *et al.* Introducing intermediate filaments: from discovery to disease. *J Clin Invest* **119**, 1763-1771 (2009).
172. Ponti, D., *et al.* Isolation and in vitro propagation of tumorigenic breast cancer cells with stem/progenitor cell properties. *Cancer Res* **65**, 5506-5511 (2005).
173. Ginestier, C., *et al.* ALDH1 is a marker of normal and malignant human mammary stem cells and a predictor of poor clinical outcome. *Cell Stem Cell* **1**, 555-567 (2007).
174. Prat, A. & Perou, C.M. Deconstructing the molecular portraits of breast cancer. *Mol Oncol* **5**, 5-23 (2011).
175. Keller, P.J., *et al.* Mapping the cellular and molecular heterogeneity of normal and malignant breast tissues and cultured cell lines. *Breast Cancer Res* **12**, R87 (2010).
176. Parker, J.S., *et al.* Supervised risk predictor of breast cancer based on intrinsic subtypes. *J Clin Oncol* **27**, 1160-1167 (2009).

177. Nielsen, T.O.*, et al.* A comparison of PAM50 intrinsic subtyping with immunohistochemistry and clinical prognostic factors in tamoxifen-treated estrogen receptor-positive breast cancer. *Clin Cancer Res* **16**, 5222-5232 (2010).
178. Van Keymeulen, A.*, et al.* Reactivation of multipotency by oncogenic PIK3CA induces breast tumour heterogeneity. *Nature* **525**, 119-123 (2015).
179. Koren, S.*, et al.* PIK3CA(H1047R) induces multipotency and multi-lineage mammary tumours. *Nature* **525**, 114-118 (2015).
180. Lim, E.*, et al.* Aberrant luminal progenitors as the candidate target population for basal tumor development in BRCA1 mutation carriers. *Nat Med* **15**, 907-913 (2009).
181. Prabhakaran, P., Hassiotou, F., Blancafort, P. & Filgueira, L. Cisplatin induces differentiation of breast cancer cells. *Front Oncol* **3**, 134 (2013).
182. Huang, J., Li, H. & Ren, G. Epithelial-mesenchymal transition and drug resistance in breast cancer (Review). *Int J Oncol* **47**, 840-848 (2015).
183. Battula, V.L.*, et al.* Epithelial-mesenchymal transition-derived cells exhibit multilineage differentiation potential similar to mesenchymal stem cells. *Stem Cells* **28**, 1435-1445 (2010).
184. Hou, L.*, et al.* FAT4 functions as a tumor suppressor in triple-negative breast cancer. *Tumour Biol* (2016).
185. Dupont, S.*, et al.* Role of YAP/TAZ in mechanotransduction. *Nature* **474**, 179-183 (2011).
186. Bhargava, R.*, et al.* Immunohistochemical surrogate markers of breast cancer molecular classes predicts response to neoadjuvant chemotherapy: a single institutional experience with 359 cases. *Cancer* **116**, 1431-1439 (2010).
187. de Azambuja, E.*, et al.* Lapatinib with trastuzumab for HER2-positive early breast cancer (NeoALTTO): survival outcomes of a randomised, open-label, multicentre, phase 3 trial and their association with pathological complete response. *Lancet Oncol* **15**, 1137-1146 (2014).
188. Gianni, L.*, et al.* Efficacy and safety of neoadjuvant pertuzumab and trastuzumab in women with locally advanced, inflammatory, or early HER2-positive breast cancer (NeoSphere): a randomised multicentre, open-label, phase 2 trial. *Lancet Oncol* **13**, 25-32 (2012).
189. Perez, E.A.*, et al.* Intrinsic Subtype and Therapeutic Response Among HER2-Positive Breaty st Tumors from the NCCTG (Alliance) N9831 Trial. *J Natl Cancer Inst* **109**(2017).
190. Xu, X.*, et al.* HER2 Reactivation through Acquisition of the HER2 L755S Mutation as a Mechanism of Acquired Resistance to HER2-targeted Therapy in HER2+ Breast Cancer. *Clin Cancer Res* (2017).
191. Arcila, M.E.*, et al.* Prevalence, clinicopathologic associations, and molecular spectrum of ERBB2 (HER2) tyrosine kinase mutations in lung adenocarcinomas. *Clin Cancer Res* **18**, 4910-4918 (2012).
192. Anido, J.*, et al.* Biosynthesis of tumorigenic HER2 C-terminal fragments by alternative initiation of translation. *The EMBO journal* **25**, 3234-3244 (2006).
193. Parra-Palau, J.L.*, et al.* Effect of p95HER2/611CTF on the response to trastuzumab and chemotherapy. *J Natl Cancer Inst* **106**(2014).
194. Pereira, C.B.*, et al.* Prognostic and predictive significance of MYC and KRAS alterations in breast cancer from women treated with neoadjuvant chemotherapy. *PLoS One* **8**, e60576 (2013).
195. de Oliveira Taveira, M.*, et al.* Genomic characteristics of trastuzumab-resistant Her2-positive metastatic breast cancer. *J Cancer Res Clin Oncol* (2017).
196. Korkola, J.E.*, et al.* Decoupling of the PI3K Pathway via Mutation Necessitates Combinatorial Treatment in HER2+ Breast Cancer. *PLoS One* **10**, e0133219 (2015).
197. Nagata, Y.*, et al.* PTEN activation contributes to tumor inhibition by trastuzumab, and loss of PTEN predicts trastuzumab resistance in patients. *Cancer Cell* **6**, 117-127 (2004).
198. Perez, E.A.*, et al.* Impact of PTEN protein expression on benefit from adjuvant trastuzumab in early-stage human epidermal growth factor receptor 2-positive breast cancer in the North Central Cancer Treatment Group N9831 trial. *J Clin Oncol* **31**, 2115-2122 (2013).

199. O'Reilly, K.E.*, et al.* mTOR inhibition induces upstream receptor tyrosine kinase signaling and activates Akt. *Cancer Res* **66**, 1500-1508 (2006).
200. Rexer, B.N., Chanthaphaychith, S., Dahlman, K. & Arteaga, C.L. Direct inhibition of PI3K in combination with dual HER2 inhibitors is required for optimal antitumor activity in HER2+ breast cancer cells. *Breast Cancer Res* **16**, R9 (2014).
201. Chandarlapaty, S.*, et al.* AKT inhibition relieves feedback suppression of receptor tyrosine kinase expression and activity. *Cancer Cell* **19**, 58-71 (2011).
202. Stuhlmiller, T.J.*, et al.* Inhibition of Lapatinib-Induced Kinome Reprogramming in ERBB2-Positive Breast Cancer by Targeting BET Family Bromodomains. *Cell Rep* **11**, 390-404 (2015).
203. Paget, S. The distribution of secondary growths in cancer of the breast. 1889. *Cancer Metastasis Rev* **8**, 98-101 (1989).
204. Witz, I.P. The biological significance of tumor-bound immunoglobulins. *Curr Top Microbiol Immunol* **61**, 151-171 (1973).
205. Vose, B.M. Functional activity of human tumor-infiltrating macrophages. *Adv Exp Med Biol* **114**, 783-787 (1979).
206. Folkman, J., Merler, E., Abernathy, C. & Williams, G. Isolation of a tumor factor responsible for angiogenesis. *J Exp Med* **133**, 275-288 (1971).
207. Folkman, J. Anti-angiogenesis: new concept for therapy of solid tumors. *Ann Surg* **175**, 409-416 (1972).
208. Xu, B.J.*, et al.* Quantitative analysis of the secretome of TGF-beta signaling-deficient mammary fibroblasts. *Proteomics* **10**, 2458-2470 (2010).
209. Miyamoto, S.*, et al.* Matrix metalloproteinase-7 triggers the matricrine action of insulin-like growth factor-II via proteinase activity on insulin-like growth factor binding protein 2 in the extracellular matrix. *Cancer Sci* **98**, 685-691 (2007).
210. Schrader, J.*, et al.* Matrix stiffness modulates proliferation, chemotherapeutic response, and dormancy in hepatocellular carcinoma cells. *Hepatology* **53**, 1192-1205 (2011).
211. Huang, C.*, et al.* beta1 integrin mediates an alternative survival pathway in breast cancer cells resistant to lapatinib. *Breast Cancer Res* **13**, R84 (2011).
212. Butcher, D.T., Alliston, T. & Weaver, V.M. A tense situation: forcing tumour progression. *Nat Rev Cancer* **9**, 108-122 (2009).
213. Sappino, A.P., Skalli, O., Jackson, B., Schurch, W. & Gabbiani, G. Smooth-muscle differentiation in stromal cells of malignant and non-malignant breast tissues. *Int J Cancer* **41**, 707-712 (1988).
214. Kalluri, R. The biology and function of fibroblasts in cancer. *Nat Rev Cancer* **16**, 582-598 (2016).
215. Lau, E.Y.*, et al.* Cancer-Associated Fibroblasts Regulate Tumor-Initiating Cell Plasticity in Hepatocellular Carcinoma through c-Met/FRA1/HEY1 Signaling. *Cell Rep* **15**, 1175-1189 (2016).
216. Capparelli, C., Rosenbaum, S., Berger, A.C. & Aplin, A.E. Fibroblast-derived neuregulin 1 promotes compensatory ErbB3 receptor signaling in mutant BRAF melanoma. *J Biol Chem* **290**, 24267-24277 (2015).
217. Yang, X.*, et al.* FAP Promotes Immunosuppression by Cancer-Associated Fibroblasts in the Tumor Microenvironment via STAT3-CCL2 Signaling. *Cancer Res* **76**, 4124-4135 (2016).
218. Lesokhin, A.M.*, et al.* Monocytic CCR2(+) myeloid-derived suppressor cells promote immune escape by limiting activated CD8 T-cell infiltration into the tumor microenvironment. *Cancer Res* **72**, 876-886 (2012).
219. Gabrilovich, D.I. & Nagaraj, S. Myeloid-derived suppressor cells as regulators of the immune system. *Nat Rev Immunol* **9**, 162-174 (2009).
220. Monu, N.R. & Frey, A.B. Myeloid-derived suppressor cells and anti-tumor T cells: a complex relationship. *Immunol Invest* **41**, 595-613 (2012).

221. Huang, B.*, et al.* Gr-1+CD115+ immature myeloid suppressor cells mediate the development of tumor-induced T regulatory cells and T-cell anergy in tumor-bearing host. *Cancer Res* **66**, 1123-1131 (2006).
222. Mills, C.D., Kincaid, K., Alt, J.M., Heilman, M.J. & Hill, A.M. M-1/M-2 macrophages and the Th1/Th2 paradigm. *J Immunol* **164**, 6166-6173 (2000).
223. Yuan, A.*, et al.* Opposite Effects of M1 and M2 Macrophage Subtypes on Lung Cancer Progression. *Sci Rep* **5**, 14273 (2015).
224. Savage, N.D.*, et al.* Human anti-inflammatory macrophages induce Foxp3+ GITR+ CD25+ regulatory T cells, which suppress via membrane-bound TGFbeta-1. *J Immunol* **181**, 2220-2226 (2008).
225. Tai, X.*, et al.* Basis of CTLA-4 function in regulatory and conventional CD4(+) T cells. *Blood* **119**, 5155-5163 (2012).
226. Dannenmann, S.R.*, et al.* Tumor-associated macrophages subvert T-cell function and correlate with reduced survival in clear cell renal cell carcinoma. *Oncoimmunology* **2**, e23562 (2013).
227. Ruffell, B.*, et al.* Macrophage IL-10 blocks CD8+ T cell-dependent responses to chemotherapy by suppressing IL-12 expression in intratumoral dendritic cells. *Cancer Cell* **26**, 623-637 (2014).
228. Wang, R.*, et al.* Increased IL-10 mRNA expression in tumor-associated macrophage correlated with late stage of lung cancer. *J Exp Clin Cancer Res* **30**, 62 (2011).
229. Strachan, D.C.*, et al.* CSF1R inhibition delays cervical and mammary tumor growth in murine models by attenuating the turnover of tumor-associated macrophages and enhancing infiltration by CD8+ T cells. *Oncoimmunology* **2**, e26968 (2013).
230. Avanzato, D.*, et al.* Activation of P2X7 and P2Y11 purinergic receptors inhibits migration and normalizes tumor-derived endothelial cells via cAMP signaling. *Sci Rep* **6**, 32602 (2016).
231. Csoka, B.*, et al.* Adenosine promotes alternative macrophage activation via A2A and A2B receptors. *FASEB J* **26**, 376-386 (2012).
232. Cekic, C. & Linden, J. Adenosine A2A receptors intrinsically regulate CD8+ T cells in the tumor microenvironment. *Cancer Res* **74**, 7239-7249 (2014).
233. Gentles, A.J.*, et al.* The prognostic landscape of genes and infiltrating immune cells across human cancers. *Nat Med* **21**, 938-945 (2015).
234. Tong, R.T.*, et al.* Vascular normalization by vascular endothelial growth factor receptor 2 blockade induces a pressure gradient across the vasculature and improves drug penetration in tumors. *Cancer Res* **64**, 3731-3736 (2004).
235. Ozawa, C.R.*, et al.* Microenvironmental VEGF concentration, not total dose, determines a threshold between normal and aberrant angiogenesis. *J Clin Invest* **113**, 516-527 (2004).
236. Sounni, N.E.*, et al.* Stromal regulation of vessel stability by MMP14 and TGFbeta. *Dis Model Mech* **3**, 317-332 (2010).
237. Chauhan, V.P.*, et al.* Angiotensin inhibition enhances drug delivery and potentiates chemotherapy by decompressing tumour blood vessels. *Nat Commun* **4**, 2516 (2013).
238. Kim, B.J. & Forbes, N.S. Single-cell analysis demonstrates how nutrient deprivation creates apoptotic and quiescent cell populations in tumor cylindroids. *Biotechnol Bioeng* **101**, 797-810 (2008).
239. Semenza, G.L. Targeting HIF-1 for cancer therapy. *Nat Rev Cancer* **3**, 721-732 (2003).
240. Minet, E.*, et al.* ERK activation upon hypoxia: involvement in HIF-1 activation. *FEBS Lett* **468**, 53-58 (2000).
241. Karakashev, S.V. & Reginato, M.J. Hypoxia/HIF1alpha induces lapatinib resistance in ERBB2-positive breast cancer cells via regulation of DUSP2. *Oncotarget* **6**, 1967-1980 (2015).
242. Siegel, R.L., Miller, K.D. & Jemal, A. Cancer Statistics, 2017. *CA Cancer J Clin* **67**, 7-30 (2017).
243. Lin, C.H., Lee, J.K. & LaBarge, M.A. Fabrication and use of microenvironment microarrays (MEArrays). *J Vis Exp* (2012).
244. Rantala, J.K.*, et al.* A cell spot microarray method for production of high density siRNA transfection microarrays. *BMC Genomics* **12**, 162 (2011).

245. LaBarge, M.A., *et al.* Human mammary progenitor cell fate decisions are products of interactions with combinatorial microenvironments. *Integrative biology : quantitative biosciences from nano to macro* **1**, 70-79 (2009).
246. Johann A. Gagnon-Bartsch, L.J., Terence P Speed. Removing Unwanted Variation from High Dimensional Data with Negative Controls. (University of California, Berkeley, Department of Statistics, University of California, Berkeley, 2013).
247. Wands, J.R., Podolsky, D.K. & Isselbacher, K.J. Mechanism of human lymphocyte stimulation by concanavalin A: role of valence and surface binding sites. *Proc Natl Acad Sci U S A* **73**, 2118-2122 (1976).
248. Tyner, J.W., *et al.* RNAi screen for rapid therapeutic target identification in leukemia patients. *Proc Natl Acad Sci U S A* **106**, 8695-8700 (2009).
249. Slamon, D.J., *et al.* Use of chemotherapy plus a monoclonal antibody against HER2 for metastatic breast cancer that overexpresses HER2. *N Engl J Med* **344**, 783-792 (2001).
250. Piccart-Gebhart, M.J., *et al.* Trastuzumab after adjuvant chemotherapy in HER2-positive breast cancer. *N Engl J Med* **353**, 1659-1672 (2005).
251. Gomez, H.L., *et al.* Efficacy and safety of lapatinib as first-line therapy for ErbB2-amplified locally advanced or metastatic breast cancer. *J Clin Oncol* **26**, 2999-3005 (2008).
252. Eichhorn, P.J., *et al.* Phosphatidylinositol 3-kinase hyperactivation results in lapatinib resistance that is reversed by the mTOR/phosphatidylinositol 3-kinase inhibitor NVP-BEZ235. *Cancer Res* **68**, 9221-9230 (2008).
253. Yao, Z., *et al.* BRAF Mutants Evade ERK-Dependent Feedback by Different Mechanisms that Determine Their Sensitivity to Pharmacologic Inhibition. *Cancer Cell* **28**, 370-383 (2015).
254. Zunder, E.R., Knight, Z.A., Houseman, B.T., Apsel, B. & Shokat, K.M. Discovery of drug-resistant and drug-sensitizing mutations in the oncogenic PI3K isoform p110 alpha. *Cancer Cell* **14**, 180-192 (2008).
255. Wilson, T.R., *et al.* Widespread potential for growth-factor-driven resistance to anticancer kinase inhibitors. *Nature* **487**, 505-509 (2012).
256. DeNardo, D.G., *et al.* Leukocyte complexity predicts breast cancer survival and functionally regulates response to chemotherapy. *Cancer discovery* **1**, 54-67 (2011).
257. Acerbi, I., *et al.* Human breast cancer invasion and aggression correlates with ECM stiffening and immune cell infiltration. *Integrative biology : quantitative biosciences from nano to macro* **7**, 1120-1134 (2015).
258. Muranen, T., *et al.* Inhibition of PI3K/mTOR leads to adaptive resistance in matrix-attached cancer cells. *Cancer Cell* **21**, 227-239 (2012).
259. Sullivan, R., Pare, G.C., Frederiksen, L.J., Semenza, G.L. & Graham, C.H. Hypoxia-induced resistance to anticancer drugs is associated with decreased senescence and requires hypoxia-inducible factor-1 activity. *Mol Cancer Ther* **7**, 1961-1973 (2008).
260. Cancer-Genome-Atlas-Network. Comprehensive molecular portraits of human breast tumours. *Nature* **490**, 61-70 (2012).
261. Daemen, A., *et al.* Modeling precision treatment of breast cancer. *Genome Biol* **14**, R110 (2013).
262. Thomas, G., Siegmann, M. & Gordon, J. Multiple phosphorylation of ribosomal protein S6 during transition of quiescent 3T3 cells into early G1, and cellular compartmentalization of the phosphate donor. *Proc Natl Acad Sci U S A* **76**, 3952-3956 (1979).
263. Jonas, O., *et al.* An implantable microdevice to perform high-throughput in vivo drug sensitivity testing in tumors. *Sci Transl Med* **7**, 284ra257 (2015).
264. Donnelly, S.M., *et al.* P38 MAPK contributes to resistance and invasiveness of HER2-overexpressing breast cancer. *Curr Med Chem* **21**, 501-510 (2014).
265. Ni, M., *et al.* Targeting androgen receptor in estrogen receptor-negative breast cancer. *Cancer Cell* **20**, 119-131 (2011).
266. Law, A.J., Shannon Weickert, C., Hyde, T.M., Kleinman, J.E. & Harrison, P.J. Neuregulin-1 (NRG-1) mRNA and protein in the adult human brain. *Neuroscience* **127**, 125-136 (2004).

267. Takai, K.*, et al.* Hepatocyte growth factor is constitutively produced by human bone marrow stromal cells and indirectly promotes hematopoiesis. *Blood* **89**, 1560-1565 (1997).
268. Eagles, G.*, et al.* Hepatocyte growth factor/scatter factor is present in most pleural effusion fluids from cancer patients. *Br J Cancer* **73**, 377-381 (1996).
269. Moondra, V.*, et al.* Serum Neuregulin-1beta as a Biomarker of Cardiovascular Fitness. *Open Biomark J* **2**, 1-5 (2009).
270. Kanda, T., Sullivan, K.F. & Wahl, G.M. Histone-GFP fusion protein enables sensitive analysis of chromosome dynamics in living mammalian cells. *Curr Biol* **8**, 377-385 (1998).
271. Debnath, J., Muthuswamy, S.K. & Brugge, J.S. Morphogenesis and oncogenesis of MCF-10A mammary epithelial acini grown in three-dimensional basement membrane cultures. *Methods* **30**, 256-268 (2003).
272. Heiser, L.M.*, et al.* Subtype and pathway specific responses to anticancer compounds in breast cancer. *Proc Natl Acad Sci U S A* (2011).
273. Kuo, W.L.*, et al.* A systems analysis of the chemosensitivity of breast cancer cells to the polyamine analogue PG-11047. *BMC Med* **7**, 77 (2009).
274. Lee-Hoeflich, S.T.*, et al.* A central role for HER3 in HER2-amplified breast cancer: implications for targeted therapy. *Cancer Res* **68**, 5878-5887 (2008).
275. Tibes, R.*, et al.* Reverse phase protein array: validation of a novel proteomic technology and utility for analysis of primary leukemia specimens and hematopoietic stem cells. *Mol Cancer Ther* **5**, 2512-2521 (2006).
276. Runswick, S.K., O'Hare, M.J., Jones, L., Streuli, C.H. & Garrod, D.R. Desmosomal adhesion regulates epithelial morphogenesis and cell positioning. *Nat Cell Biol* **3**, 823-830 (2001).
277. Perks, C.M., Vernon, E.G., Rosendahl, A.H., Tonge, D. & Holly, J.M. IGF-II and IGFBP-2 differentially regulate PTEN in human breast cancer cells. *Oncogene* **26**, 5966-5972 (2007).
278. Mehrian-Shai, R.*, et al.* Insulin growth factor-binding protein 2 is a candidate biomarker for PTEN status and PI3K/Akt pathway activation in glioblastoma and prostate cancer. *Proc Natl Acad Sci U S A* **104**, 5563-5568 (2007).
279. Busund, L.T.*, et al.* Significant expression of IGFBP2 in breast cancer compared with benign lesions. *J Clin Pathol* **58**, 361-366 (2005).
280. Park, K.H.*, et al.* Insulin-like growth factor-binding protein-2 is a target for the immunomodulation of breast cancer. *Cancer Res* **68**, 8400-8409 (2008).
281. Cecil, D.L.*, et al.* Elimination of IL-10-inducing T-helper epitopes from an IGFBP-2 vaccine ensures potent antitumor activity. *Cancer Res* **74**, 2710-2718 (2014).
282. Engelman, J.A.*, et al.* MET amplification leads to gefitinib resistance in lung cancer by activating ERBB3 signaling. *Science* **316**, 1039-1043 (2007).
283. Nahta, R., Yuan, L.X., Zhang, B., Kobayashi, R. & Esteva, F.J. Insulin-like growth factor-I receptor/human epidermal growth factor receptor 2 heterodimerization contributes to trastuzumab resistance of breast cancer cells. *Cancer Res* **65**, 11118-11128 (2005).
284. Huang, X.*, et al.* Heterotrimerization of the growth factor receptors erbB2, erbB3, and insulin-like growth factor-i receptor in breast cancer cells resistant to herceptin. *Cancer Res* **70**, 1204-1214 (2010).
285. Harbeck, N.*, et al.* HER2 Dimerization Inhibitor Pertuzumab - Mode of Action and Clinical Data in Breast Cancer. *Breast Care (Basel)* **8**, 49-55 (2013).
286. Zhang, Q., Park, E., Kani, K. & Landgraf, R. Functional isolation of activated and unilaterally phosphorylated heterodimers of ERBB2 and ERBB3 as scaffolds in ligand-dependent signaling. *Proc Natl Acad Sci U S A* **109**, 13237-13242 (2012).
287. Dobin, A.*, et al.* STAR: ultrafast universal RNA-seq aligner. *Bioinformatics* **29**, 15-21 (2013).
288. Robinson, M.D., McCarthy, D.J. & Smyth, G.K. edgeR: a Bioconductor package for differential expression analysis of digital gene expression data. *Bioinformatics* **26**, 139-140 (2010).
289. Robinson, M.D. & Oshlack, A. A scaling normalization method for differential expression analysis of RNA-seq data. *Genome Biol* **11**, R25 (2010).

290. Bullard, J.H., Purdom, E., Hansen, K.D. & Dudoit, S. Evaluation of statistical methods for normalization and differential expression in mRNA-Seq experiments. *BMC Bioinformatics* **11**, 94 (2010).
291. Risso, D., Schwartz, K., Sherlock, G. & Dudoit, S. GC-content normalization for RNA-Seq data. *BMC Bioinformatics* **12**, 480 (2011).
292. McCarthy, D.J., Chen, Y. & Smyth, G.K. Differential expression analysis of multifactor RNA-Seq experiments with respect to biological variation. *Nucleic Acids Res* **40**, 4288-4297 (2012).
293. He, W*., et al.* Cell-free expression of functional receptor tyrosine kinases. *Sci Rep* **5**, 12896 (2015).
294. Grant, B.D. & Donaldson, J.G. Pathways and mechanisms of endocytic recycling. *Nat Rev Mol Cell Biol* **10**, 597-608 (2009).
295. Finisguerra, V*., et al.* MET is required for the recruitment of anti-tumoural neutrophils. *Nature* **522**, 349-353 (2015).
296. O'Quigley, J. & Chevret, S. Methods for dose finding studies in cancer clinical trials: a review and results of a Monte Carlo study. *Stat Med* **10**, 1647-1664 (1991).